MECHANISMS AND INHIBITION OF DEALLOYING IN AN ALPHA BRASS

By

WILLIAM CLARENCE FORT, III

A DISSERTATION PRESENTED TO THE GRADUATE COUNCIL
OF THE UNIVERSITY OF FLORIDA
IN PARTIAL FULFILLMENT OF THE REQUIREMENTS FOR THE
DEGREE OF DOCTOR OF PHILOSOPHY

UNIVERSITY OF FLORIDA

1975

Dedicated to my wife, Deborah.

ACKNOWLEDGEMENTS

I would like to express my appreciation to the chairman of my supervisory committee, Dr. Ellis D. Verink, Jr., for his encouragement and inspiration throughout the course of my studies and research. Thanks are extended to Dr. R. T. DeHoff, Dr. R. W. Gould, and Dr. G. M. Schmid for serving as members of the supervisory committee, and to Dr. C. M. Chen for his many helpful suggestions.

I wish to acknowledge the financial assistance made available by the College of Engineering of the University of Florida, the NDEA Title IV fellowship Program, the Office of Naval Research, and the International Nickel Company. In addition, certain of the equipment used in these investigations was purchased with funds from the Office of Saline Water.

I also extend special appreciation to Mr. P. M. Russell, Mr. M. H. Froning, Mr. J. T. Healey, and Dr. R. G. Connell for their unselfish assistance in the final moments. I am indebted to Mr. W. A. Acree, Mr. E. J. Jenkins, Mr.E.C. Logsdon, Mr. C. J. Minier, and Mr. C. Simmons for their expert technical assistance during the course of the investigation.

TABLE OF CONTENTS

Page

ACKNOWLEDGEMENTS iii

LIST OF TABLES vi

LIST OF FIGURES. vii

ABSTRACT xiii

CHAPTER 1 INTRODUCTION 1

CHAPTER 2 LITERATURE REVIEW 4

2.1. Selective Leaching Mechanism 5
2.2. Dissolution and Replating Mechanism 20
2.3. The Role of Arsenic as an Inhibitor of Dezincification 29

CHAPTER 3 EXPERIMENTAL PROCEDURE 34

3.1. Potentiokinetic Polarization Experiments . . 34
3.2. Selective Leaching Experiments 37
3.3. Controlled Anodic Dissolution Experiments . . 38
3.4. Artificial Occluded Cell Experiments 39
3.5. Auger Electron Spectroscopic Analyses 42
3.6. X-Ray Identification of Corrosion Products . 51

CHAPTER 4 RESULTS AND DISCUSSION 52

4.1. Electrochemical Characterization of Copper, Zinc, and Cu30Zn 52
4.2. Dealloying of Cu30Zn by Selective Leaching . 66
4.3. Dealloying of Cu30Zn by Dissolution and Replating 103
4.4. Effect of Arsenic Additions on Dealloying of Cu30Zn 150

CHAPTER 5 CONCLUSIONS 165

CHAPTER 6 RECOMMENDATIONS FOR FURTHER RESEARCH . . . 169

TABLE OF CONTENTS (Continued)

Page

APPENDICES

1 SAMPLE CHARACTERIZATION AND PREPARATION. . . 171

2 SOLUTION CHARACTERIZATION AND PREPARATION. . 174

3 STANDARD POLARIZATION CELL 175

4 LIST OF EQUIPMENT 178

5 AUGER ELECTRON SPECTROSCOPY 179

6 CALIBRATION OF THE ARGON SPUTTERING RATE . . 185

7 FREE ENERGY DATA USED IN CALCULATED EQUILIBRIA 187

BIBLIOGRAPHY 188

BIOGRAPHICAL SKETCH 193

LIST OF TABLES

Table		Page
1	Conditions of Exposure for the Cu30Zn Selective Leaching Samples	67
2	Rate of Zinc Dissolution from Cu30Zn Under Selective Leaching Conditions	72
3	Thicknesses of the Zinc-Depleted Surface Layers	93
4	Summary of Diffusion Analysis Data	99
5	Plateau Values of Dissolved Copper Concentrations Measured in Controlled Anodic Dissolution Experiments	132

LIST OF FIGURES

Figure		Page
1	Superposition of calculated equilibria for the Cu-0.1M Cl^--H_2O and Zn-H_2O systems and experimental potential versus pH diagram for Cu30Zn alloy in 0.1M chloride solutions, after Verink and Heidersbach (18).	7
2	Kink-step-terrace model of a dissolving alloy surface, after Pickering and Wagner. . .	10
3	Schematic of the equipment set-up for generation of potentiokinetic polarization curves	35
4	Artificial occluded cell electrode assembly . .	40
5	Schematic of the electrical circuit for the artificial occluded cell experiments . . .	43
6	Schematic of the AES system used to analyze selective leaching samples	45
7	Typical Auger spectrum from the surface of a Cu30Zn sample	46
8	Effect of the composition of Cu-Zn alloys on the Cu/Zn ratio obtained by AES analysis. .	49
9	Auger composition profile obtained for Cu-15 w/o alloy	50
10	Experimental potential versus pH diagram for pure copper in nitrogen saturated, 0.1M chloride solutions	54
11	Superposition of polarization data for pure copper in 0.1M chloride solutions and the equilibrium potential versus pH diagram calculated for the system Cu-0.1M Cl^--H_2O at 25°C, after Van Muylder *et al*. (71)	57

LIST OF FIGURES (Continued)

Figure		Page
12	Experimental potential versus pH diagram for pure zinc in nitrogen-saturated 0.1M chloride solutions	59
13	Superposition of polarization data for pure zinc in 0.1M chloride solutions and the equilibrium potential versus pH diagram calculated for the system Zn-H_2O at 25°C, after Pourbaix (72)	61
14	Experimental potential versus pH diagram for Cu30Zn in nitrogen-saturated 0.1M chloride solutions	62
15	Variation of the corrosion potential of Cu30Zn with time of exposure in 0.1M chloride solutions of pH 2 and pH 4.	64
16	Zinc dissolved from Cu30Zn samples potentiostated at -0.700 V_{SCE} in 89°C, 0.1M chloride solutions of pH 4	70
17	Zinc dissolved from Cu30Zn samples potentiostated at electrode potentials between -0.500 and -0.900 V_{SCE} at 89°C	71
18	Pitting of Cu30Zn sample exposed 4 days at -0.450 V_{SCE}. 3700X	75
19	Typical surface of Cu30Zn samples potentiostated below -0.450 V_{SCE}. From a Cu30Zn sample exposed 4 days at -0.600 V_{SCE}. 3500X	76
20	Auger composition profile obtained from an unexposed Cu30Zn sample	78
21a	Auger composition profile obtained from a Cu30Zn sample potentiostated at -0.450 V_{SCE} for 1 day	80
21b	Auger composition profile obtained from a Cu30Zn sample potentiostated at -0.450 V_{SCE} for 4½days	81

LIST OF FIGURES (Continued)

Figure		Page
21c	Auger composition profile obtained from a Cu30Zn sample potentiostated at -0.450 V_{SCE} for 7 days	82
22	Auger composition profile obtained from a Cu30Zn sample potentiostated at -0.500 V_{SCE} for 4 days	84
23	Auger composition profile obtained from a Cu30Zn sample potentiostated at -0.600 V_{SCE} for 4 days	85
24a	Auger composition profile obtained from a Cu30Zn sample potentiostated at -0.700 V_{SCE} for 2 days	86
24b	Auger composition profile obtained from a Cu30Zn sample potentiostated at -0.700 V_{SCE} for 4 days	87
24c	Auger composition profile obtained from a Cu30Zn sample potentiostated at -0.700 V_{SCE} for 7 days	88
24d	Auger composition profile obtained from a Cu30Zn sample potentiostated at -0.700 V_{SCE} for 10 days	89
25	Auger composition profile obtained from a Cu30Zn sample potentiostated at -0.800 V_{SCE} for 4 days	90
26	Auger composition profile obtained from a Cu30Zn sample potentiostated at -0.900 V_{SCE} for 4 days	91
27	Infinite diffusion model used in zinc diffusion analysis	95
28	Log-log plot of the zinc diffusion data taken from composition profiles obtained by AES from Cu30Zn samples selectively leached at -0.700 V_{SCE}	100

LIST OF FIGURES (Continued)

Figure		Page
29	Simplified potential versus pH diagram for Cu30Zn in 0.1M chloride solutions outlining conditions of exposure for controlled anodic dissolution experiments	104
30	Etched surface of a Cu30Zn sample potentiostated 13 days at -0.200 V_{SCE} in pH 4, 0.1M chloride solution. 1500X	107
31	Curves showing the concentrations of copper and zinc present in solution during dissolution of Cu30Zn at -0.200 V_{SCE}.	108
32a	Pitting observed on etched Cu30Zn sample exposed 10 days at -0.100 V_{SCE}. Two copper crystals formed on the surface are marked by arrows. 125X	111
32b	Detail of one of the crystals found on the sample described in figure 32a. The tetrahedral shape is outlined in the accompanying sketch. 300X	112
32c	Cross section of one of the copper crystals detailing the Cu30Zn grain boundary artifacts visible in the dezincified structure. 75X	113
33	Concentrations of copper and zinc measured in the solution of a cell containing a Cu30Zn sample polarized 10 days at -0.100 V_{SCE}	115
34	Dezincification noted on a Cu30Zn sample exposed 3 days at 0.000 V_{SCE}. 1000X	117
35	Dezincification noted on a Cu30Zn sample exposed 13 days at 0.000 V_{SCE}. 60X	118
36	Results of solution analysis for Cu30Zn samples potentiostated at 0.000 V_{SCE} for 7 days and 13 days	119

LIST OF FIGURES (Continued)

Figure		Page
37	Dezincification noted on a Cu30Zn sample exposed 10 days at +0.100 V_{SCE}. 1000X	121
38	Results of solution analysis for a Cu30Zn sample potentiostated 10 days at +0.100 V_{SCE}.	122
39	Detail of sample surface of a Cu30Zn sample exposed 13 days at +0.200 V_{SCE}, covered by a layer of cuprous chloride. 1500X	123
40	Results of solution analysis for a Cu30Zn sample potentiostated 13 days at +0.200 V_{SCE}	125
41	Results of solution analysis for a Cu30Zn sample potentiostated 10 days at +0.500 V_{SCE}	126
42	Extent of dezincification noted on a Cu30Zn sample exposed 10 days at +0.500 V_{SCE}. 60X	127
43	Equilibria calculated for the Cu-Cl^--H_2O system at pH = 4 showing agreement between equilibrium calculations and constant copper concentrations observed in the controlled anodic dissolution experiments	133
44	Cu30Zn sample potentiostated 4 days at +0.500 V_{SCE}, showing separation between the brass and the copper sponge structure. 250X	138
45	Results of artificial occluded cell experiments showing occluded cell potential and occluded cell current measured as a function of time	141
46	Results of solution analysis for arsenical Cu30Zn potentiostated at -0.200 V_{SCE} in pH 4, 0.1M chloride solution	154

LIST OF FIGURES (Continued)

Figure		Page
47	Results of solution analysis for arsenical Cu30Zn potentiostated at -0.100 V_{SCE} in pH 4, 0.1M chloride solution	155
48	Results of solution analysis for arsenical Cu30Zn potentiostated at -0.000 V_{SCE} in pH 4, 0.1M chloride solution	157
49	Results of solution analysis for arsenical Cu30Zn potentiostated at +0.100 V_{SCE} in pH 4, 0.1M chloride solution	158
50	Results of solution analysis for arsenical Cu30Zn potentiostated at +0.200 V_{SCE} in pH 4, 0.1M chloride solution	159
51	Results of solution analysis of arsenical Cu30Zn potentiostated at +0.500 V_{SCE} in pH 4, 0.1M chloride solution	161
52	Standard polarization cell	176
53	Energy level diagram depicting a KLM Auger transition	180
54	Schematic energy spectrum and experimental AES curve for silver excited in a 1000 eV electron beam	182
55	Composition profile of a 1026±25Å copper film deposited on a zinc substrate, used to calibrate the argon sputtering rate	186

Abstract of Dissertation Presented to the Graduate Council of the University of Florida in Partial Fulfillment of the Requirements for the Degree of Doctor of Philosophy

MECHANISMS AND INHIBITION OF DEALLOYING IN AN ALPHA BRASS

By

William Clarence Fort, III

July, 1975

Chairman: Dr. Ellis D. Verink, Jr.
Major Department: Materials Science and Engineering

Dealloying of a single-phase binary alpha brass in pH 4, 0.1M chloride solution was investigated in terms of the operative mechanism. Selective leaching of zinc from the brass was produced under conditions of cathodic polarization. Auger electron spectroscopy was employed to measure composition versus depth profiles of the resulting zinc-depleted surface layers. The selective leaching mechanism was found to be based on enhanced volume diffusion of zinc to the brass surface. Dealloying by dissolution of the brass as a whole, followed by redeposition of the copper, was found to occur exclusively under occluded cell conditions. The mechanism was examined in terms of the copper-chloride equilibria established at the dissolving brass surface. The redeposition of copper was found to proceed by reduction of cuprous chloride near the brass surface. The inhibitive effect of arsenic was determined to be the prevention of the cuprous chloride reduction reaction.

CHAPTER 1

INTRODUCTION

Since the initial description of the dealloying phenomenon in brasses more than 100 years ago (1), the metals literature has witnessed an ongoing debate as to the mechanism(s) responsible. Notwithstanding that rather early in the century the practical problem of dezincification of alpha brasses was solved by alloying with arsenic (2), a considerable amount of research effort is even now being directed towards understanding the phenomena involved.

This can be at least partly attributed to ongoing discoveries of dealloying behavior in a host of diverse alloy systems (3). In addition, several reports in more recent years have linked dealloying behavior with stress corrosion cracking in several systems of interest (4-8). It remains the goal of researchers in this area of investigation to apply a basic understanding of the mechanisms of dealloying in brasses to solve the dealloying problems encountered in other systems, and to predict when dealloying might be expected in new applications.

Two principal mechanisms for dealloying* of single phase binary alloys in aqueous environments have gained wide acceptance:

(1) Selective leaching of the less noble component of the alloy from the metal matrix into solution without corresponding dissolution of the more noble component; and

(2) Total dissolution of the alloy (both components entering solution at rates proportional to their respective concentrations in the alloy) followed by redeposition of the more noble component metal on or adjacent to the dissolving alloy surface.

Almost without exception, one or the other of these mechanisms has been assigned to each reported dealloying occurrence. Efforts to resolve the nature of the mechanism operating for any one system have resulted, for the most part, in confusing and often contradictory conclusions.

It is the goal of this research to clarify the mechanisms responsible for dealloying in a defined system — Cu-30 w/o (weight percent) Zn [hereafter designated as Cu30Zn] exposed in aqueous solutions containing 0.1 molar of chloride ion. The choice of this system is based on several factors. Cu30Zn has been and remains the most important binary brass alloy. For this reason, if none other, it has also received the majority of research attention. Consequently, a large

---

*Dealloying is defined as the corrosion process whereby one constituent of an alloy is preferentially removed from an alloy, leaving an altered residual structure (3).

volume of literature concerning its corrosion and physical properties is available. The fact that it is a single phase alloy eliminates complications which might otherwise result from galvanic interactions between dissimilar phases. The possibility of phase changes under corrosion conditions is likewise eliminated.

Further, a large proportion of the dezincification failures reported have occurred in saline environments. Thus, the role of the chloride ion in causing or in enhancing dezincification cannot be overlooked.

This investigation is divided into four main sections:

(1) Definition of the polarization behavior of the system in order to establish a firm basis for predicting the conditions which lead to dealloying, and the effects of these conditions on the mechanism;

(2) Elucidation of the detailed mechanism involved in selective leaching of zinc from the brass matrix through use of surface sensitive techniques;

(3) Clarification of the chemical and electrochemical equilibria which govern dezincification of alpha brass in chloride-containing environments; and

(4) Clarification of the role played by arsenic additions to alpha brass in inhibiting dezincification.

Special attention is payed to the role of crevice or occluded cell phenomena in the initiation and propagation of the attack.

CHAPTER 2

LITERATURE REVIEW

Investigations of dealloying mechanisms have been limited almost entirely to the binary copper-zinc and copper-gold systems. The research popularity of non-commercial copper-gold alloys is due to the following factors: (1) the system is isomorphous, hence phase changes with accompanying compositional changes need not be considered; (2) gold exhibits a very noble single electrode potential, and does not dissolve under ordinary circumstances (the dissolving component in this case is copper); (3) there is little overlap in the X-ray spectra of copper and gold; and (4) the melting points of copper and gold are similar, and alloying is relatively simple.

Dealuminification of the commercially important aluminum bronzes has received only limited attention regarding mechanisms, primarily because the problem has been remedied through slight compositional adjustments and improved heat treatment procedures (9-11). The literature concerning dealloying in other systems is almost entirely limited to reports of in-service failures. Several excellent reviews covering the entire dealloying spectrum are available (3, 12-15).

2.1. Selective Leaching Mechanism

The theoretical aspects of dealloying by a selective leaching mechanism have been described most eloquently by Pickering and Wagner (16). They state that preferential removal of the less noble component of a binary alloy undergoing anodic dissolution requires that: (1) there be a sufficiently large difference (i.e., several RT/F) between the single electrode potentials of the two constituent metals; and (2) the electrode potential of the alloy be higher than that of the less noble component and significantly lower than that of the more noble component. Such is the case for Cu-Au alloys and beta brass. The electrode potential of alpha brass, however, is nearly the same as that of its more noble component, copper (17).

The important condition here is that, at a given alloy electrode potential, there be a much greater tendency for the more active component atoms to dissolve than for the noble component to dissolve, based on the respective single electrode potentials of the component metals. Thus, alpha brass polarized several RT/F below the single electrode potential for copper (i.e., cathodically) meets this requirement.

Verink and Heidersbach (18) have proposed that the electrochemical conditions outlined above as necessary for dealloying by a selective leaching mechanism can be rather

simply predicted by comparing the calculated and experimental potential versus pH diagrams for the system of interest. Thus, referring to figure 1, selective leaching of zinc from a Cu30Zn alloy exposed in neutral and acidic 0.1M chloride solutions free of copper ions would occur at potentials more noble than the calculated $Zn/Zn^{++}(10^{-6}M)$ equilibrium and less noble than the experimentally determined corrosion potentials for Cu30Zn (area of small dots).

The authors tested this hypothesis by exposing Cu30Zn samples in buffered 0.1M chloride solutions of pH 4 for up to 13 days at several potentials in the predicted range (19). They report that zinc is dissolved into the electrolyte with no discernable accompanying copper dissolution. However, the formation of a dezincified layer was not confirmed although tarnishing was observed. The identity of tarnish layer could not be determined by any of the then currently available techniques.

The results of Verink and Heidersbach are consistent with earlier investigations of selective dissolution of Cu-Zn and Cu-Au alloys. Pickering and Byrne (20) measured partial currents (by solution analysis) for the dissolution of copper and zinc from alpha, gamma, and epsilon brass specimens held at potentials between -1.000 and +0.500 V_{SHE} in acetate buffered (pH = 5) 1N Na_2SO_4 alloy where only zinc was dissolved in detectable quantities. At potentials more noble than certain critical potentials, simultaneous

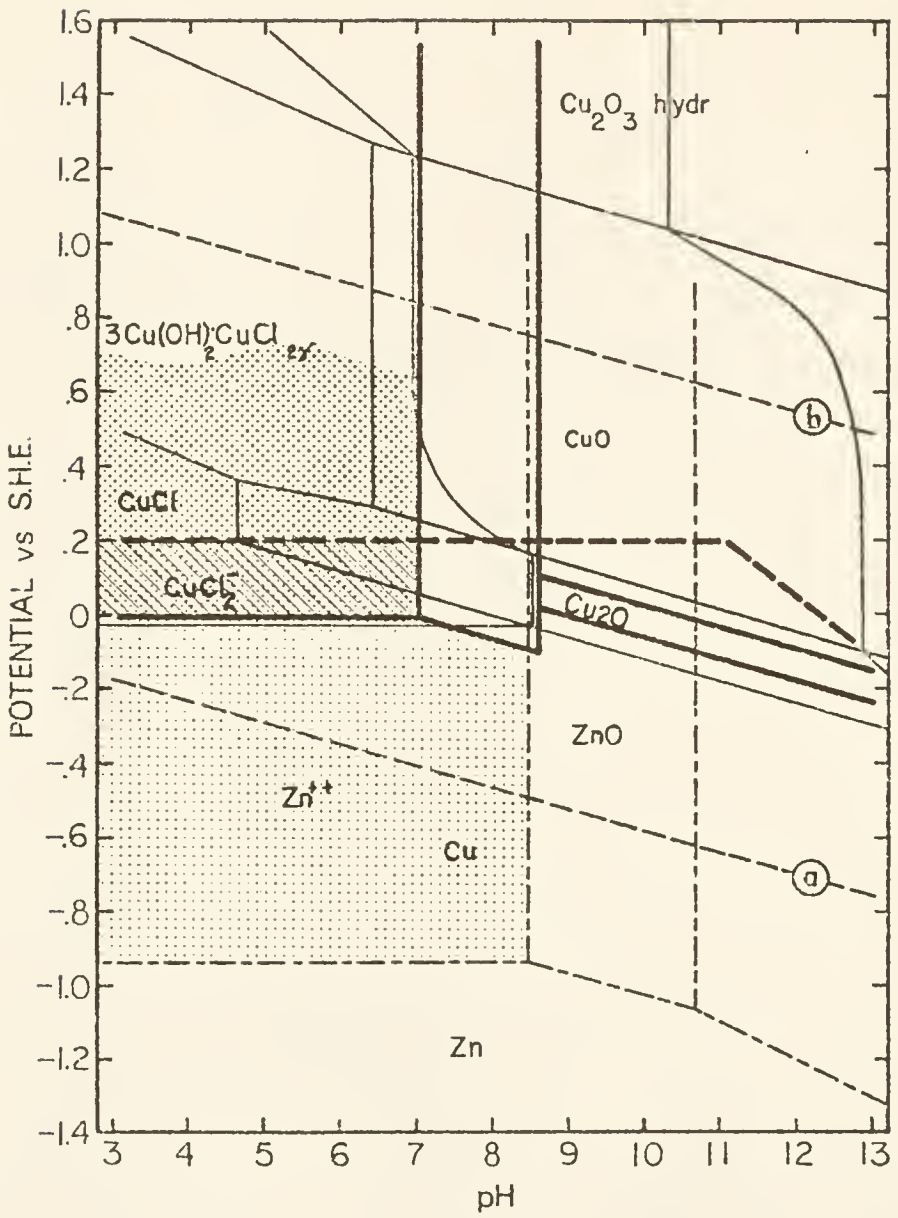

Figure 1. Superposition of calculated equilibria for the Cu-0.1M Cl^--H_2O and Zn-H_2O systems and experimental potential versus pH diagram for Cu30Zn alloy in 0.1M chloride solutions, after Verink and Heidersbach (18).

dissolution* of the alloys occurred.

Similar results were reported by the same authors for Cu-13a/o (atomic percent) Au and Cu-18a/o Au alloys potentiostated between -0.350 and +0.875 V_{SHE} in 1N Na_2SO_4-0.01N H_2SO_4 solutions (21). In this case, however, simultaneous dissolution does not occur above the critical potentials. Instead, severe roughening of the alloy surface was noted. These results are in substantial agreement with those of earlier investigators (22) for the same system.

Ionization of the less noble component results in rapid accumulation of the other components' atoms on the alloy surface. If selective dissolution is to continue, some means must be established to provide the atoms of the more active component access to the liquid-solid interface.† The two likely possibilities are

(1) Aggregation of the more noble component atoms by surface diffusion, exposing new alloy surface containing active atoms; and

(2) Transport by volume diffusion of active metal atoms to the liquid-solid interface.

---

*Simultaneous dissolution is defined by both alloy components entering solution at rates proportional to their respective concentrations in the alloy.

†Implicit in this argument is that the ionization of the active atoms at the liquid-solid interface and their consequent diffusion into the bulk electrolyte is fast and not rate-controlling. This assumption has been recently discussed in detail by Rubin (17).

Pickering and Wagner (16) favor the latter possibility and have proposed a divacancy diffusion mechanism which counters the classical argument against such a concept (i.e., the sluggishness of transport by simple bulk diffusion at ambient temperatures). The mechanism is based on a kink-step-terrace model of the surface of the dissolving metal alloy A-B, figure 2.

Ionization of the less noble component atom A at kink position 1 proceeds by its moving along the step and onto the terrace as an adsorbed atom, from where it passes into solution as an ion. The more noble component atom B initially at step position 2 may then move along the step, and become adsorbed, but not ionized, or it may desorb. As this process continues, the concentration of adsorbed B atom increases, thereby increasing the probability that adsorbed B atoms desorb to kink sites, and consequently decreasing the probability that active A atoms occupy kink sites. This leads to increased electrochemical polarization and increased driving force for ionization of A atoms. The increased driving force makes possible direct adsorption of A atoms (position 6) from step sites and, eventually, direct adsorption from terrace sites. The step and surface vacancies resulting from such events may in some cases be filled by subsurface atoms, thereby introducing excess monovacancies and divacancies into the alloy matrix. The buildup of an excess vacancy concentration in the vicinity of the surface would enhance chemical diffusion (i.e., diffusion in

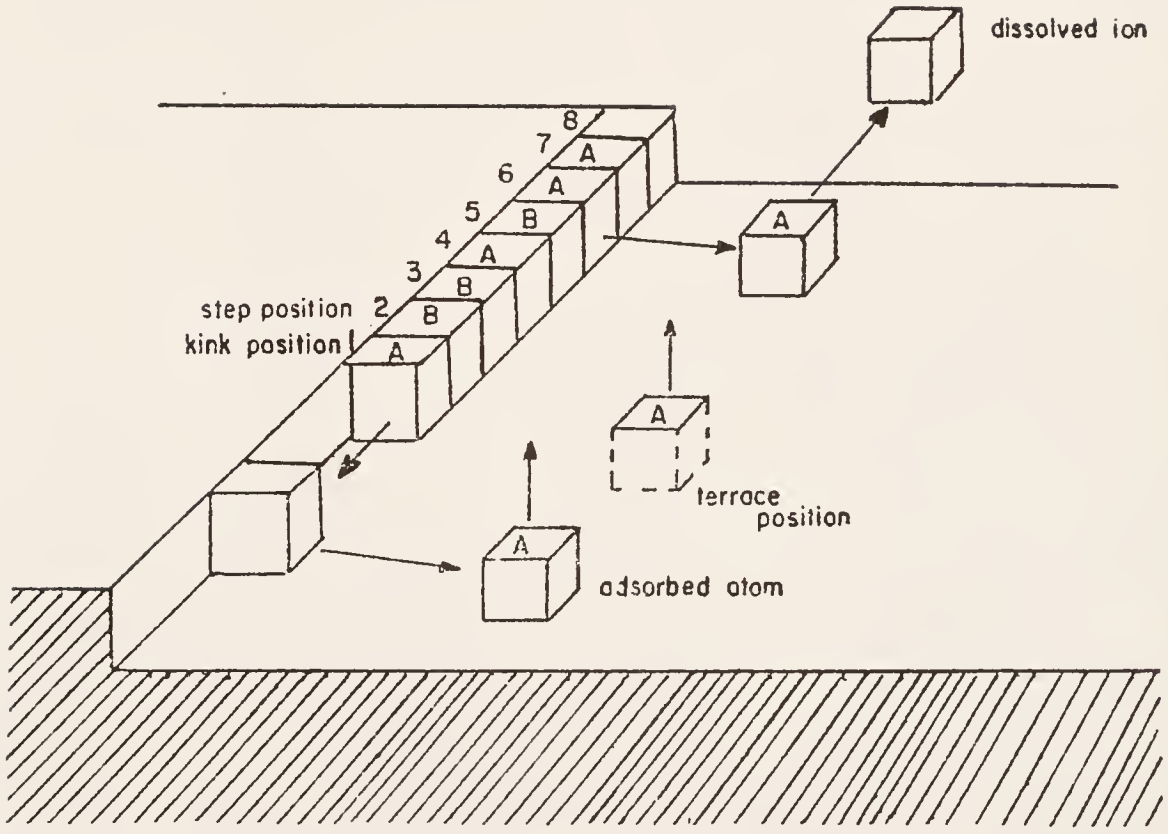

Figure 2. Kink-step-terrace model of a dissolving alloy surface, after Pickering and Wagner.

the concentration gradient due to enrichment of the surface in component B) of A atoms towards the surface and B atoms into the subsurface layers.

The authors have presented calculations of the current density and effective diffusion zone thickness expected for dissolution of copper from a Cu-10 a/o Au alloy at 25°C. Several assumptions have been made which are open to question (17), among them:

(1) the concentration of divacancies near the surface is taken to be as high as 10^{-2} a/o;

(2) the accuracy of divacancy diffusion coefficient values extrapolated to 25°C are realistic;

(3) the diffusion coefficient value used is assumed to be composition independent; and

(4) contributions to the total diffusion rate by short-circuit diffusion paths (subgrain boundaries and dislocations) are ignored.

Notwithstanding these criticisms, the authors calculate a current density of about 2×10^{-4} amp/cm^2 and an effective diffusion zone thickness equal to about 10^{-6} cm (0.01 μm) after 1 000 seconds' exposure.

Experimental verification of the model calculations presented above were undertaken by the authors. Cu-10 a/o Au sheets dissolved at 1 ma/cm^2 for 320 min (19.2 coulombs/cm^2 passed) in 1N H_2SO_4 or in buffered 1N NaCl solution developed gold-rich surface layers approximately 8 μm thick. Based on

the amount of charge passed in the experiments, 8 μm is very close to the depth from which total dissolution of copper would occur. Calculation of the effective diffusion zone thickness from the divacancy diffusion model gives the maximum thickness as only about 0.7 μm for 320 min exposure.

These conflicting results can be reconciled by considering the surface roughening noted to have occurred in the gold-rich layers (23). As the attack proceeds, the surface roughening effect introduces channel-like penetrations and porosity, thereby significantly increasing the surface area of the gold-rich surface layers. Consequently, a much larger surface area is exposed to the solution, and can undergo selective dissolution. This mechanism results in the formation of a leached structure significantly thicker than could be formed without roughening.

The operation of a selective leaching mechanism does not preclude simultaneous operation of dissolution and replating mechanism. Pickering and Wagner have discounted the possibility that significant numbers of gold atoms are ionized on the basis of rotating ring disk electrode measurements on a Cu-10 a/o Au alloy specimen dissolved at polentials up to +0.900 V_{SHE}. The limitations of this method in measuring very small concentrations has been pointed out by Rubin (17). At any rate, the effects of increased overpotentials on the mobilities of adsorbed gold atoms and any resultant surface diffusion effects are unknown.

Under appropirate polarization conditions, complete dissolution and selective leaching might be expected to occur simultaneously. Such would be the case if a Cu-Au alloy were dissolved at potentials close to the single electrode potential for gold, or if alpha brass were dissolved at very low anodic overpotentials. The consequent effect of the receding metal-solution interface on the interdiffusion zone thickness has been treated by Holliday and Pickering (24) for the case where the rate of selective leaching and the rate of total dissolution are similar. After an initial period during which the metal diffusion profiles are established, a stationary state is reached, wherein simultaneous dissolution from the surface critically enriched in the more noble component occurs. Thereafter, the rate of selective leaching of the more active component is proportional to the total alloy dissolution rate, and the diffusion profiles adjacent to the surface (i.e., the level of surface enrichment of the more noble component) remain constant as dissolution continues.

The role played by surface diffusion in the selective dissolution mechanism has received relatively little attention. Pickering and Wagner (16) discount its importance, pointing out that noble component atoms migrating on the metal surface would agglomerate and form small crystals. As these crystals grow to impingement, blockage of the active atoms' access to the liquid-solid interface occurs, and the leaching process is stifled.

The ease with which blockage would occur presumably is related to the alloy composition, i.e., alloys containing larger percentages of the noble element would be more immune to significant leaching than those containing more of the active component. This possible explanation of the fact that high brasses, containing less than about 10 w/o of zinc, have not been observed to dezincify has been hinted at by Feller (25). Feller discounts normal unaided isothermal surface diffusion as being too slow to produce measurable effects. Instead he proposes that under appropriate high anodic potentials, surface diffusion is enhanced. This viewpoint is supported by Tischer and Gerischer (26), who report that surface mobility of gold depends on the electrode potential.

Rubin (17) has recently proposed that noble and active atoms might combine via surface diffusion to form patches of alloy having a composition more stable under the prevailing surface condition than the initial alloy composition. As is pointed out, the mechanism could be used to explain the detection of intermediate compositions in dealloyed Cu-Au alloys, to be discussed subsequently.

Direct experimental evidence for the operation of the selective leaching mechanism in dealloying is rare. Furthermore, quantitative data concerning leaching rates, layer thickness, and the detailed diffusion processes involved are almost completely lacking.

The optical metallographical evidence for selective leaching is primarily speculative in nature, and has in most instances been successfully challenged (3). Aside from the obvious comment, that the extent of attack found in most dealloying experiments cannot be accounted for by even the most optimistic diffusion mechanism, consideration is rarely given to the factors and processes which result in the formation of the grossly porous residual metal sponges often found.* Explanation of the formation of such structures by a selective leaching mechanism is difficult.

X-ray and electron diffraction examinations of dealloyed metals have yielded the best evidence to date. The applicability of the method to dealloying measurement rests on the assumption that the lattice parameter of the alloy undergoing selective leaching will evolve in some orderly fashion from its initial value towards that of the more noble component. Thus, the diffraction pattern obtained from a partially leached alloy would contain "bands" of intensity limited by the normal diffraction line positions of the alloy and the noble metal. Furthermore, if dealloying has taken place by a dissolution and replating mechanism, then only the lines corresponding to the initial alloy and to the more noble metal should be detected.

---

*Some experiments by Lucey (27) are the notable exceptions.

Graf's early X-ray diffraction experiments (28, 29) indicated the formation of a series of crystals containing from 60 to 80 atomic percent of gold on Cu-10 a/o Au alloy specimens exposed in alcohol-picric acid solutions or in alkaline solutions of sodium tartrate at 25°C. He found, however, that Cu-25 a/o Au specimens, dealloyed in more highly oxidizing nitric acid solutions at 70°C, formed no regions of intermediate composition;only diffraction spectra for the original alloy and for pure gold were found.

Pickering and Wagner (16) refined Graf's method and applied it to Cu-10 a/o Au foils dissolved in room temperature 1N H_2SO_4 and in 1N NaCl solution at current densities up to 20 ma/cm^2. They report the emergence of maxima in diffracted intensity between the Cu-10 a/o Au peaks and the pure copper peaks. These maxima move towards the gold peaks as the amount of dissolution increases. Later electron diffraction experiments on a series of copper-rich Cu-Au alloys exposed under the same conditions were reported to confirm the findings for the earlier stages of dissolution (30, 31). The positions of the intensity maxima observed in patterns from dealloyed Cu-Au alloys containing 3, 5, and 10 a/o of gold were observed to be nearly the same, and to correspond to those of an alloy of approximate composition Cu-69 a/o Au. Similar formation of equivalent intermediate compositions by a series of alloys has been described in the Cu-Ni

system (17). In this case the stability of an intermediate composition was attributed to altered thermodynamic conditions present at the surface of the dissolving metal.

Similar X-ray diffraction determinations were carried out by Heidersbach and Verink (19) on alpha (Cu-30 w/o Zn) and beta (Cu-48 w/o Zn) brass specimens exposed in 5N HCl for 20 and 30 days and 2 days, respectively. Their X-ray patterns from the alpha brass show a band of increased intensity between the peaks due to copper and to the Cu3OZn alloy. A similar pattern reported for a beta brass sample shows peaks for beta brass and copper and a peak whose position corresponds to an alpha brass containing approximately 36 w/o of zinc (32).

The diffraction results described above embody the only undisputed evidence for the operation of a selective leaching mechanism in dealloying. The diffraction methods are limited, however, in that they yield very little information about the distribution in the dealloyed structure of new alloy compositions.

In both investigations discussed above, the electron microprobe was employed to obtain profiles of composition across all or part of the dealloyed layers. The gold and copper profiles reported for dealloyed Cu-10 a/o Au specimens show a monotonic increase in gold concentration and a corresponding decrease in copper concentration over the

width (∿10 μm) of the dealloyed layer (30, 31). Zinc composition profiles reported for alpha and beta brass were taken only close to the interface between the bulk metal and the dezincified layer (19, 32). The widths of layers in which the zinc contents drop from 30 w/o to zero are less than 10 μm for alpha brass exposed in 1N NaCl for 7 days at room temperature and in 5N HCl for 10 days at 75°C, but about 30 μm wide for beta brass exposed in 5N HCl for 2 days at 75°C.

It should be pointed out that concentration profiles obtained by spectrographic techniques reflect only the average composition of the material in the volume of measurement. Thus, a profile obtained from a binary alloy sample having a uniform gradient of depletion in one element may be indistinguishable from a sample composed of fine particles of each of its constituents and having only a uniform gradient in the fraction of particles of each element. For this reason, such profiles by no means represent unequivocal proof of the operation of a selective leaching mechanism.

The possibility that selective dissolution might result in the formation of stable phases having compositions intermediate to the starting alloy and the more noble component has been tested in two investigations of dealloying in high zinc content brasses. Stillwell and Turnipseed (33) used X-ray diffraction to study epsilon brass (∿ Cu-80 w/o Zn) samples exposed in a series of acid solutions. They found

that in acetic acid or dilute HCl, gamma brass (∿ Cu-65 w/o Zn), beta brass, and alpha brass or copper were successively formed on the epsilon brass substrate. However, in stronger acids (HNO_3, H_2SO_4, and concentrated HCl), only copper was formed, or complete dissolution took place.

Pickering (34) has extended the analysis to epsilon (Cu-86 a/o Zn) and gamma (Cu-65 a/o Zn) brasses dissolved anodically (1 to 5 ma/cm^2) in 1N H_2SO_4 and in a series of buffered (pH = 5) solutions. He reports the formation of alpha brass on the gamma samples and alpha and gamma brass on the epsilon brass samples. In addition, the starting brass compositions were observed to shift towards higher copper contents, thus reflecting depletion of zinc.

In summation, several important conclusions can be drawn about our knowledge of the selective leaching phenomenon as it pertains to metal corrosion.

(1) The theoretical aspects of dealloying by selective leaching of the less noble component from the alloy matrix are rather well-developed, detailed models having been proposed.

(2) Undisputed experimental evidence for the occurrence of selective leaching in the Cu-Au and Cu-Zn alloy systems exists in the form of X-ray diffraction measurements of lattice parameter changes.

(3) No direct measurements of the physical scale of dealloyed layers resulting from the operation of a selective leaching mechanism exist.

(4) Consequently, little is known of the operational details of the selective leaching mechanism(s).

These conclusions clearly point out the need for a new experimental approach in analyzing leached structures. Such an approach is contemplated in Auger electron spectroscopy, a highly surface-sensitive experimental technique.

2.2. Dissolution and Replating Mechanism

In contrast to the Cu-Au alloys which undergo selective dissolution rather easily, the alloys of the Cu-Zn system normally dissolve simultaneously in aqueous environments. This observation led early investigators to conclude that the porous layers of copper remaining on brass after dezincification must certainly be the result of redeposition (at favorable sites on the brass surface) of copper which had previously passed into solution.

Pickering and Wagner (16) have analyzed the conditions for simultaneous dissolution and replating of a binary alloy for the case where no complexing reactions are possible and no solid products are formed. Consider dissolution of a binary Cu-Zn alloy by the reactions

$$Cu[Cu\text{-}Zn] \rightarrow Cu^{+n} + ne^-, \quad n = 1, 2 \qquad (1)$$

$$Zn[Cu\text{-}Zn] \rightarrow Zn^{++} + 2e^-, \qquad (2)$$

If the reactions are independent, then the single electrode

potentials for dissolution of each component are given by

$$E_{Cu[Cu\text{-}Zn]} = E^{\circ}_{Cu} + \frac{RT}{nF} \ln \frac{a_{Cu^{+n}}}{a_{Cu[Cu\text{-}Zn]}} , \qquad (1a)$$

and by

$$E_{Zn[Cu\text{-}Zn]} = E^{\circ}_{Zn} + \frac{RT}{2F} \ln \frac{a_{Zn^{+2}}}{a_{Zn[Cu\text{-}Zn]}} . \qquad (2a)$$

Subsequent redeposition of dissolved copper ions at copper-rich surface sites, by the reaction

$$Cu^{+n} + ne^{-} \rightarrow Cu[Cu \text{ sites}], \qquad (3)$$

occurs at an electrode potential given by

$$E_{Cu[Cu \text{ sites}]} = E^{\circ}_{Cu} + \frac{RT}{nF} \ln \frac{a_{Cu^{+n}}}{a_{Cu[Cu \text{ sites}]}} . \qquad (3a)$$

The activity of copper on the brass surface, $a_{Cu[Cu\text{-}Zn]}$, is less than unity. Consideration of equations (1a) and (3a) for these conditions leads to the conclusion that the single electrode potential for dissolution of copper from the brass, $E_{Cu[Cu\text{-}Zn]}$, is more noble than the potential for deposition of copper, $E_{Cu[Cu \text{ sites}]}$. Consequently, redeposition does not occur.

If, however, the copper and zinc dissolution reactions are not independent, then copper atoms may tend to remain adsorbed on the surface as the zinc dissolves. These

adsorbed copper atoms tend to aggregate on the surface. An isolated adsorbed copper atom not surrounded by other copper atoms possesses a higher activity than a copper atom which has aggregated and been surrounded by other copper atoms. Due to this activity reversal, the single electrode potential for deposition of copper at copper-rich sites, equation (3a), becomes more noble than the single electrode potential for dissolution of copper from the Cu-Zn surface, equation (1a). Under these circumstances, copper dissolving from the brass surface may be plated out on copper-rich areas on the surface.

The necessity of copper-rich sites as areas for initiation of replating is intuitively attractive. Formation of such cathodic sites has been attributed to selective leaching of zinc from zinc-rich impurities at grain boundaries (35), traces of beta brass, or compositional inhomogenieties (36, 37).

This rather simple argument has a basic flaw in that it fails to explain why dezincification of high brasses (i.e., brasses containing less than 15 w/o of zinc) has not been observed. Surely for such dilute alloys, the difference in single electrode potentials for dissolution and replating of copper, equations (1a) and (3a), respectively, is much smaller than in the case of brasses with higher zinc content, which do dezincify.

Additionally, Pickering and coworkers have shown, both through analysis of metal ion pickup in solution (20) and by a soft X-ray diffraction technique (24), that simultaneous dissolution of Cu-30 a/o Zn in acid sulfate solution is preceded by an enrichment of the brass surface in copper. Similar results were obtained by Bumbulis and Graydon (38) for dissolution of a Cu-15 w/o Zn alloy. In each of these cases, no tendency towards further dezincification by redeposition of copper was observed. Thus the existence of copper-rich sites on a dissolving brass surface does not necessarily represent a sufficient condition for the occurrence of copper redeposition.

The situation discussed above is critically altered if the concentration of dissolved copper ions adjacent to a portion of the surface is increased above the equilibrium value corresponding to the average surface potential. Then, $E_{Cu[Cu\ sites]}$ may become larger than $E_{Cu[Cu-Zn]}$, and deposition of copper will occur. In connection with dealloying failures in service, copper concentrations higher than the equilibrium concentrations have been attributed to: (1) stagnant conditions (15); (2) decreased flow rates (19, 36); (3) porous surface films or deposits (39, 40); and (4) crevices or pits (41-43). It should be noted that the porous copper deposits resulting from dezincification produce stagnant conditions in the solutions adjacent to the corroding

brass surfaces beneath. Deposits of copper (27, 44, 45) and of nickel (46) have been employed to initiate dezincification on brasses.

The traditional, extensive use of brasses in saline environments has made the effects of chloride ions in promoting dezincification well known. Several early investigators recognized the importance of the complex salts of copper and chlorine which are commonly observed on dezincification failures.

Bengough, Jones, and Pirret (2) observed that brass immersed in aerated sodium chloride solution becomes covered by a film of sparingly soluble cuprous chloride

$$Cu[Cu\text{-}Zn] + Cl^- \rightarrow CuCl + e^- \qquad (4)$$

which eventually is oxidized to cuprite and cupric chloride by the reaction

$$4CuCl + \tfrac{1}{2}O_2 \rightarrow Cu_2O + 2CuCl_2 . \qquad (5)$$

The authors hypothesized that the cupric chloride formed by this reaction attacks the brass according to the reactions

$$CuCl_2 + Cu \rightarrow 2CuCl \qquad (6a)$$

and

$$CuCl_2 + Zn \rightarrow ZnCl_2 + 2Cu. \qquad (6b)$$

Of these reaction products, copper is deposited at the brass surface, soluble $ZnCl_2$ passes into solution, and sparingly soluble CuCl is available to continue the reaction cycle.

Abrams (39) demonstrated in a classic series of experiments the ability of cuprous chloride reaction product membranes — as well as artificial membranes — to produce dezincification. He was also able to show that conditions which retard the formation of dense CuCl films, e.g., low pH and agitation, also retard preferential dissolution.

More recently, Lucey (27) noted the physical similarities between pits in copper and dezincified areas in brasses formed in chloride containing environments. He reasoned that most of the copper dissolved from a pit is precipitated in the pit as cuprous chloride, some of which is subsequently oxidized to cuprite. A more detailed discussion of pit formation and morphology has been presented by Van Muylder et al. (47). In the case of dezincification, however, the cuprous chloride formed through dissolution of the brass is reduced to copper. Further, beta brass is capable of direct cathodic reduction of cuprous ions. Alpha brass, having a much higher electrode potential, can reduce only cupric ions, which are formed by disproportionation of cuprous chloride

$$2CuCl \rightleftarrows Cu + CuCl_2 . \qquad (7)$$

Therefore, according to this reasoning, dezincification of alpha brass is dependent upon the formation of cupric ions. Unfortunately, Lucey's rather low experimental value for the potential of a film-free alpha brass surface is unsubstantiated, making the validity of this mechanism questionable.

Heidersbach and Verink (18, 19) have also recognized the importance of the copper-cuprous chloride reaction in producing dealloying in copper alloys. They observed the deposition of copper on Cu30Zn and Cu10Ni samples polarized below a certain critical electrode potential during cyclic polarization in acid 0.1M chloride solutions. This critical potential, +0.200 V_{SHE}, also observed by Efird (48), corresponds closely to the equilibrium potential of the copper-cuprous chloride reaction

$$Cu + Cl^- \rightarrow CuCl + e^- \quad . \qquad (8)$$

On this basis, the authors have predicted the conditions of electrode potential for which copper alloys having polarization behavior similar to that of pure copper may undergo dealloying by a dissolution and replating mechanism in neutral and acid chloride environments. Referring to figure 1, Cu30Zn undergoes simultaneous dissolution at electrode potentials more noble than its corrosion potential, the area of large dots. However, at potentials less noble than this critical potential, cuprous chloride formed on the brass surface as a result of dissolution may be reduced to copper.

Thus, in the potential range bounded by the corrosion potential of the brass and the critical potential, the area of crosshatching, dealloying by dissolution and replating may take place.

Substantiation of this prediction was undertaken by potentiostating alpha and beta brass samples in deaerated 0.1M chloride solutions of pH 4 at several potentials in the predicted potential range. All beta brass samples were dezincified after a few days' exposure. The alpha brass samples dezincified only if their solutions were unstirred or after several weeks in stirred solutions. This result is consistent with earlier observations of agitation on the formation of adherent cuprous chloride layers (39). Essentially identical potential dependence has been reported by Marshakov and Bogdanov (49) for dealloying of several alpha, beta, and duplex brasses polarized anodically in 0.5M NaCl solutions. Comparable results have been obtained by Robinson and Shalit (50) and by Sugawara and Ebiko (51) for similar series of brasses potentiostated in 3½% NaCl solutions.

Additionally, Heidersbach and Verink exposed alpha and beta brass samples in solutions known to produce dezincification. The steady state electrode potentials were measured, and in each case were found to fall within the predicted potential range for dealloying.

The uncertainties involved in specifying electrode potentials required to produce, or to inhibit, dealloying have been pointed out by several investigators (19, 21, 48, 51). Potential drops due to anodic films, dealloyed layers, and crevices can alter the electrode potential at the attack interface. For example, as dealloying attack proceeds, the formation of a thick, porous residual metal sponge over the sample surface changes significantly the conditions adjacent to the dissolving alloy surface. This process is in many ways analogous to the development of pitting or crevice attack (52). By the same token, as the initiation and the propagation stages of pitting attack can be treated as separate processes (53), so ought the initiation and propagation stages of dealloying attack. A case in point is the initiation of dezincification in brass by deposition of copper onto the brass surface. Early investigators (54) referred to such a deposit as "apparent dezincification." The resulting dezincification which occurs beneath the deposit is true dezincification, and the conditions which sustain the attack are very probably quite different from those initiating it. The determination of conditions at the dealloying attack interface is the prerequisite necessary for understanding how the attack proceeds and, ultimately, how to stop it. Unfortunately, heretofore very little work has been directed towards this area of investigation.

2.3. The Role of Arsenic as an Inhibitor of Dezincification

Extensive research early in this century concerning the interplay of compositional variables and dezincification of brass condenser tubes resulted in the discovery of arsenic's inhibitive properties (2). Since that time, the addition of 0.02 to 0.04 w/o of arsenic to alpha brasses has become the standard means of preventing their dezincification (3). Research into the cause(s) of the effect, however, has proceeded haltingly, and no concensus has been reached concerning the identity of the mechanism(s) involved. The several theories which have been proposed to explain the effect can be loosely classified into two groups:

(1) Arsenic acts as an anodic inhibitor, interfering with dissolution of the brass or its zinc component; and

(2) Arsenic acts as a cathodic inhibitor, interfering with copper deposition.

Fink (36) first proposed the former mechanism, stating that arsenic dissolved from the brass combined with copper to form copper arsenide films over the most "active" or zinc-rich points on the brass surface. The protective action of the arsenic films prevented any subsequent enrichment in copper of the active spots by dealloying, thereby eliminating potential sites for deposition of copper from solution. The small amount of arsenic found in commercial brasses precludes the formation of a continuous arsenical film over the entire

surface (12, 55), hence, arsenic affects only dezincification attack, and has little influence on general dissolution rates.

More recently, West (56) has proposed that the effect of arsenic under certain conditions of pH may be to render the brass surface passive. According to this theory, arsenic in solution is stable as arsenite, $As(OH)_4^-$, under the local slightly alkaline conditions present during oxygen reduction. These arsenite ions readily adsorb onto the positively charged metal surface, forming strong bonds with the copper atoms, and particularly with the zinc atoms, at the surface. The effect of this bonding is to stabilize the surface by rendering the surface atoms in an essentially passive state. West points out, however, that in the acid environments expected within pits, some other mechanism must be operative. Under these conditions the arsenyl ion, AsO^+, is the stable dissolved arsenic species. This ion would possess little tendency to adsorb onto a positively charged metal surface.

The theory that arsenic prevents redeposition of copper at the brass surface has been proposed in many forms over the years. Masing (57) found that the overpotential for hydrogen reduction on brass surfaces was less in solutions containing dissolved arsenic than in arsenic-free solutions. On the basis of his observation he proposed that for arsenical brasses undergoing corrosion, the cathodic

copper reduction reaction was replaced by the hydrogen reduction reaction, hence, no dezincification (i.e., no copper redeposition) occurred. More recent polarization data reported by Sugawara and Shimodaira (58) point out a possible flaw in Masing's experiments. They found that anodic and cathodic polarization of copper and copper-zinc alloys is influenced by additions of sodium arsenite to the test solution (3% NaCl). However, arsenical brasses exposed in solutions without arsenic additions exhibited polarization data identical to those of the non-arsenical brasses. The disagreement between the two works is by no means conclusive. The detection of the influences of trace element additions to alloys by electrochemical polarization curves can be insensitive to very subtle effects (59). Nevertheless, similar indications that the source of arsenic, whether from the alloy or from the bulk solution, influences its inhibitive effects have been reported by other investigators (27, 60, 61).

Hollomon and Wulff (60) have presented the only experimental data concerning the identity of the black or gray films normally found on the surfaces of corroded arsenical brasses. Their film-structure experiments consisted of immersing samples of copper and Cu30Zn containing up to about 0.5 w/o of arsenic in 2N and 5N nitric acid and in 2N and 5N hydrochloric acid, followed by examination of the corroded surfaces by electron diffraction. Arsenious oxide,

As_2O_3, films were observed to form on arsenical copper and Cu30Zn in all solutions tested. Significantly, elemental copper was also found on the Cu30Zn samples. These results were interpreted in terms of a dissolution and replating mechanism. As the brass dissolves, redeposition of copper and, later, of arsenic takes place. The arsenic deposits are subsequently oxidized to arsenious oxide.

The detection of copper on the arsenical brass surfaces in this investigation has significant implications, namely: either arsenic additions have limited effects in inhibiting redeposition of copper on Cu30Zn (contrary to experience); or dezincification of brass by a selective leaching mechanism may proceed even when arsenic is present.

Hollomon and Wulff later extended their investigations, exposing arsenical and non-arsenical Cu30Zn samples in a series of environments designed to produce dissolution of the copper component of the brass to either cuprous or to cupric ions. They concluded that non-arsenical alpha brass undergoes simultaneous dissolution and that dezincification occurs by the reduction of cuprous ions to copper on the brass surface. In the case of arsenical brass, the arsenic dissolved from the alloy is subsequently deposited on the brass surface. The arsenical film thus formed increases the effective electrode potential of the brass surface such that reduction of cuprous ions to copper is impossible.

Lucey (27) has also stated that arsenic interferes with the copper deposition step of dezincification. According to this author's mechanism, copper deposition at the advancing corrosion interface proceeds by the disproportionation of cuprous ions to form cupric ions and copper,

$$2Cu^{+} \rightarrow Cu^{++} + Cu. \qquad (9)$$

When arsenic is present at the interface, the disproportionation reaction is suppressed by the following pair of reactions:

$$3Cu^{+2} + As \rightarrow 3Cu^{+} + As^{+3} \qquad (10)$$

$$3Cu + As^{+3} \rightarrow 3Cu^{+} + As\ . \qquad (10a)$$

A noteworthy feature of this mechanism is that the arsenic is recycled between the As^{+3} and metallic states. Consequently, only a very small amount of arsenic is required for protection. This is consistent with the fact that only traces of arsenic are required to protect alpha brasses against dezincification.

In summary, it can be said that the mechanisms proposed to explain arsenic's role in the inhibition of dezincification have been influenced by the investigators' choices for the detailed dezincification mechanism. Thus, it is clear that complete clarification of the inhibition phenomenon awaits final determination of the mechanism(s) of dezincification.

CHAPTER 3

EXPERIMENTAL PROCEDURE

Characterization of the metals used in this investigation and the details of sample preparation are discussed in Appendix 1. Details of solution compositions and preparation are given in Appendix 2. The standard polarization cell as used in potentiokinetic testing, and its modification for subsequent tests, are described in Appendix 3. A list of the equipment used in these investigations is given in Appendix 4.

3.1. Potentiokinetic Polarization Experiments

Potentiokinetic polarization tests on copper, zinc, and Cu30Zn were conducted in the standard polarization cell, described in Appendix 3. Details of the potentiokinetic technique and theory have been presented elsewhere (62, 63). A schematic of the experimental set-up is presented in figure 3.

Each test was conducted in a fresh solution of about 500 ml volume. Samples were introduced into the cell only after the solution was thoroughly purged with nitrogen.

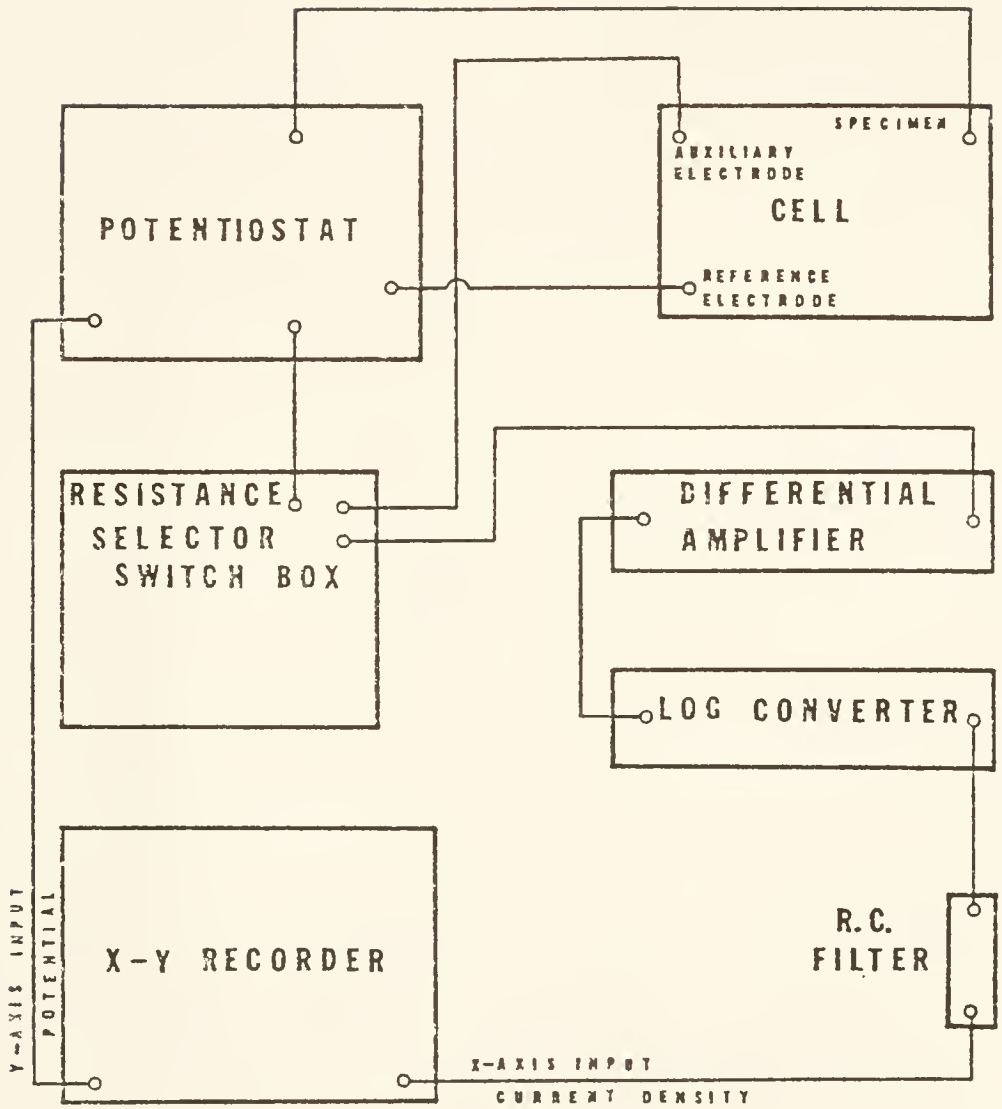

Figure 3. Schematic of the equipment set-up for generation of potentiokinetic polarization curves.

Equilibration of the sample corrosion potential was monitored with an electrometer. Zinc samples achieved stable potentials within a few minutes. Copper and Cu30Zn samples, however, were sluggish, exhibiting changes in potential after several hours. It was soon discovered that a prepolarization treatment, consisting of a 5-minute cathodic polarization to -1.000 V_{SCE}, resulted in much faster attainment of steady corrosion potentials. A sample was considered to have achieved a steady corrosion potential when its potential changed less than about 30 mV in 30 minutes.

Polarization curves were obtained by scanning the sample's electrode potential from low cathodic overpotentials to the appropriate anodic overpotential, both in the forward (i.e, active-to-noble potential) and in the reverse (noble-to-active) directions. The curves were plotted on potential versus log current coordinates on an X-Y recorder. The effect of scan rate on the polarization curves was investigated for copper by comparing curves obtained at scan rates varying from 10 to 70 mV/min with step scans made in steps of 50 mV every 5 min (64). As a result of these comparisons, 1 V/hour (16.67 mV/min) was chosen as the optimum scan rate consistent with reproducible characteristic potential features on the polarization curves.

3.2. Selective Leaching Experiments

Potentiostatic selective leaching experiments were carried out in the modified standard polarization cell, as described in Appendix 3. All experiments were on polished Cu30Zn samples immersed in 0.1M chloride solutions of pH = 4.0±0.1. Cells containing 500 ml of solution were brought up to temperature and purged with purified nitrogen for 12 hours prior to introduction of the samples. The potentiostat was switched on simultaneously with the introduction of the sample.

Cell temperature was monitored throughout the tests. A constant temperature bath was employed to maintain cell temperature at 89±½°C throughout the tests. Cell potential and cell current were noted frequently.

Solution aliquots of 25 ml volume were pipetted from each of the 89°C cells before introduction of the sample and at approximately 24-hour intervals during the test. The solution drawn off was replaced with 25 ml aliquots of fresh, nitrogen saturated solution. Solution samples were submitted to atomic absorption spectrophometric analysis for dissolved copper and zinc. Details of the analytical procedure have been presented elsewhere (32). The experimental limits of detection were 0.10 ppm for copper and 0.05 ppm for zinc.

At the conclusion of each test, the potentiostat was switched off as the sample was removed from the cell. Each

sample was rinsed in a stream of distilled and deionized water and dried with a blast of compressed dusting gas. The sample connecting wire was ripped away, and the stop-off lacquer was peeled off. Each sample was inspected scrupulously for evidence of leaks in the stop-off lacquer. These were usually easily recognized as patches of deposited copper on the sides or back of the sample. Any indication of leaks was cause for rejection of the experiment.

The exposed (projected) surface area of each sample was measured by direct comparison with a celluloid sheet inscribed with a 15 mm x 15 mm grid. The accuracy of these measurements was about ± 0.005 cm^2. Most samples were carefully sectioned with a jeweler's saw across a diameter. Half of the sample was submitted to Auger analysis; the other half examined by scanning electron microscopy (SEM).

Solution pH was checked before and after each experiment, and was found in every case not to have changed. Final solution volume was measured in order to correct atomic absorption data for evaporation losses.

3.3. Controlled Anodic Dissolution Experiments

Potentiostatic anodic dissolution experiments were conducted in the standard polarization cell, modified as described in Appendix 3. Experiments were carried out on Cu30Zn and Arsenical Cu30Zn specimens in pH 4, 0.1M chloride solutions of 600 ml volume. Cell temperature was maintained

by a constant temperature bath at 30±1°C. Details of cell operation are as described for the selective leaching experiments, section 3.2.

At the conclusion of tests, samples were sectioned across diameters. One half was mounted and polished for metallographic examination; the other half was examined by SEM. Analysis of solution samples was accomplished through atomic absorption analysis. The experimental lower limit of detection for arsenic was 0.01 ppm.

3.4. Artificial Occluded Cell Experiments

The artificial occluded cell was designed to simulate the restricted flow and electrochemical conditions adjacent to the internal dissolving brass surface of a partially dezincified sample.

The electrode assembly, detailed in figure 4, consisted of a Cu30Zn sample positioned horizontally to, and shielded from the bulk solution by, a porous copper screen. The sample holder was constructed from three pieces of 0.0625 inch thick polycarbonate sheet, bonded together with epoxy. A length of 0.7 mm inside diameter "spaghetti" tube, inserted through a slot cut in the middle sheet, connected the 1 cm^2 hole between the Cu30Zn and the copper screen with the top of the assembly. The entire sample assembly was inserted in a slot in the rubber stopper. The end of the

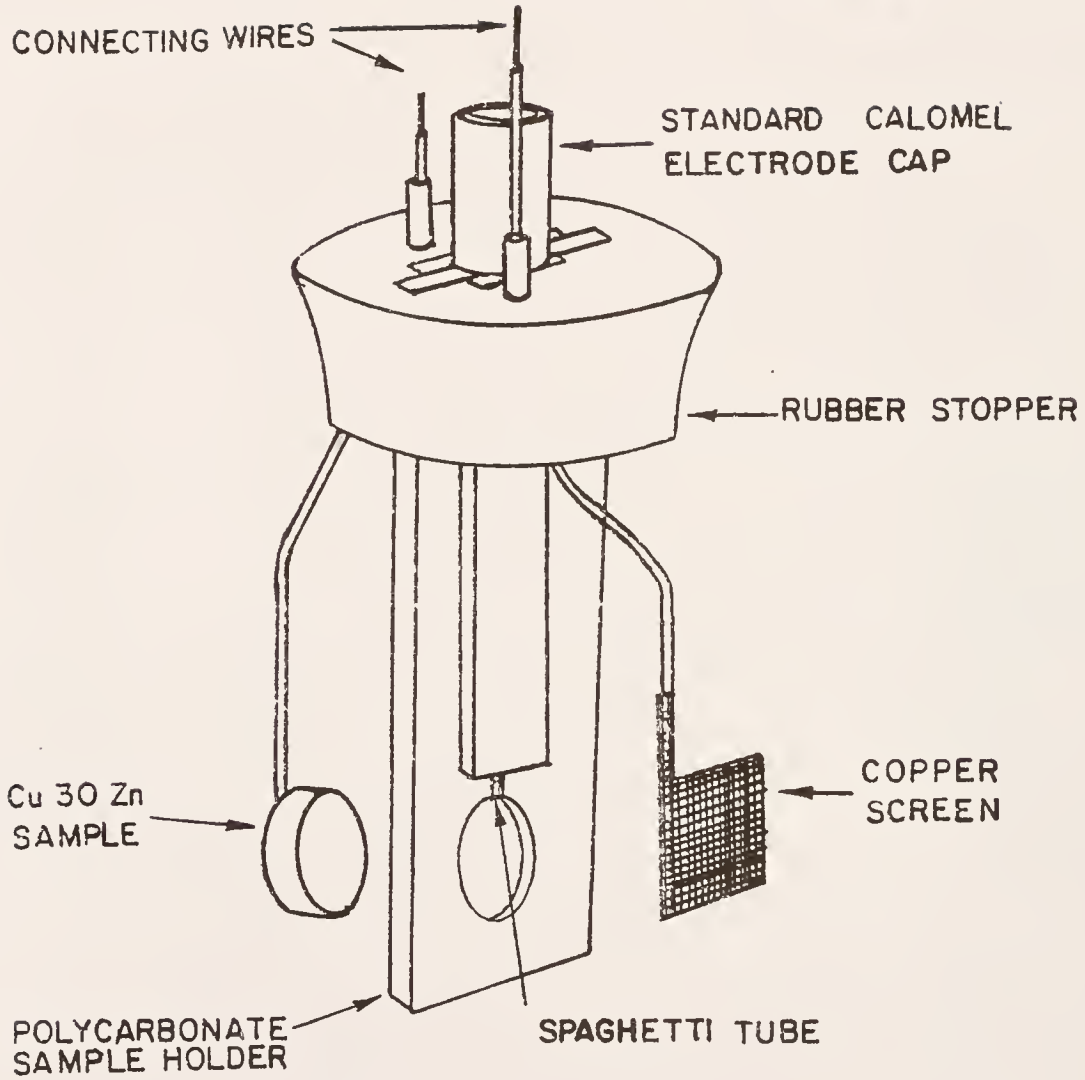

Figure 4. Artificial occluded cell electrode assembly.

spaghetti tube was inserted into the bottom of a standard calomel electrode storage cap, which was bonded to the top of the assembly.

The copper screen was fabricated from a 18 mm x 18 mm, number 100 mesh bronze, copper-plated in a saturated $CuSO_4$ bath to a total thickness of about 0.6 mm. The platinum auxilliary electrode, Haber-Luggin probe, gas disperser, and gas outlet, all similar to those used on the standard polarization cell, were inserted through holes in the rubber stopper to complete the assembly. The cell container consisted of a glass jar. A saturated calomel reference electrode, SCE 2, was connected to the Haber-Luggin probe through a salt bridge of the test solution.

Before each experiment, a fresh Cu30Zn specimen and copper screen were carefully attached to opposite sides of the 1 cm^2 hole with a quantity of Miccroflex stop-off lacquer. The connecting wires were fed through glass tubes set in the stopper. The volume of the occluded cell cavity between the two electrodes was approximately 0.154 ml.

All experiments were conducted potentiostatically at room temperature in approximately 300 ml of stirred, nitrogen-saturated, 0.1M chloride solutions of pH = 4. The assembled cell was purged with nitrogen prior to introduction of the solution and during the test. A saturated calomel electrode, SCE 1, was inserted into the electrode cap at the top of the cell. The occluded cell cavity, spaghetti tube, and electrode

cap were then filled by drawing solution up from the cell with a hypodermic syringe and needle inserted through the side of the electrode cap.

The Cu30Zn sample and copper screen were connected through a zero-resistance ammeter (53). The electrode assembly was connected to the working electrode terminal of the potentiostat. The bulk cell potential, E_B, was monitored by an electrometer connected between the working electrode assembly and SCE 2. The occuded cell potential, E_C, was similarly monitored by a second electrometer connected between the working electrode assembly and SCE 2. The occluded cell current, i_c, passing between the Cu30Zn sample and the copper screen was measured by the zero-resistance ammeter. A schematic diagram of the electrical circuit is given in figure 5. When the potentiostat was switched on, the occluded cell current and occluded cell potential were recorded on identical strip-chart recorders.

3.5. Auger Electron Spectroscopic Analyses

Auger electron spectroscopy (AES), coupled with argon sputtering, was employed to determine the thickness of the dezincified layers formed on the Cu30Zn samples subjected to selective leaching as described in section 3.2. The theory of AES analysis and of the argon sputtering process is discussed in detail in Appendix 5.

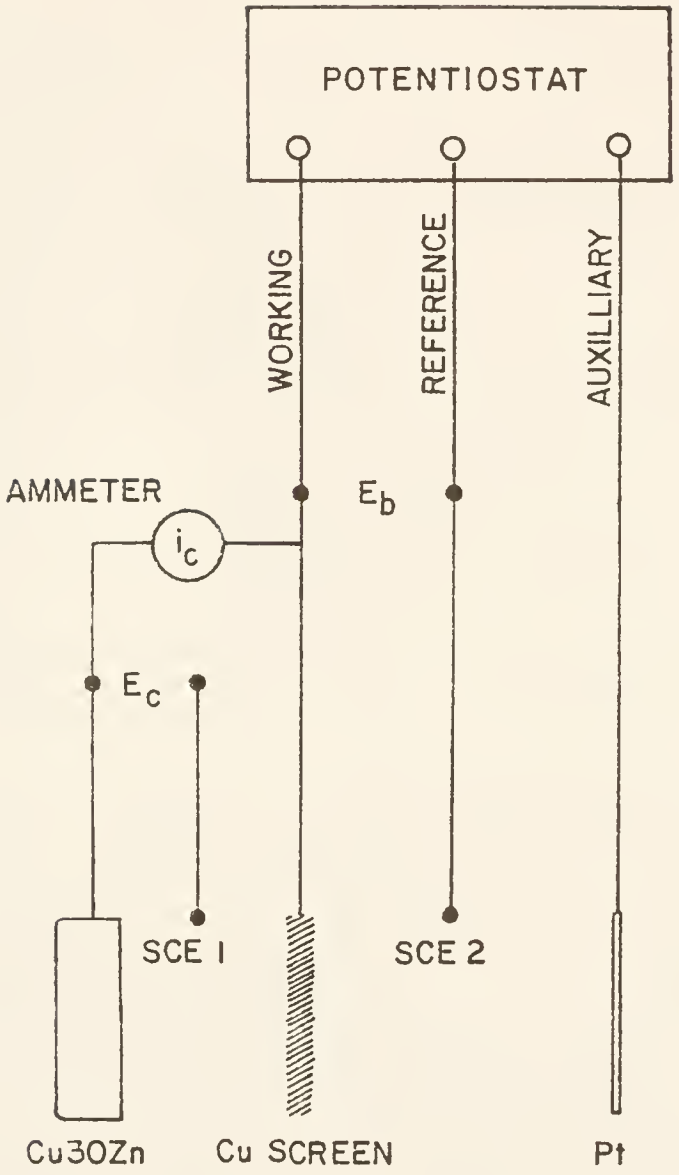

Figure 5. Schematic of the electrical circuit for the artificial occluded cell experiments.

The AES system in the Department of Materials Science and Engineering of the University of Florida is employed routinely in the determination of glass surface compositions and in the measurement of near-surface compositional profiles of metals, glasses, and composites. The system consists of a high vacuum chamber and accompanying pumping systems, an electron gun, a cylindrical-mirror energy analyzer, a sputter-ion gun, and accompanying control and data treatment and acquisition systems. A schematic diagram of the AES system is presented in figure 6.

As many as six samples were attached (by copper clips) to the externally manipulated carrousel sample holder. The vacuum chamber was evacuated to a base pressure no higher than 5×10^{-8} atm. Auger surface composition measurements were made with the electron gun operating at 3 keV. The electron beam diameter was about 0.5 mm, and the beam current about 25 μa. The angle of incidence was about 45 degrees from normals to the sample surface. Energies from zero to 1800 eV were normally scanned, however, only the portions of interest were scanned as generation of the composition profiles proceeded. A typical spectrum obtained from the surface of a Cu30Zn sample is shown in figure 7.

Composition profiles were obtained by successive removal of layers of metal by argon sputtering and recording the Auger spectra of freshly exposed surfaces. Argon was leaked into the evacuated chamber until a pressure of

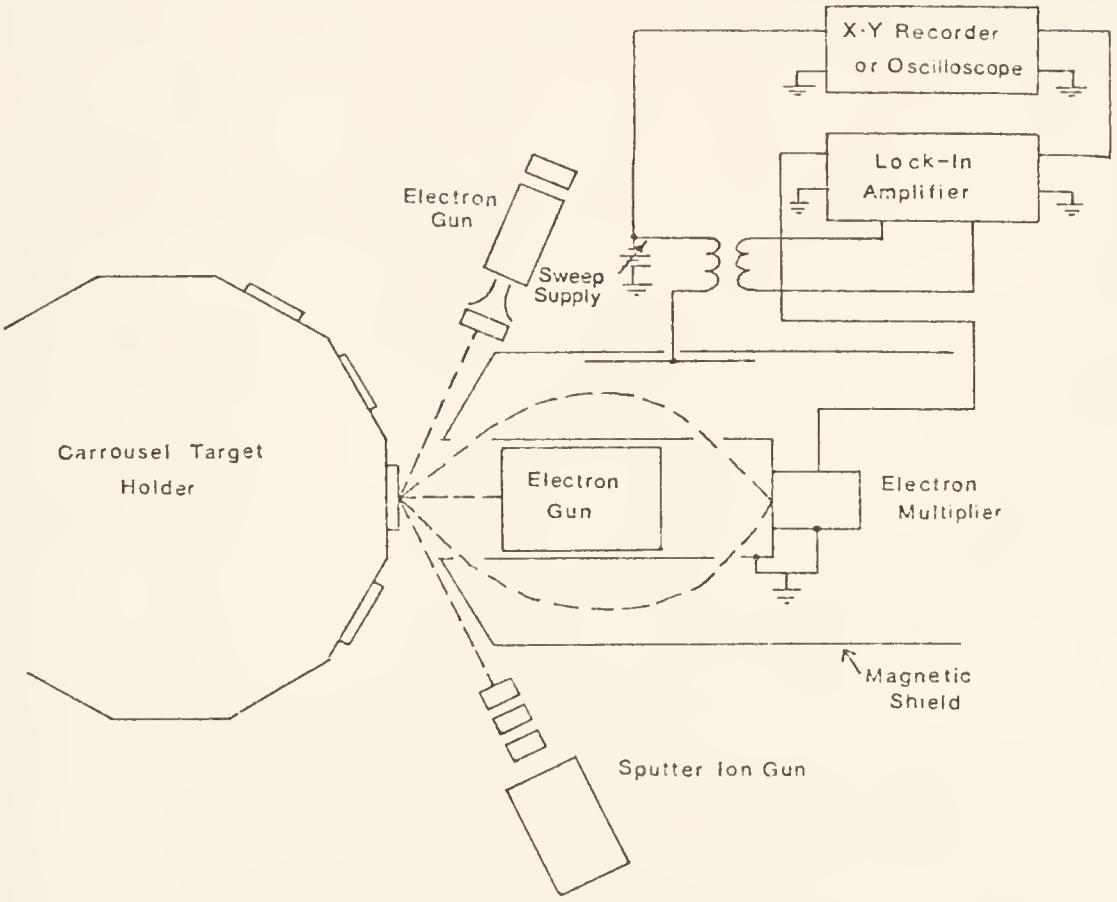

Figure 6. Schematic of the AES system used to analyze selective leaching samples.

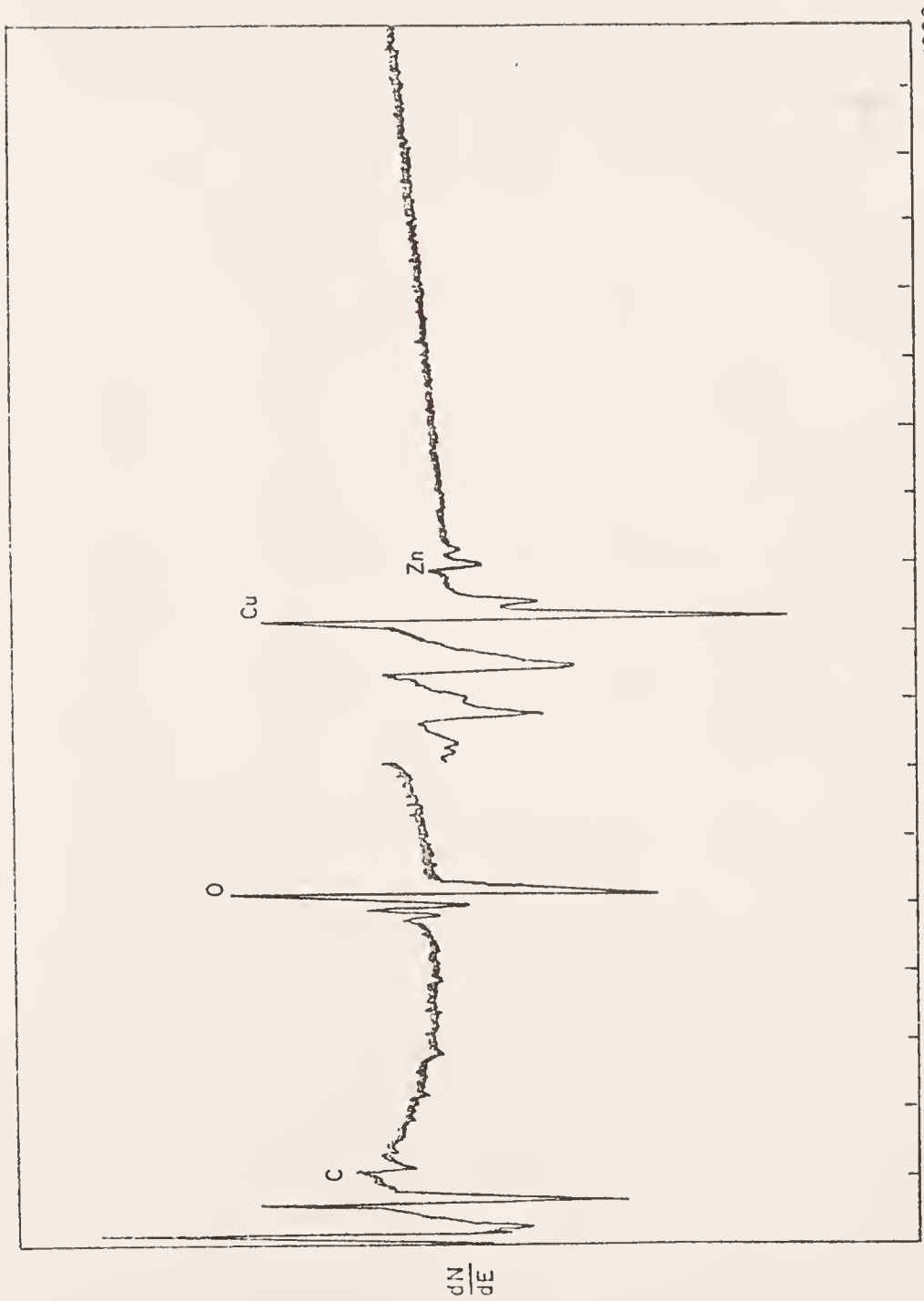

Figure 7. Typical Auger spectrum from the surface of a Cu30Zn sample.

$5\text{-}6\text{x}10^{-5}$ atm was reached. The sputter-ion gun was then switched on and the Argon sputtering begun. The area of the surface affected by the sputtering was about 5 mm in diameter. The electron gun and the sputter ion gun were aligned so that the incident electron beam was concentric with the sputtering crater. The sputter-ion gun was switched off while the Auger spectra were measured. The peak-to-peak heights measured for each element of interest were plotted as a function of sputtering time to produce the composition profiles.

Calibration of the Auger peak-to-peak heights with absolute concentrations was not attempted in this investigation. The primary reason for this was the uncertainty in measurement introduced by the argon sputtering process. In particular, the effects of differential sputtering rates of copper and zinc from the brass surface on the measured peak-to-peak heights are unknown. Also, smearing or averaging of the surface due to sputtering is likely. Secondly, the introduction of excess vacancies or porosity into the near surface layers of brass samples by the selective leaching process could lead to false results. Consequently, the ratio of the peak-to-peak heights for copper and zinc (Cu/Zn ratio) was introduced as a qualitative indicator of the level of selective leaching determined at each depth from the sample surface.

An indication of the peak-to-peak ratios to be expected from surface layers leached of part of their zinc contents can be seen in figure 8. The data points on this plot represent the Cu/Zn ratios measured from binary copper-zinc alloys having 90, 85, 80, and 70 w/o of copper. Two important points are to be noted from the curve.

(1) The Cu/Zn ratio measured for the Cu30Zn alloy has a value of about 5.

(2) A small change in alloy composition away from 30 w/o of zinc towards pure copper is accompanied by a significant increase in the measured Cu/Zn ratio.

Referring to figure 9, the composition profile recorded for the Cu-15 w/o Zn alloy, one can see that a steady Cu/Zn ratio is reached after about four minutes of sputtering. The initial period of sputtering, before the ratio becomes constant, corresponds to a "cleaning" of the surface of adsorbed gases, fingerprints, etc. which are the inevitable results of handling samples outside the vacuum chamber. This "steady state" Cu/Zn ratio reflects any effects which may be present due to differential sputtering rates.

Calibration of the argon sputtering rate was undertaken in order to assign numerical values to the depth axes of the composition profiles obtained from selectively leached Cu30Zn samples. Details of the calibration procedure are given in Appendix 6.

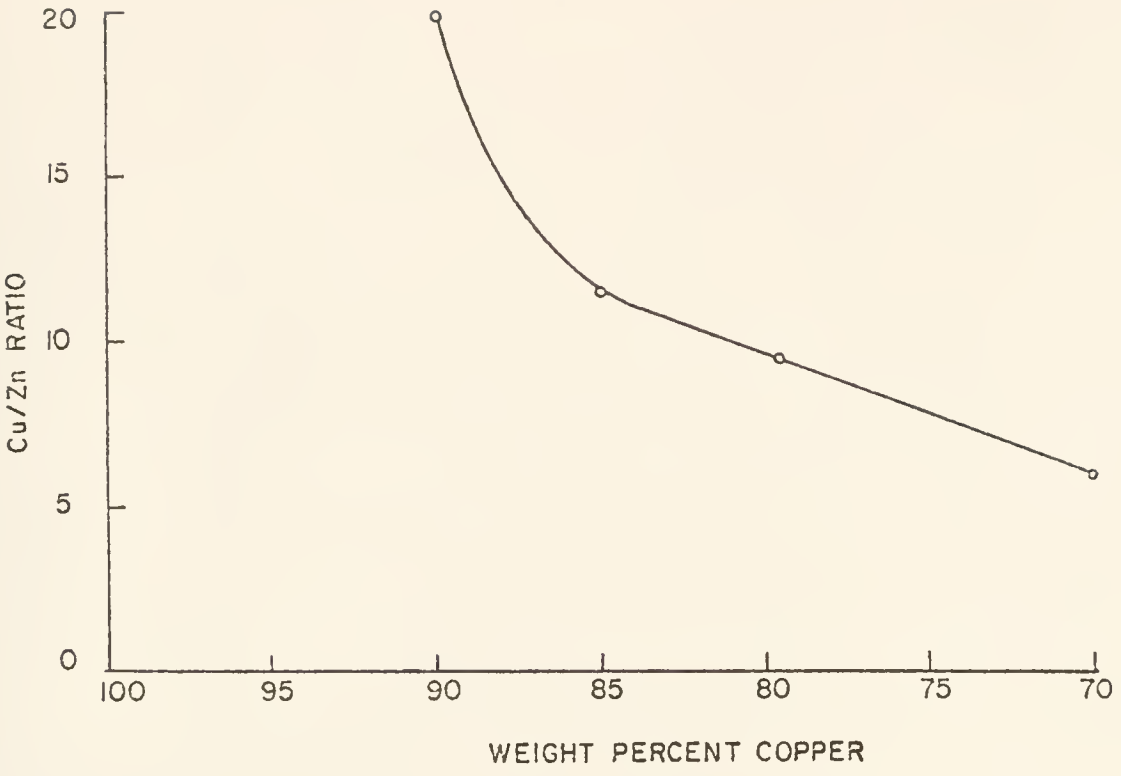

Figure 8. Effect of the composition of Cu-Zn alloys on the Cu/Zn ratio obtained by AES analysis.

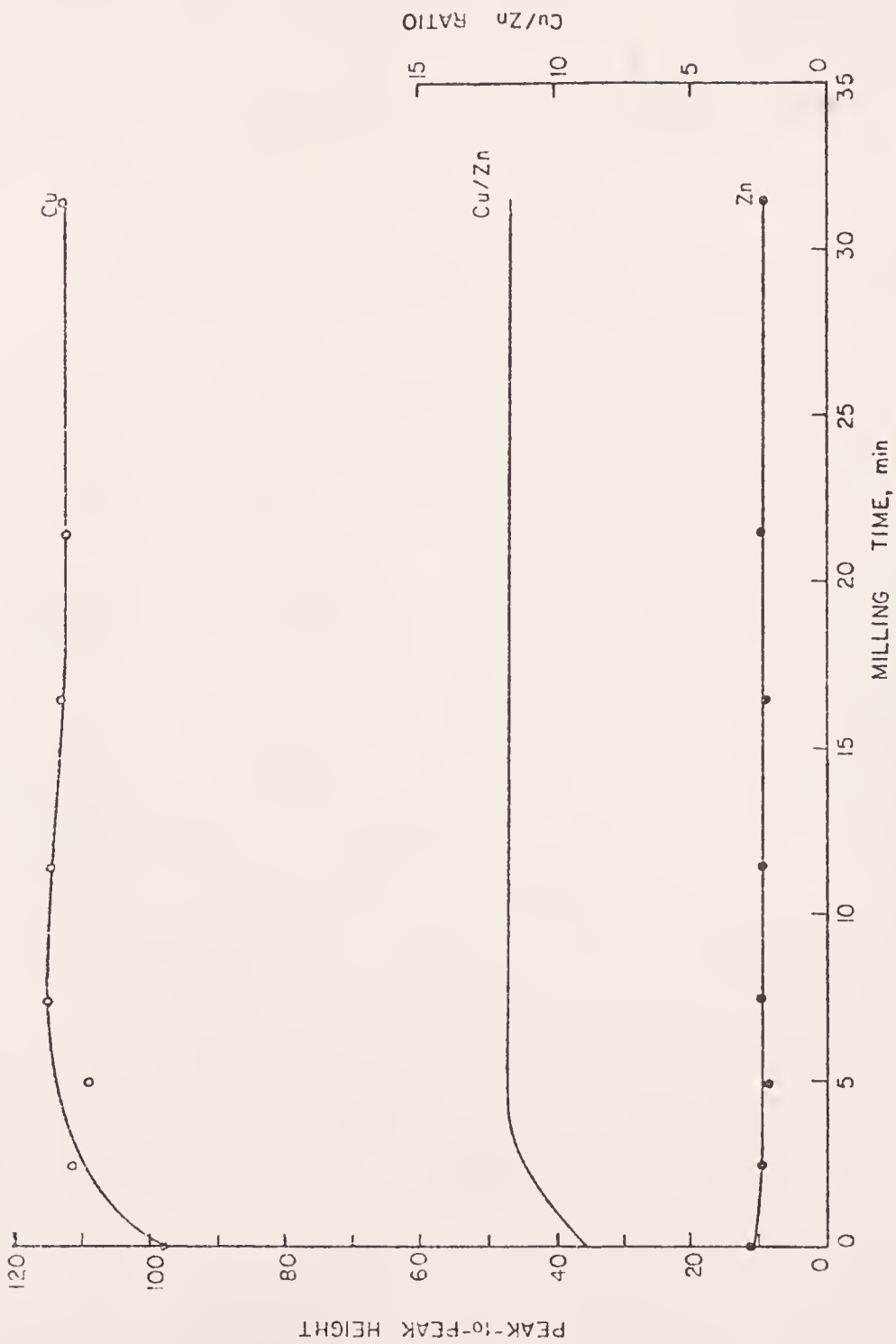

Figure 9. Auger composition profile obtained for Cu-15 w/o alloy.

3.6. X-Ray Identification of Corrosion Products

Solid corrosion products were examined by the X-ray powder diffraction method (65). Standard Debye-Scherrer powder cameras of 57.3 mm of 114.6 mm diameter were employed. Nickel-filtered copper radiation or manganese-filtered iron radiation was used in all cases. Product identification was made by the comparison of d-spacings derived from the X-ray films with those listed in the ASTM Powder Diffraction Files.

Identification of some complex hydroxy-chlorides of copper was simplified considerably by reference to the d-spacings published for these compounds by Feitknecht and Maget (66).

CHAPTER 4

RESULTS AND DISCUSSION

4.1. Electrochemical Characterization of Copper, Zinc, and Cu30Zn

Electrochemical characterization of copper, zinc, and the Cu30Zn alloy in deaerated 0.1M chloride solutions was undertaken in order to establish a firm basis for predicting the experimental conditions which lead to dealloying behavior in the system. Further, the effects of these experimental conditions on the choice of dealloying mechanisms were explored.

Potentiokinetic polarization experiments described in section 3.1., were employed throughout this phase of the investigation. Wherever possible, experimental polarization results were compared with calculated equilibria. Identification of corrosion products was accomplished through X-ray powder diffraction experiments.

4.1.1. Polarization of Copper in 0.1M Chloride Solutions

Cyclic polarization curves were generated for pure copper samples immersed in a series of room temperature

(25±3°C), nitrogen-saturated, 0.1M chloride solutions having pH values between 1 and 13. The characteristic features of the polarization curves are summarized in figure 10 as an experimental potential versus pH diagram, after the method of Pourbaix (67). The general regions of immunity, passivity, and corrosion are so marked. A similar diagram has been published (59).

The diagram can be divided into two parts according to the change in the corrosion behavior of the system from general corrosion to active-passive at pH 8. In solutions of pH between 3 and 8, copper exhibited pH-independent polarization behavior. Its corrosion potential was about -0.260 V_{SCE} in this pH range. General corrosion behavior was noted at more noble (higher) potentials. A maximum in anodic current density ($\sim$ 5 ma/cm^2) occurred at about 0.060 V_{SCE}. The formation of a film of white cuprous chloride, CuCl, on the sample surface preceded the current maximum (68, 69). At electrode potentials more noble than about 0.100 V_{SCE}, increases in corrosion current with potential were again noted. If the polarization scan was reversed at this point, the current fell with decreasing electrode potential until the protection potential* (-0.060 V_{SCE}) was reached, whereupon the current changed polarity to cathodic. As the potential was decreased

---

*Strictly speaking, the protection potential has no significance under active corrosion conditions.

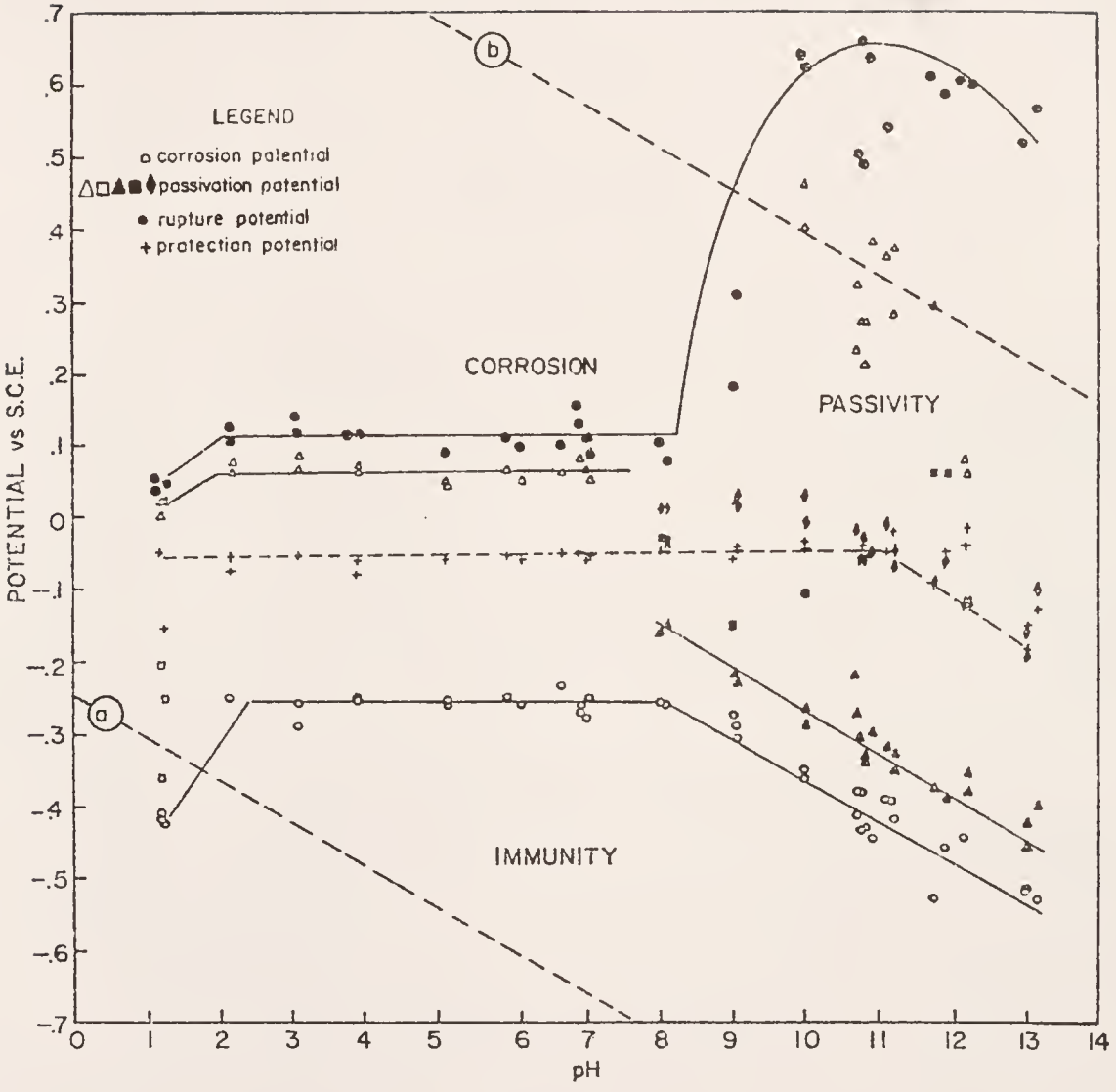

Figure 10. Experimental potential versus pH diagram for pure copper in nitrogen saturated, 0.1M chloride solutions.

further, the CuCl on the copper surface was reduced to copper.

In solutions of pH > 8, copper exhibited pH-dependent corrosion potentials and active-passive polarization behavior (70). When polarized anodically, the copper became covered by a tarnish film, identified (by X-ray diffraction) as Cu_2O, and the current density began to decrease at potentials about 90 mV above the corrosion potential. One or more current maximum features was observed as the electrode potential was subsequently increased. Such maxima are labelled in figure 10 as passivation potentials. Breakdown of passivity occurred when the rupture potential was exceeded. Initial breakdown of the passive film occurred at small, apparently random, spots on the surface. The spots quickly became covered with voluminous corrosion products identified variously as different forms of copper-hydroxy-chloride combined with CuCl. The action of stirring sometimes dislodged the products, causing them to smear over the sample face. This action resulted in the breakdown of passivity on the copper surface beneath the product. The likely mechanism involved is acidification of the solution held between the hydroxy-chloride corrosion product and the passive metal surface resulting from copper dissolution,

$$Cu + 2H_2O \rightarrow Cu(OH)_2 + 2H^+ + 2e^- . \qquad (11a)$$

The resulting pH decrease, in turn promotes dissolution of the Cu_2O passive film,

$$Cu_2O + 2H^+ + 4Cl^- \rightarrow 2CuCl_2 + H_2O + 2e^- . \quad (11b)$$

In figure 11, the polarization data for copper in 0.1M chloride solutions are superimposed over the equilibrium potential versus pH diagram calculated for the Cu-0.1M Cl^- - H_2O system at 25°C. Similar calculations have been presented elsewhere (18, 71). A list of the free energy data employed in these and later equilibrium calculations can be found in Appendix 7. Excellent agreement is noted between the experimentally measured corrosion potentials and the calculated lines corresponding to the equilibrium between copper and the $CuCl_2^-$ ion (ion activity = 10^{-6}) and between copper and cuprite, Cu_2O. The measured value of the protection potential coincides well with the calculated equilibrium between copper and cuprous chloride. The locus of the rupture potentials for solutions of pH < 9 indicates that the current increases observed at more noble potentials are due to oxidation of cuprous ions at the sample surface to cupric ions (69).

It is significant that the protection potential has the same value in both acid and alkaline solutions up to pH 11. This indicates that the Cu-CuCl equilibrium is established under localized corrosion conditions (47). The

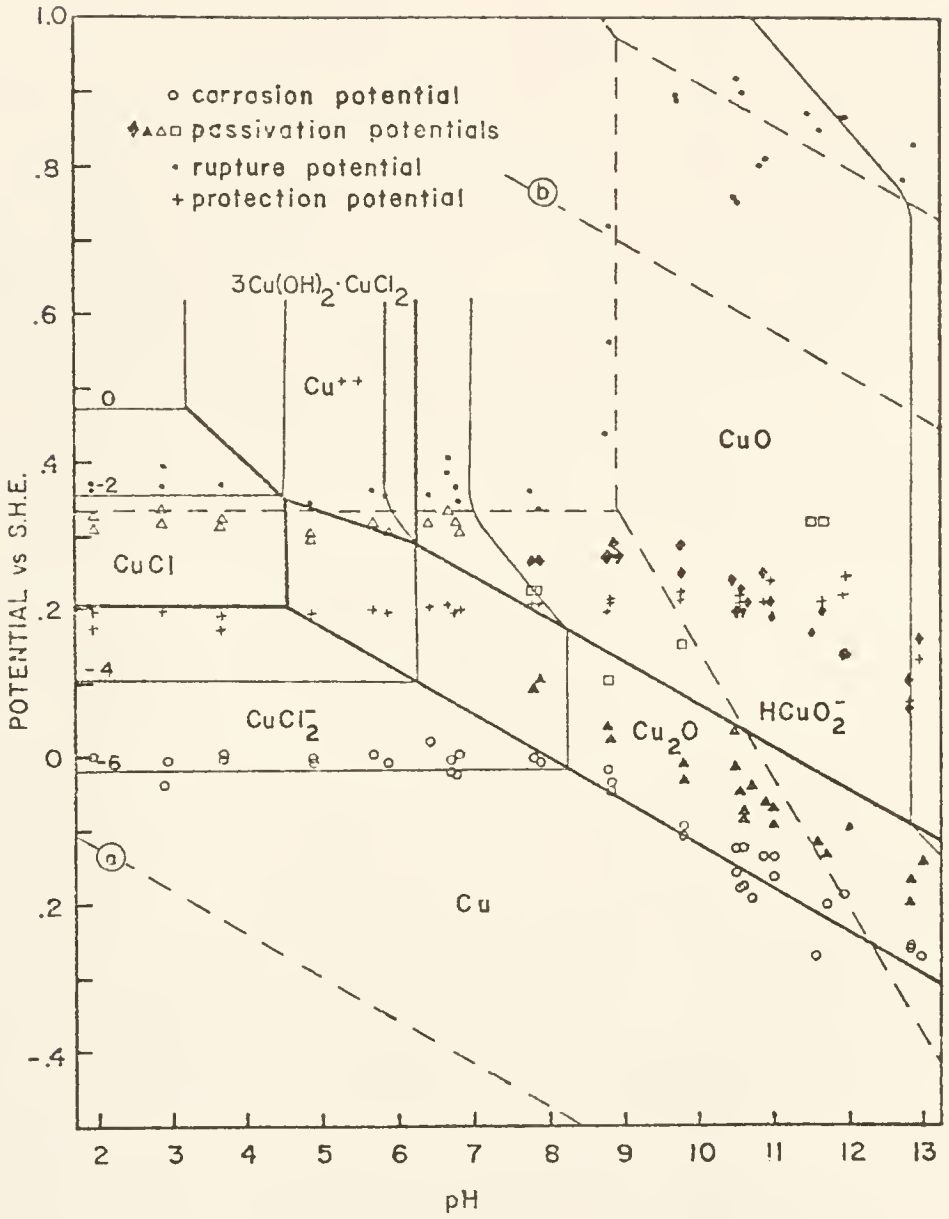

Figure 11. Superposition of polarization data for pure copper in 0.1M chloride solutions and the equilibrium potential versus pH diagram calculated for the system Cu-0.1M Cl^--H_2O at 25°C, after Van Muylder *et al.* (71).

equilibrium was at least partially confirmed by the detection (by X-ray diffraction) of CuCl in the corrosion products.

4.1.2. Polarization of Zinc in 0.1M Chloride Solutions

Cyclic polarization curves were generated for pure zinc at room temperature in stirred, nitrogen-saturated 0.1M chloride solutions having pH values between 2 and 14. The data are plotted on potential versus pH coordinates in figure 12. Apparent from the shape of the diagram is the fact that zinc exhibits amphoteric behavior, undergoing general corrosion in both acid solutions and in highly basic solutions. Equally obvious is that zinc corrodes freely in deoxygenated solutions, its corrosion mixed potentials falling well below the domain of stability for water (with respect to the H_2O/H_2 equilibrium, line a).

The region of passivity between pH values of about 7.5 and 13 is virtually insignificant since the pitting potentials also fall almost entirely below the lower limit of stability for water. When zinc samples are polarized above these potentials, severe pitting occurs. No regions of complex ion formation were suggested by the polarization data. The voluminous white corrosion products resulting from pitting attack could not be identified by X-ray diffraction but are assumed to be amorphous zinc hydroxides as predicted by previous calculations (72).

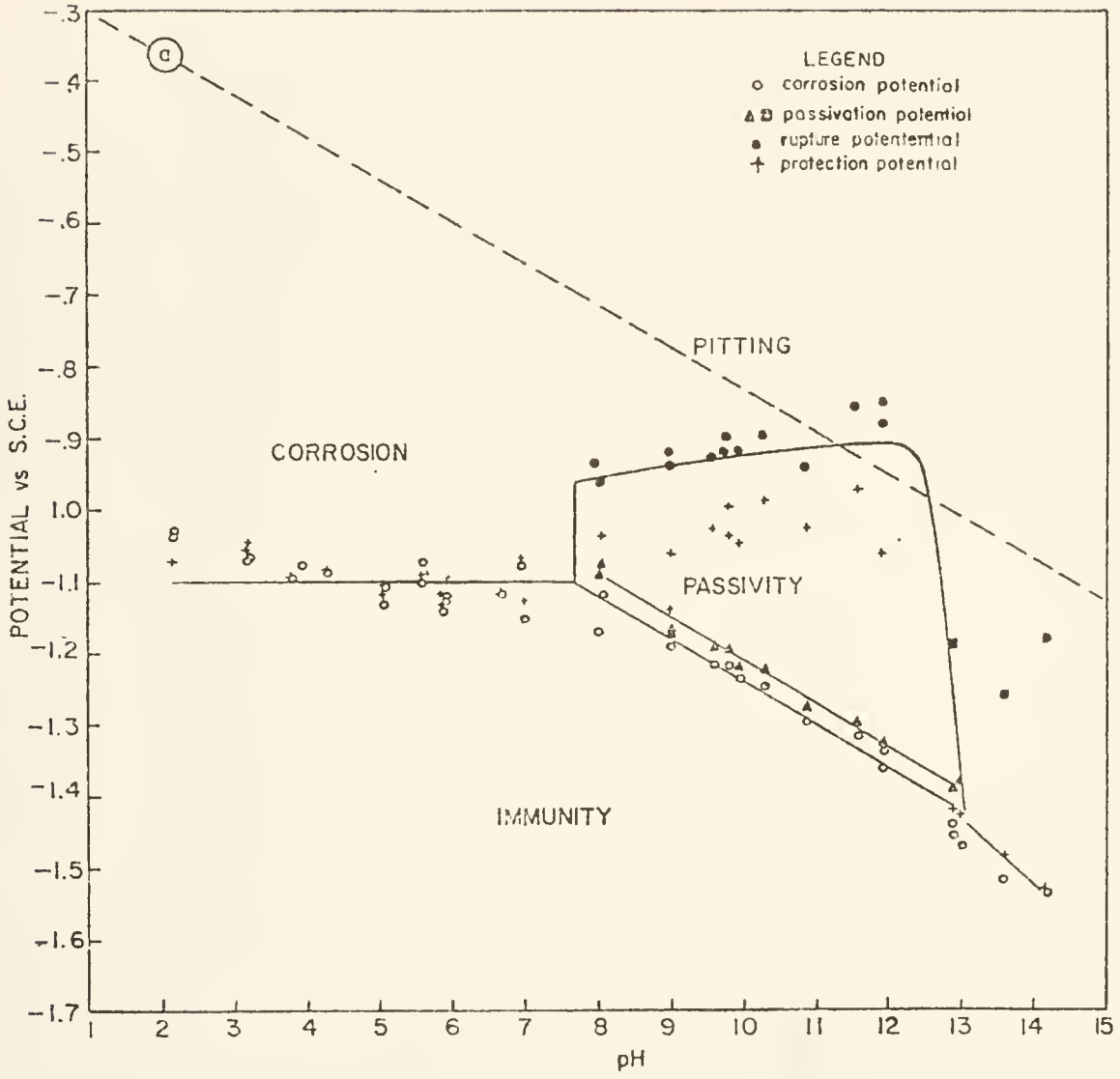

Figure 12. Experimental potential versus pH diagram for pure zinc in nitrogen-saturated 0.1M chloride solutions.

In figure 13, the experimental polarization data for pure zinc in 0.1M chloride solutions are superimposed over the stable equilibria calculated for the Zn-H_2O system at 25°C, after Pourbaix (72). Again, excellent agreement is found between calculated and experimental behavior.

It can be concluded from these data that there is a very large tendency for zinc atoms to pass into solution at all electrode potentials more noble than about -1.100 V_{SCE}.

4.1.3. Polarization of Cu30Zn in 0.1M Chloride Solutions

Cyclic polarization curves were generated for the Cu30Zn alloy in nitrogen-saturated 0.1M chloride solutions at room temperature and at 89°C. The characteristic electrode potential features of the polarization curves generated at room temperature are presented in figure 14.

With a few exceptions, these results are very similar to those obtained for pure copper. The locus of corrosion potentials between pH 4 and pH 8 is -0.260 V_{SCE}, as it was for pure copper. There is, however, a sharp drop in measured corrosion potentials between pH 3 and pH 4 to a steady value of about -0.450 V_{SCE} at lower pH's. The drop-off in corrosion potential was confirmed by exposing two Cu30Zn samples in nitrogen-saturated pH 2 and pH 4 solutions for 34 days and 50 days, respectively. The variation in measured corrosion potential was recorded as a function of

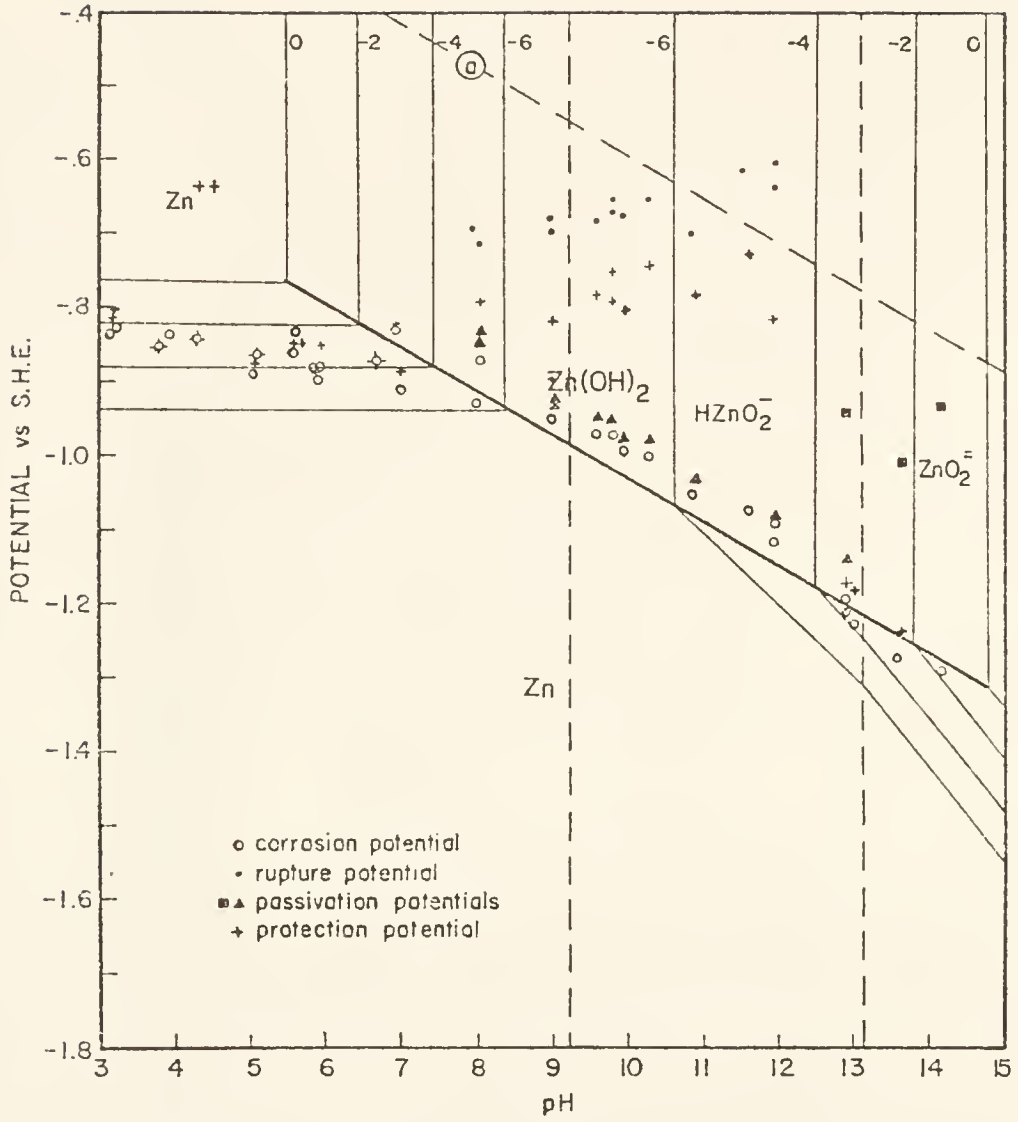

Figure 13. Superposition of polarization data for pure zinc in 0.1M chloride solutions and the equilibrium potential versus pH diagram calculated for the system Zn-H_2O at 25°C, after Pourbaix (72).

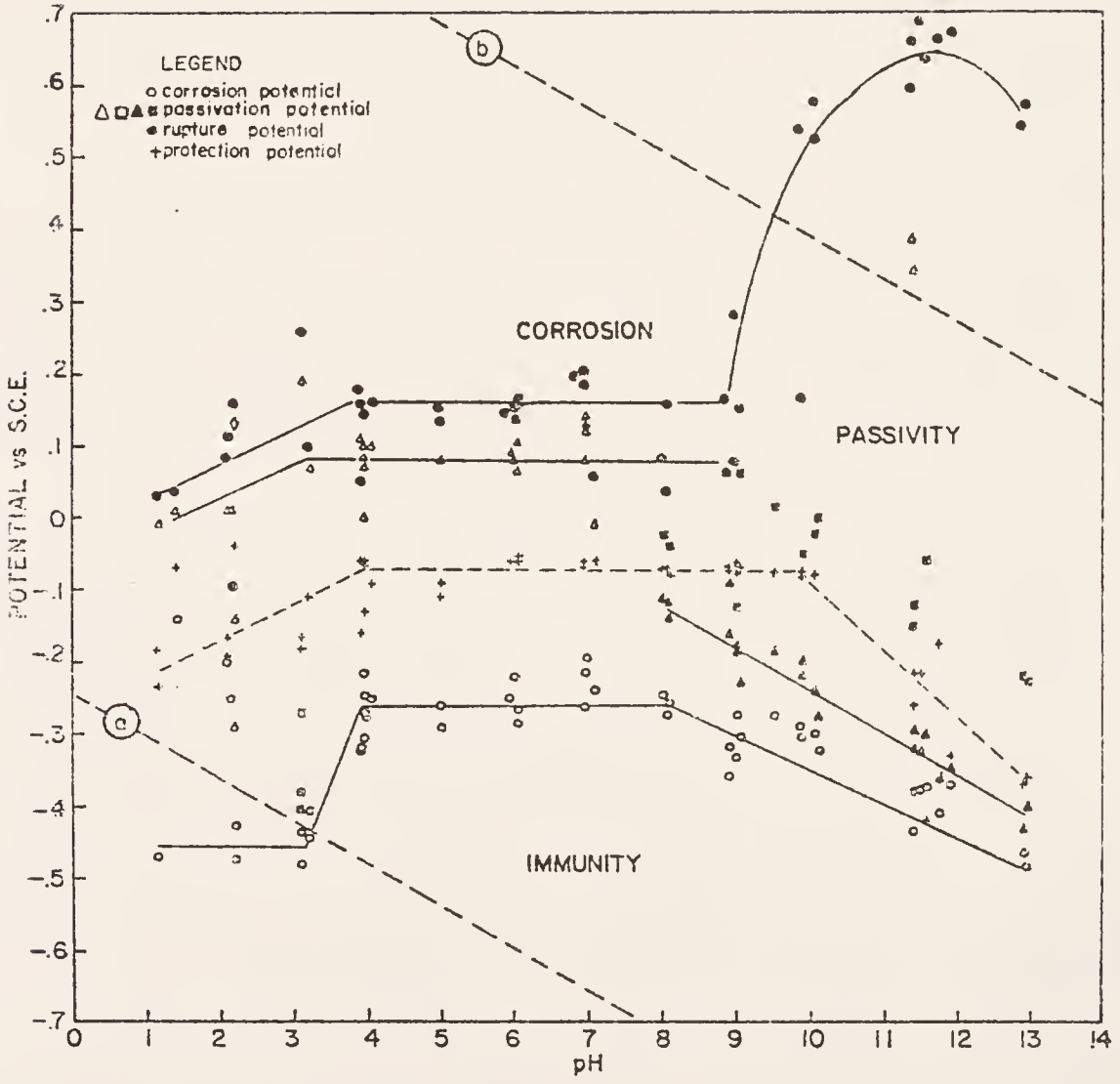

Figure 14. Experimental potential versus pH diagram for Cu30Zn in nitrogen-saturated 0.1M chloride solutions.

time, figure 15. The value of the corrosion potential measured in solutions of pH < 3 can be explained by considering the equilibrium between copper and the $CuCl_3^-$ ion:

$$Cu + 3Cl^- \rightleftarrows CuCl_3^{-2} + e^- \quad . \qquad (12)$$

Using the free energy data compiled in Appendix 7, the equilibrium potential for reaction (12) at 25°C is given by:

$$E = -.011 + .0591 \log \frac{a_{CuCl_3^{-2}}}{(a_{Cl^-})^3} \quad . \qquad (13)$$

Assuming $a_{CuCl_3^{-2}} = 10^{-6}$, the equilibrium potential of the $Cu\text{-}CuCl_3^{-2}$ reaction is -0.427 V_{SCE}. This value is in fair agreement with the experimental corrosion potential value. Indications of the establishment of this equilibrium on copper in acid chloride solutions have been reported elsewhere (73).

The locus of the protection potential determined by cyclic polarization of Cu30Zn samples is -0.070 V_{SCE}, virtually the same as that found for copper. The protection potential takes on a new significance in the case of the brass (48), since when the electrode potential of the cuprous chloride-covered brass sample was brought below the protection potential, deposition of copper occurred. This was found to be the case not only in acid and neutral solutions, but also in basic solutions when the rupture potential was

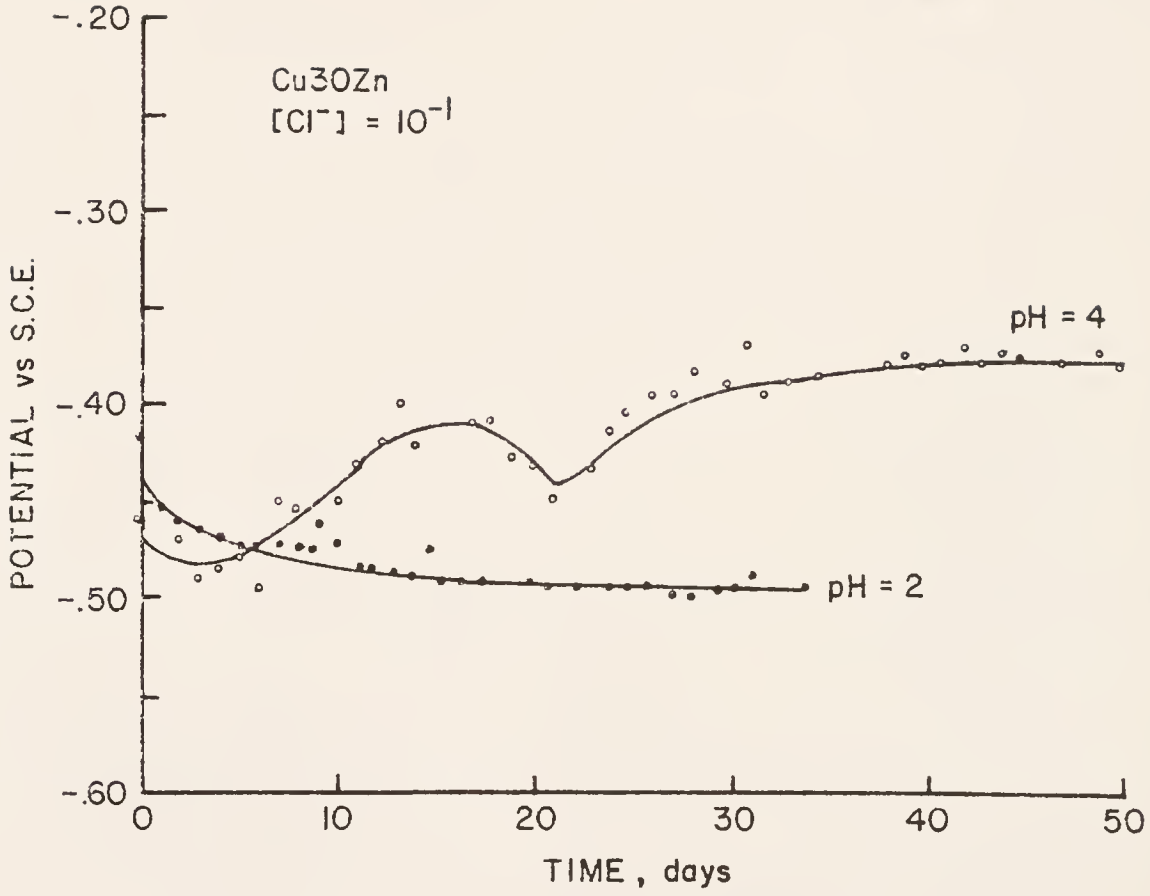

Figure 15. Variation of the corrosion potential of Cu30Zn with time of exposure in 0.1M chloride solutions of pH 2 and pH 4.

exceeded and copper-hydroxy-chloride corrosion products were formed over part of the surface. Upon passing through the protection potential, deposition of copper took place on the brass surface beneath the corrosion products, but not on the areas of the surface still remaining passive. If the rupture potential was not exceeded during the polarization scan, then no deposition of copper was detected when the sample electrode potential was brought below the protection potential.

In the context of producing dezincification of the Cu30Zn alloy, the breakdown of passive behavior can be thought of as an activation step. The concept of activation has received considerable attention in connection with the initiation of pitting on Fe-Cr alloys (53, 62, 74). Van Muylder *et al*. (47) have described the initiation of pitting of copper in aqueous chloride solutions by the introduction of oxygen at local sites on copper surface. This action of the oxygen in destroying passivity was attributed to its ability to increase the electrode potential of the copper surface above its critical potential.

A limited number of cyclic polarization experiments were conducted on Cu30Zn in 0.1M chloride solutions at 89°C. Through these experiments the corrosion potential of Cu30Zn at 89$\pm\frac{1}{2}$°C in solutions of pH 4 was established at -0.580 V_{SCE}.

4.2. Dealloying of Cu30Zn by Selective Leaching

4.2.1. Conditions of Exposure

The electrochemical requirements for operation of a selective leaching dealloying mechanism were outlined in section 2.1. According to the proposal of Verink and Heidersbach (18), selective leaching of an alloy's active component may be expected when the alloy is polarized to electrode potentials between its corrosion potential and the corrosion potential of its active component.

In the previous section (section 4.1.), the electrochemical characterization of copper, zinc, and Cu30Zn was undertaken in order to establish the domain of electrode potentials in which selective leaching of the Cu30Zn alloy could be studied. Referring to figures 12 and 14, this region is bounded in room temperature neutral and weakly acidic solutions by the corrosion potential of Cu30Zn, -0.380 V_{SCE}, and by the corrosion mixed potential of zinc, -1.100 V_{SCE}. At 89°C, the upper boundary is displaced to a somewhat lower value, -0.480 V_{SCE}.

Accordingly, potentiostatic selective leaching experiments, described in section 3.2., were conducted on samples of Cu30Zn exposed in pH 4, 0.1M chloride solutions at $89\pm\frac{1}{2}$°C. Table 1 is a list of the applied electrode potentials and times of exposure for the samples reported. Note that three samples

Table 1

Conditions of Exposure for the Cu30Zn Selective Leaching Samples

Electrode Potential volts (S.C.E.)	Time days
-0.450	4½
-0.450	1
-0.450	7
-0.500	4
-0.600	4
-0.700	2
-0.700	4
-0.700 (2 samples)	7
-0.700	10
-0.800	4
-0.900	4

were exposed at -0.450 V_{SCE}, slightly above the measured corrosion potential of the Cu30Zn alloy. It is expected that these samples would show both the effects of anodic (simultaneous) dissolution at low rates and of selective leaching.

4.2.2. Results of Solution Analysis

Atomic absorption spectroscopy was employed to analyze the copper and zinc contents of solution samples taken from the cells before the start of and during each experiment. As stated previously, the experimental limits of detection were approximately 0.10 ppm for copper and 0.05 ppm for zinc. Smaller amounts, or traces of copper and zinc could be detected, but the accuracy of measurement of concentrations below the limits of detection is questionable.

For the conditions of exposure outlined in table 1, no detectable amounts of copper are expected to enter solution. Such was found to be the case for all experiments reported. Whenever significant quantities of copper were detected in solution, failure of the stop-off lacquer to protect unexposed portions of the sample was determined to be the cause, and the experiment was rejected.

Calculation of the amount of zinc leached from each Cu30Zn sample was made from measurements, by atomic absorption analysis, of the zinc content of the solution during the course of the experiment. Corrections were made for

changes in the solution volume due to evaporation and for the quantities of zinc removed from the cells in aliquots taken for analysis. The total amount of zinc dissolved at any time during an experiment is reported in micrograms per square centimeter of sample surface (projected) area ($\mu g/cm^2$). Calculations were completed for all samples listed in table 1, except those exposed at -0.450 V_{SCE}.

Figure 16 summarizes the zinc dissolution data calculated for the five samples exposed at -0.700 V_{SCE}. Considerable variation in the rates of zinc dissolution from sample to sample is evident. However, the data denote a marked tendency towards linear zinc dissolution kinetics.

Figure 17 summarizes the zinc dissolution data from samples exposed at potentials between -0.500 and -0.900 V_{SCE}. The data points plotted for -0.700 V_{SCE} at each time of exposure represent the average of the data points shown in figure 15 for the five -0.700 V_{SCE} samples. Again, linearity is evident in each of the plots, at least for four days of exposure. The rates of zinc dissolution measured at each electrode potential are summarized in Table 2. The third column gives the partial current density for the dissolution of zinc to its divalent ion from Cu30Zn, as calculated from the zinc dissolution rates.

Pickering and Byrne (20) have presented data for dissolution currents of zinc from Cu30Zn exposed potentiostatically at 23°C in an acetate-buffered 1N Na_2SO_4 solution

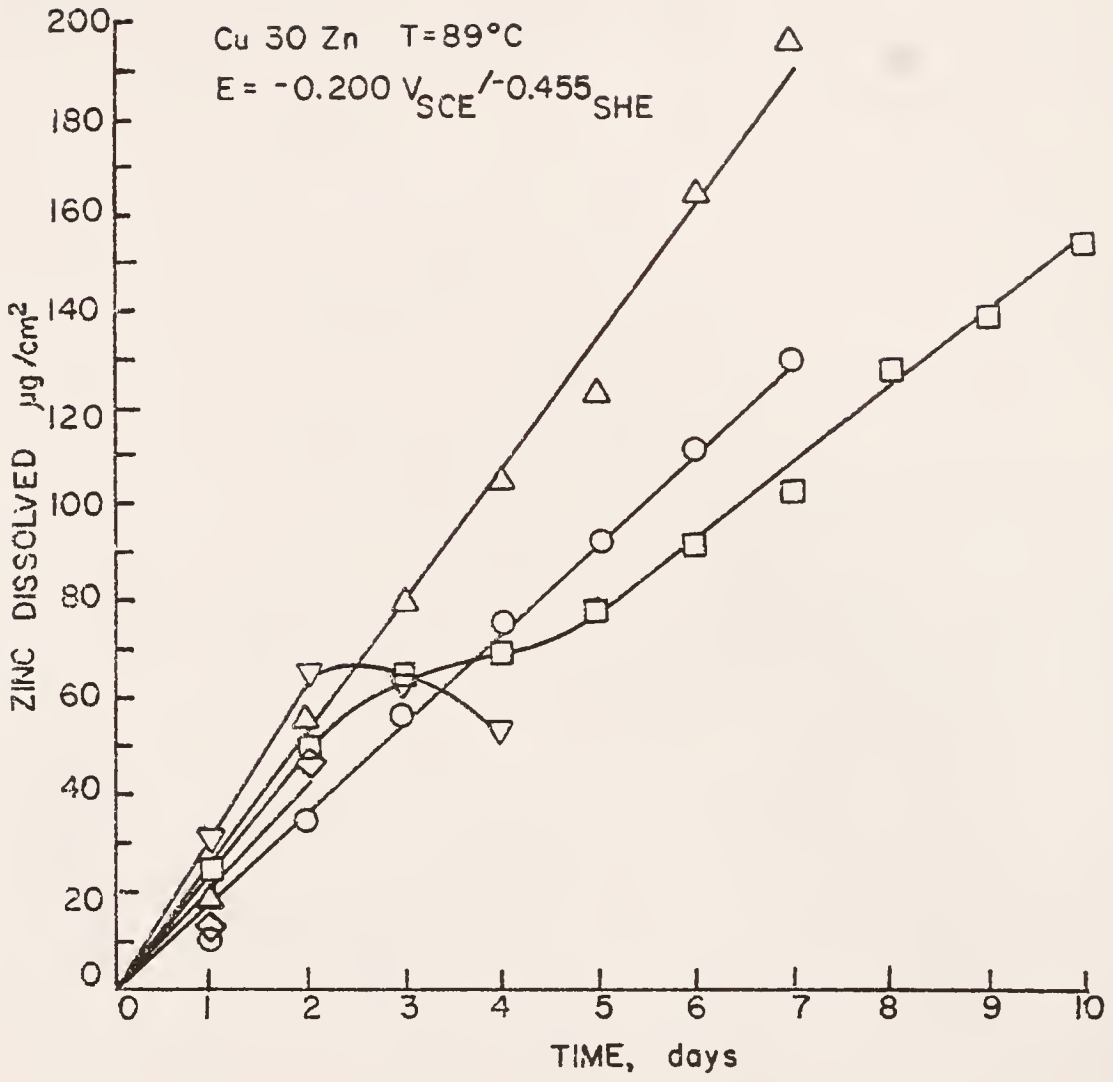

Figure 16. Zinc dissolved from Cu30Zn samples potentiostated at -0.700 V_{SCE} in 89°C, 0.1M chloride solutions of pH 4.

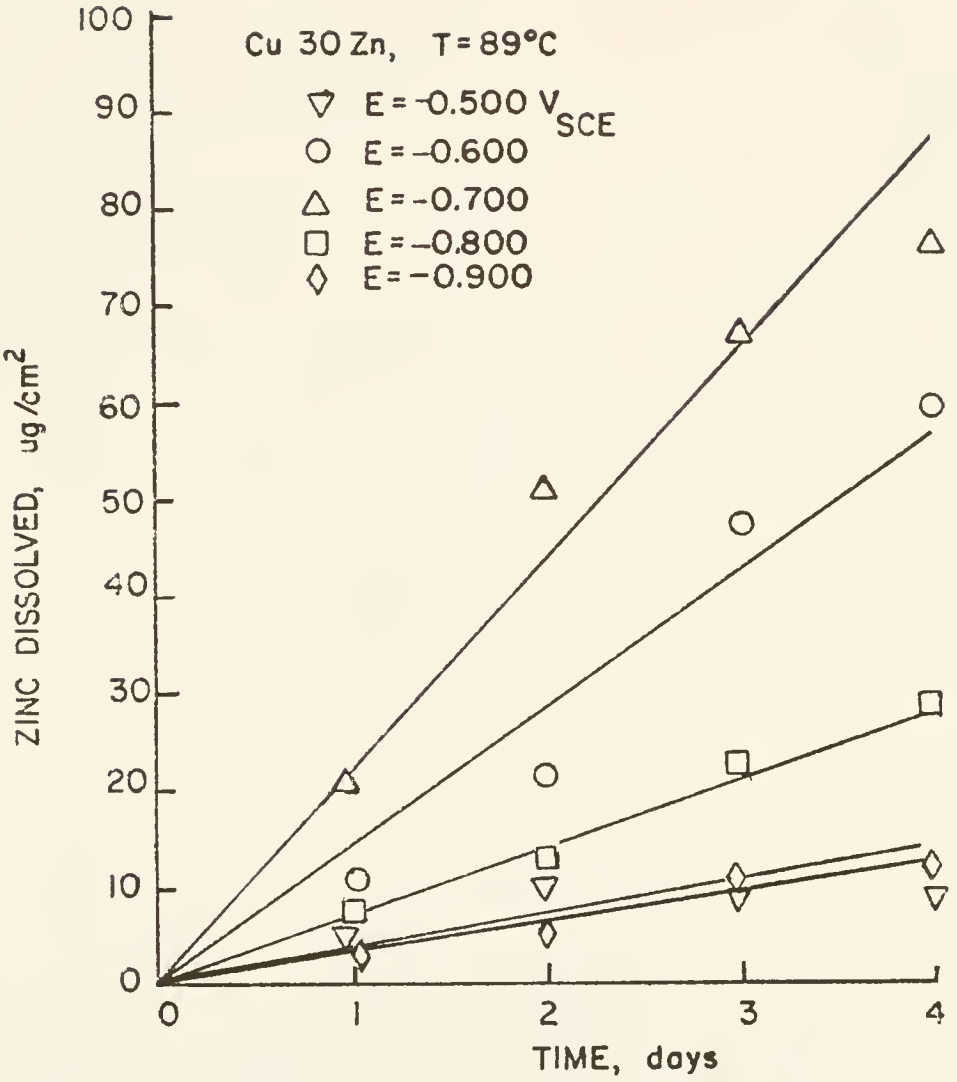

Figure 17. Zinc dissolved from Cu30Zn samples potentiostated at electrode potentials between -0.500 and -0.900 V_{SCE} at 89°C.

Table 2

Rate of Zinc Dissolution from Cu30Zn Under Selective Leaching Conditions

Electrode Potential volts (S.C.E.)	Rate of Zinc Dissolution $g/cm^2/day$	Zinc Dissolution Current Density a/cm^2
-0.500	3.5	1.2×10^{-7}
-0.600	14	4.8×10^{-7}
-0.700	22	7.5×10^{-7}
-0.800	7.0	2.4×10^{-7}
-0.900	3.3	1.1×10^{-7}

of pH 5. In the region of electrode potential between -0.600 and -0.200 V_{SHE}, they report zinc dissolution current values between 7 x 10^{-8} and 2 x 10^{-7} a/cm^2. These current values are in qualitative agreement with those measured in the present investigation for selective leaching of zinc from Cu30Zn at 89°C.

4.2.3. Surface Morphology

Visual examination of the Cu30Zn samples after exposure under selective leaching conditions indicated that dealloying had occurred in all cases. The unmasked portions of the sample surfaces exhibited the pink or reddish color characteristic of dezincified brass. For the two series of samples exposed for different periods of time at -0.450 and -0.700 V_{SCE}, a definite deepening of the surface color with increasing times of exposure was noted. In all cases, the masked surfaces of the samples showed no detectable change in color from the characteristic yellow color of the Cu30Zn alloy.

Further examination of the surfaces of the selectively leached Cu30Zn samples was accomplished by scanning electron microscopy. Cu30Zn samples were polished through 1 micron diamond paste before being subjected to selective leaching. In this way, any gross surface effects resulting from the selective leaching process could be easily recognized.

Figure 18 shows a typical area on the exposed surface a Cu30Zn sample potentiostated 4 days at -0.450 V_{SCE}. It is apparent from this photograph that the sample has undergone anodic dissolution, as was expected for samples potentiostated above the corrosion potential measured for the Cu30Zn alloy. The anodic dissolution appears to have taken place primarily in pits, which tend to lie on polishing scratches. Similar surface appearance was noted for the Cu30Zn sample exposed 7 days at the same electrode potential.

Figure 19 shows an area from the surface of a Cu30Zn sample exposed 4 days at -0.600 V_{SCE}. The surface was featureless and could not be distinguished from the unexposed surface, except by the fact that it developed a pinkish color. Figure 19 exemplifies the appearance of Cu30Zn surfaces after selective leaching at electrode potentials below -0.450 V_{SCE}. It should be noted that the resolution in figure 19 is better than 0.2 μm.

Surface roughening has been cited as a factor contributing to selective leaching in copper-gold alloys (16, 21, 31), and predicted as a possible factor in the case of copper-zinc alloys (16). In agreement with the results of Pickering and Byrne (20), no evidence for surface roughening of Cu30Zn exposed under conditions expected to produce selective leaching has been found in this investigation. Only in the case of the samples exposed under slightly anodic

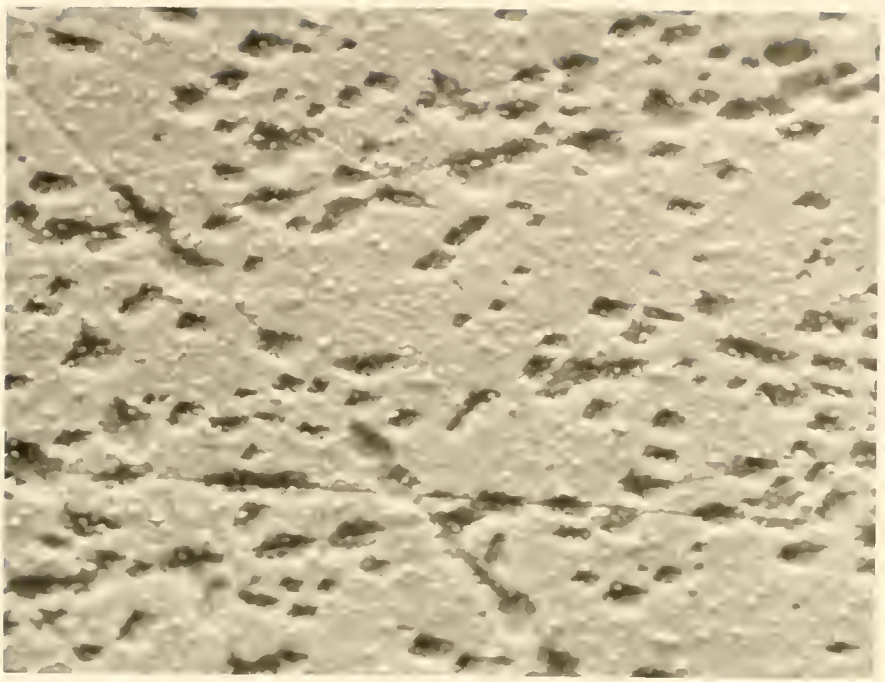

Figure 18. Pitting of Cu30Zn sample exposed 4 days at -0.450 V_{SCE}. 3700X

Figure 19. Typical surface of Cu30Zn samples potentiostated below -0.450 V_{SCE}. From a Cu30Zn sample exposed 4 days at -0.600 V_{SCE}. 3500X

conditions (at -0.450 V_{SCE}) were any changes in surface appearance noted.

4.2.4. Auger Composition Profiles

Composition profiles of the near-surface layers of the dealloyed samples listed in table 1 were obtained through Auger electron spectroscopic analysis coupled with argon sputtering, described in section 3.5. The present study describes the first reported use of Auger electron spectroscopy in the characterization of dealloyed structures.

Figure 20 is a composition profile of an area on the unexposed surface of a Cu30Zn sample which has undergone selective leaching. The dimensions on the abscissa of the profile are based on the measured argon sputtering rate of 25 Ångstroms/min, determined as in Appendix 6. The sharp increase in the copper peak-to-peak heights below ~100 Ångstroms is characteristic of all the profiles measured during the investigation. This initial period of sputtering can be assigned to cleaning of the metal surface of gases and oil adsorbed on the surface during handling. After the first few minutes of sputtering the "cleaned" metal surface is uncovered and Auger electron spectra characteristic of the metal structure are measured.

As stated previously, the ratio of the peak-to-peak heights of copper and zinc serves as an indication of the relative level of enrichment of the measured surface in these

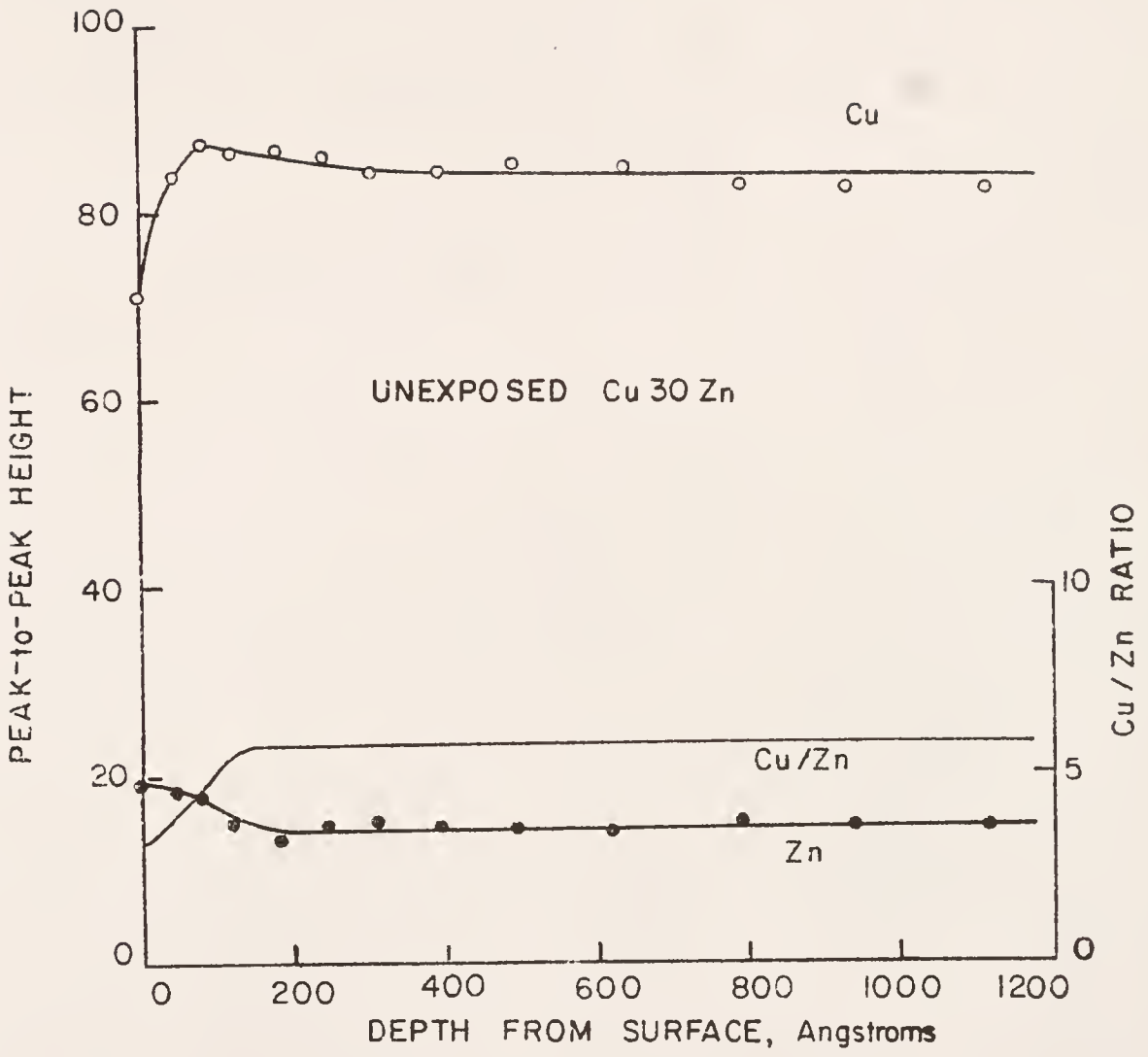

Figure 20. Auger composition profile obtained from an unexposed Cu30Zn sample.

two components. The relationship between the composition of a brass surface uncovered during sputtering and its measured peak-to-peak ratio was presented in figure 8, in section 3.5. A measured Cu/Zn ratio $\approx$ 5 is indicative of a brass surface containing 30 w/o zinc. A higher measured Cu/Zn ratio signifies decreased zinc content, and a lower ratio would indicate enrichment of the surface in zinc. Referring again to figure 20, a constant Cu/Zn ratio $\approx$ 5 is reached after sputtering about 5 minutes (125 Å). If the initial four minutes of sputtering is assigned to cleaning of the surface, then it is evident that no detectable enrichment of the Cu30Zn surface in either component has taken place.

Figures 21a, b, and c are the composition profiles measured for Cu30Zn samples potentiostated at -0.450 V_{SCE} for 1, 4½, and 7 days, respectively. In each case, depletion of the zinc content of the near-surface layers is evidenced by initially low peak-to-peak heights for zinc. With increasing depth from the sample surface, the amount of zinc measured increases until a constant value is reached. The peak-to-peak heights measured for copper remain relatively constant (after the initial "cleaning" period) with depth. In some cases, e.g., figure 21c, the copper peak-to-peak heights show a decrease after reaching maximum values. The cause of this effect is unclear, but is thought to be a result of the argon-sputtering process.

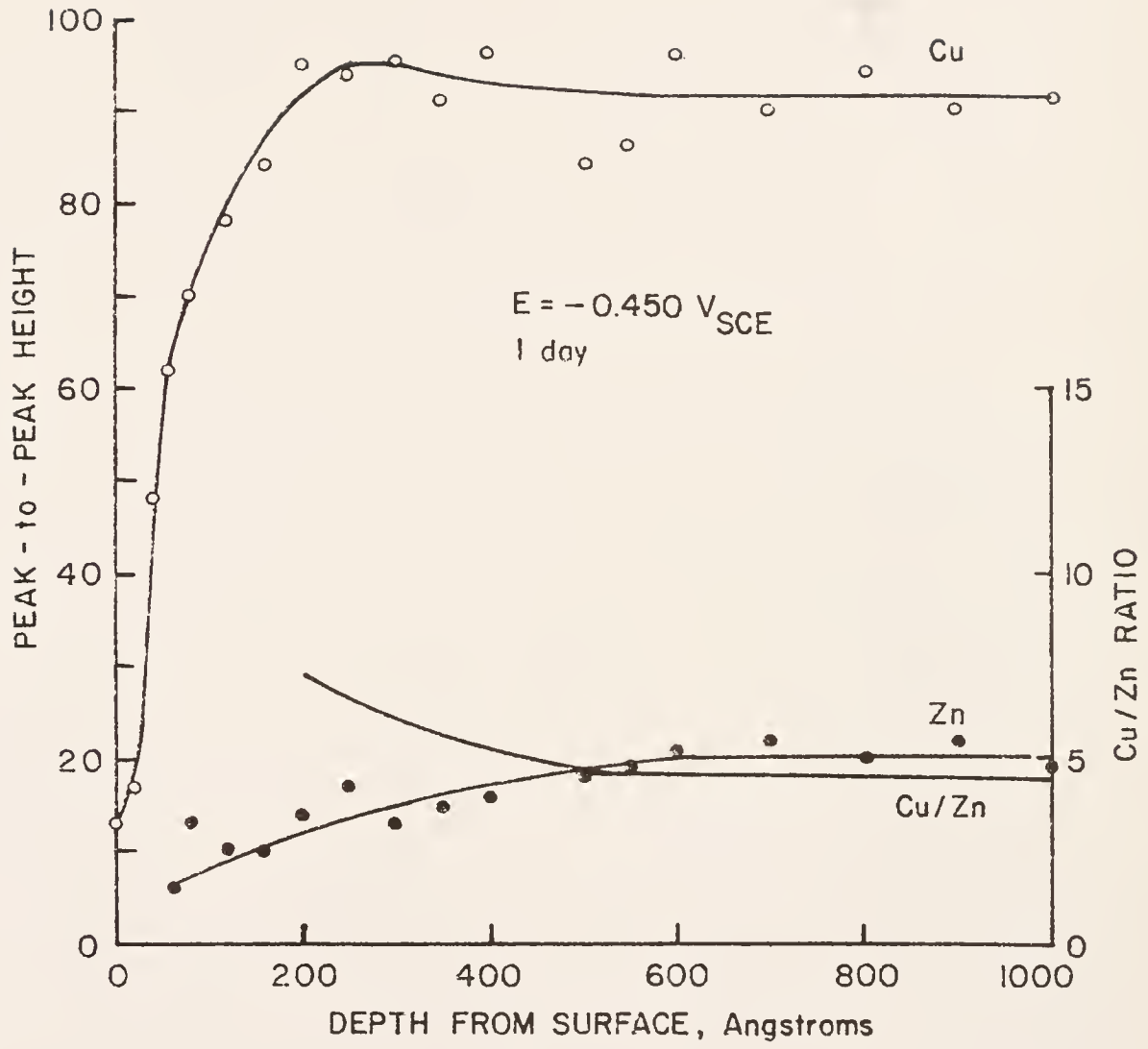

Figure 21a. Auger composition profile obtained from a Cu30Zn sample potentiostated at -0.450 V_{SCE} for 1 day.

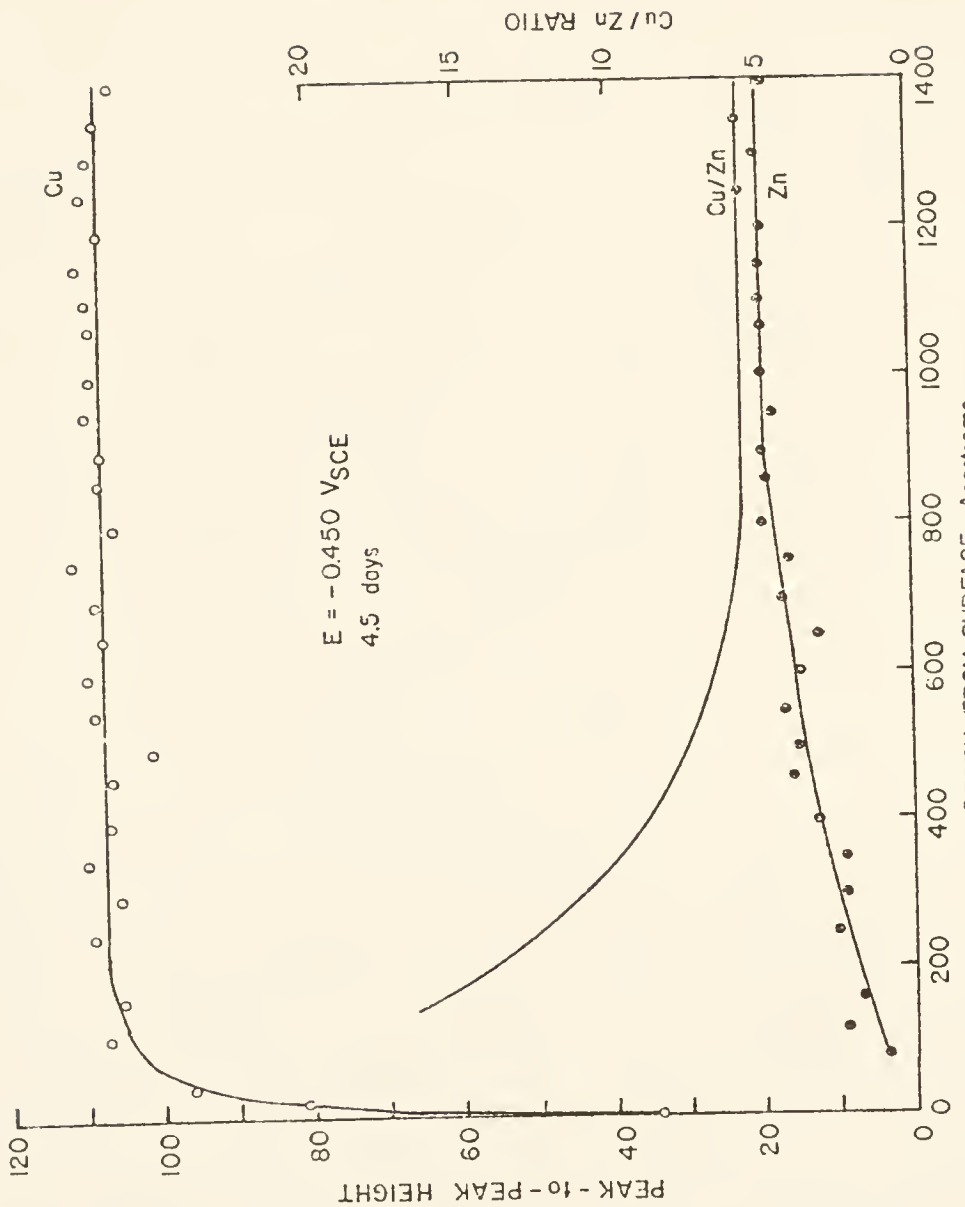

Figure 21b. Auger composition profile obtained from a Cu30Zn sample potentiostated at -0.450 V_{SCE} for 4½ days.

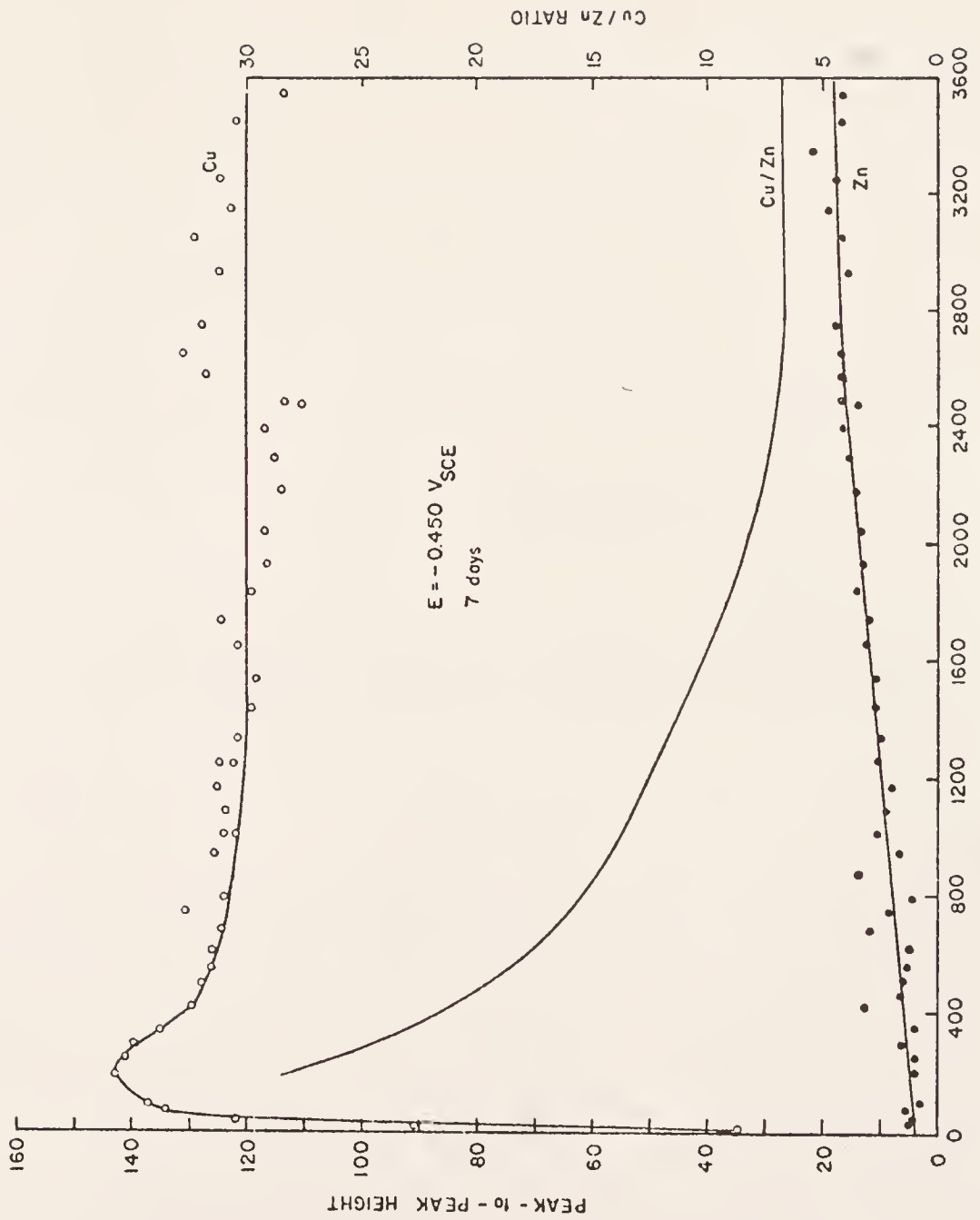

Figure 21c. Auger composition profile obtained from a Cu30Zn sample potentiostated at -0.450 V_{SCE} for 7 days.

The Cu/Zn ratio curves plotted on each profile indicate the level of dealloying at each point in the composition versus depth profiles. Comparison of these curves in figures 21a, b, and c shows that the level of zinc depletion at the surface increases with increasing time of exposure. Similarly, the depths of the zinc-depleted surface layers, indicated by the attainment of constant values ≈ 5 by the Cu/Zn ratio curves, increase with increasing time of exposure.

Figure 22 and 23 are the composition profiles obtained from Cu30Zn samples exposed 4 days at -0.500 V_{SCE} and -0.600 V_{SCE}, respectively. Depletion of the zinc content of the surface is evident, but appears to be less drastic than in the -0.450 V_{SCE} sample exposed $4\frac{1}{2}$ days.

Figures 24a, b, c, and d are the composition profiles obtained from Cu30Zn samples potentiostated at -0.700 V_{SCE} for 2, 4, 7 and 10 days, respectively. Comparison of the Cu/Zn ratio curves for this series shows that the levels of zinc depletion at the surface and the depths of zinc-depleted layers fall roughly in order according to the times of exposure.

Figure 25 and 26 are the composition profiles obtained from Cu30Zn samples potentiostated 4 days at -0.800 V_{SCE} and -0.900 V_{SCE}. The sample at -0.800 V_{SCE} gives a profile similar to those measured for the previous samples. The -0.900 V_{SCE} sample exhibits a radically different profile.

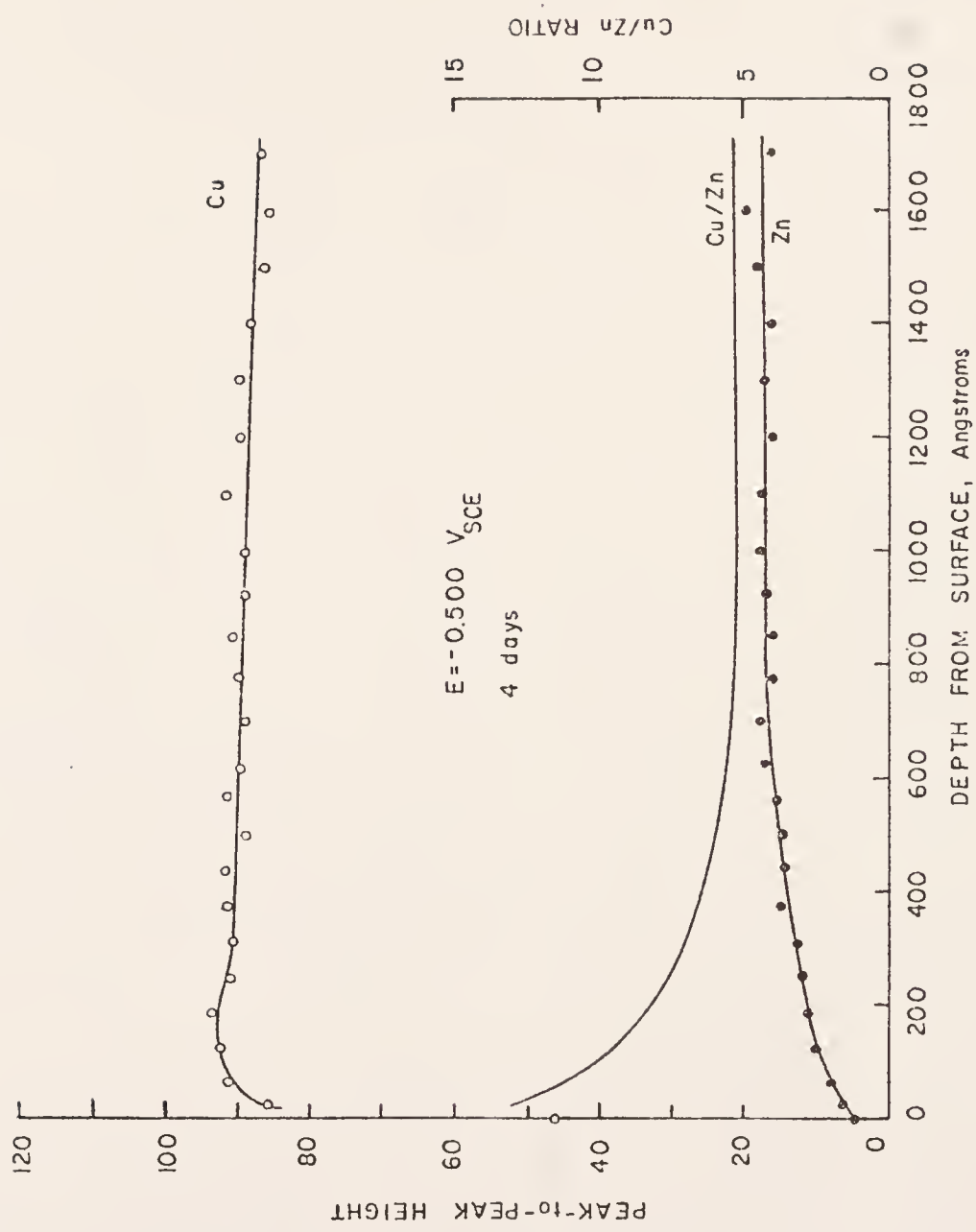

Figure 22. Auger composition profile obtained from a Cu30Zn sample potentiostated at -0.500 V_{SCE} for 4 days.

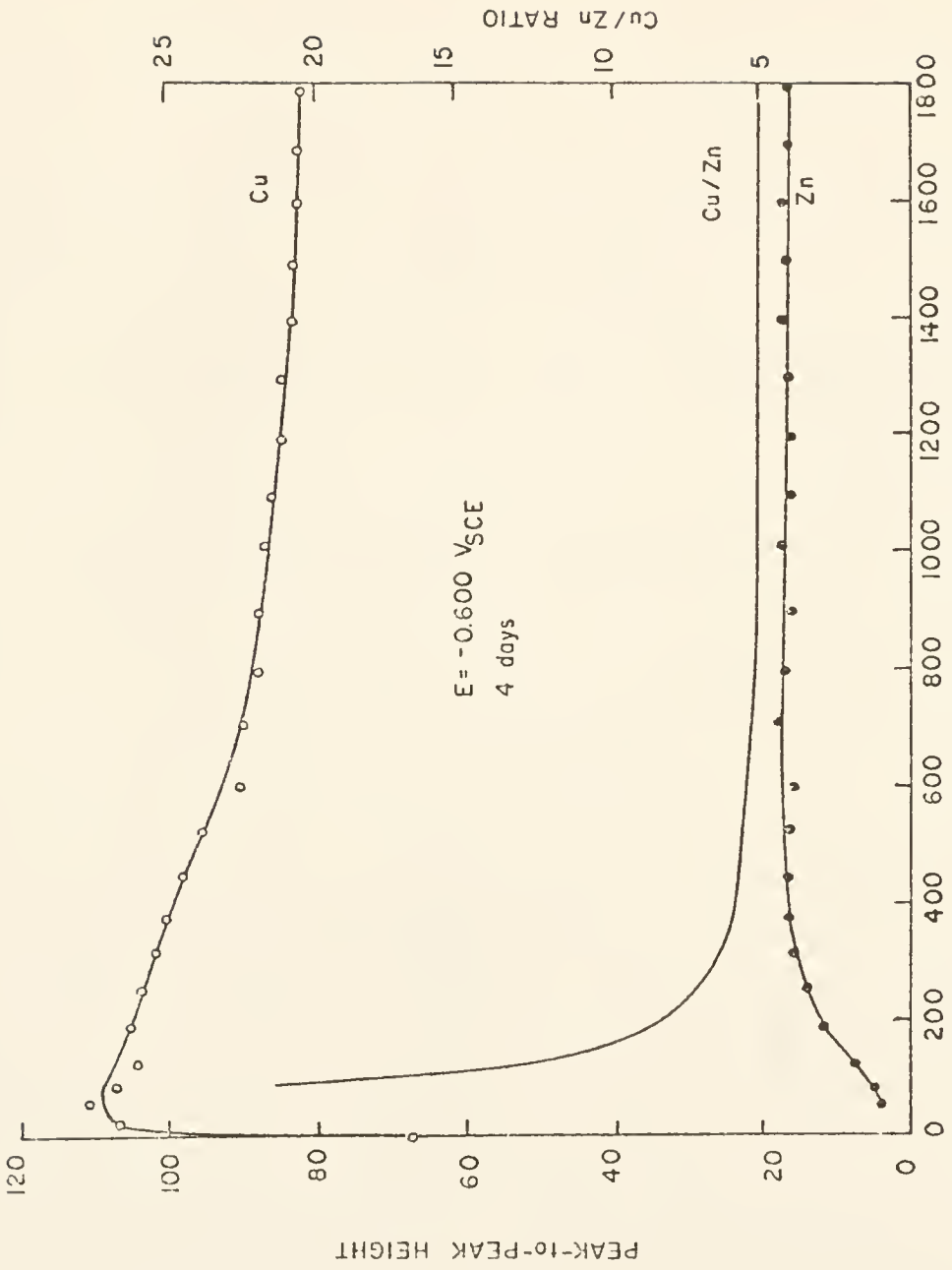

Figure 23. Auger composition profile obtained from a Cu30Zn sample potentiostated at -0.600 V_{SCE} for 4 days.

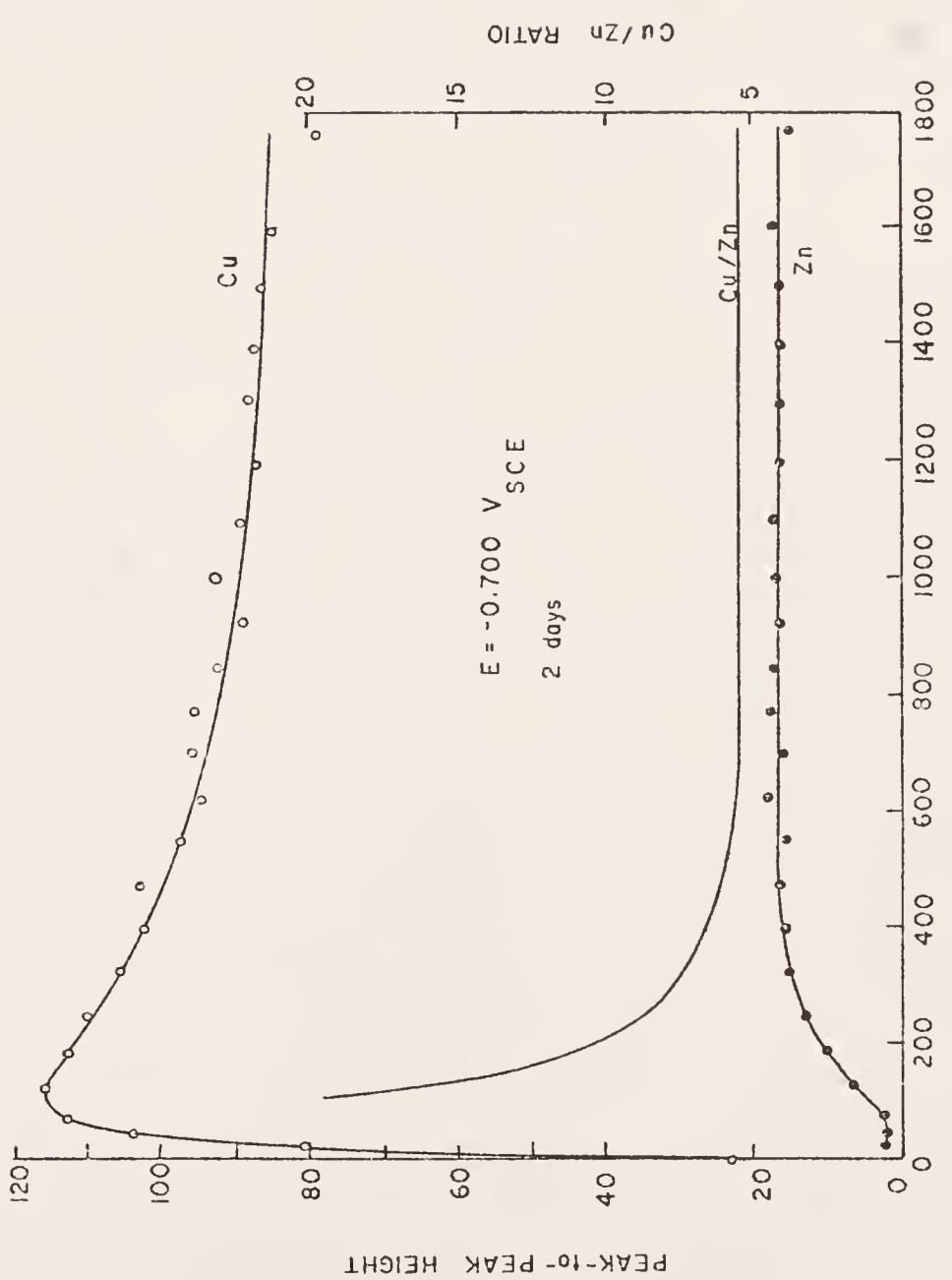

Figure 24a. Auger composition profile obtained from a Cu30Zn sample potentiostated at -0.700 V_{SCE} for 2 days.

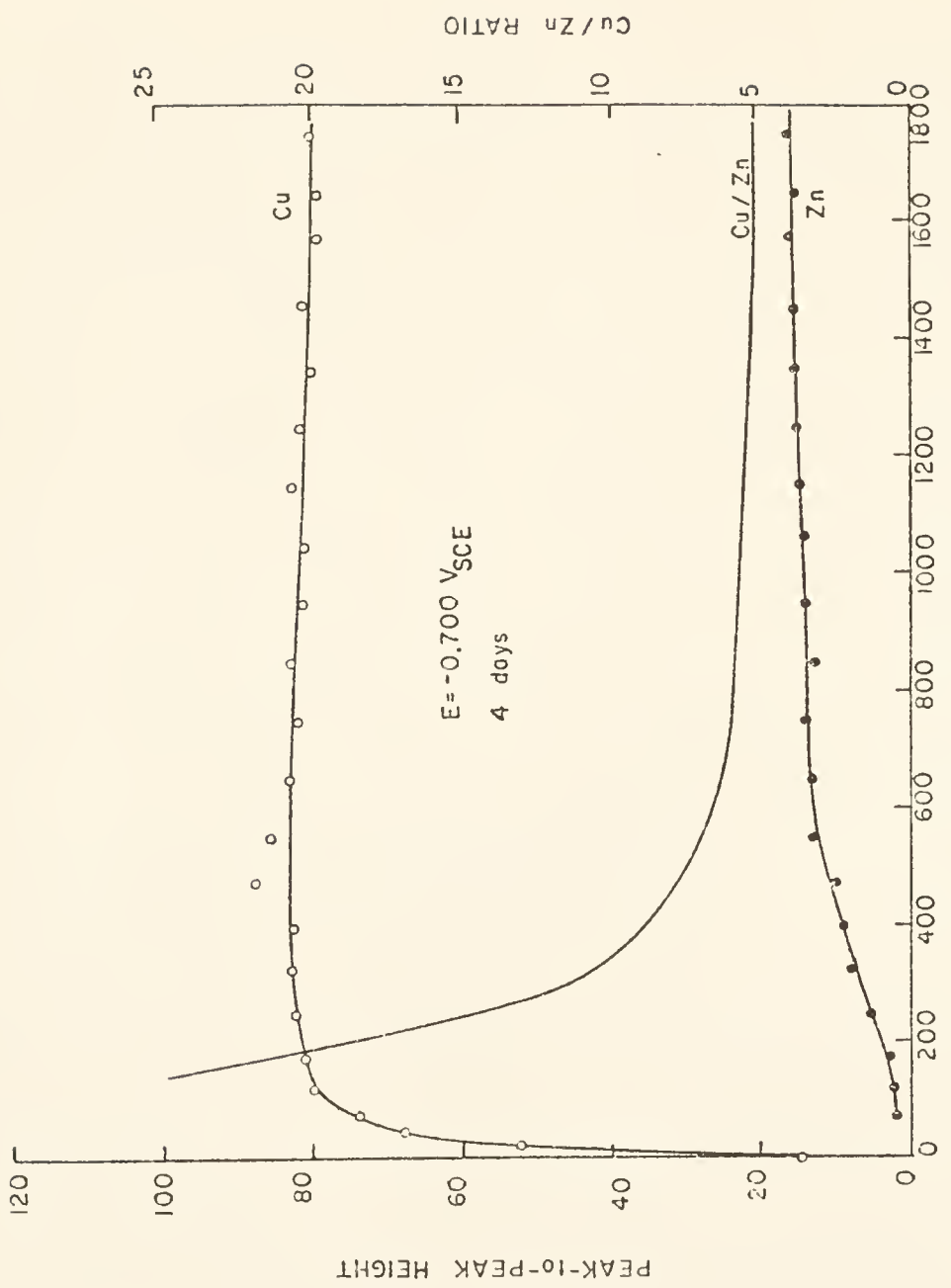

Figure 24b. Auger composition profile obtained from a Cu30Zn sample potentiostated at -0.700 V_{SCE} for 4 days.

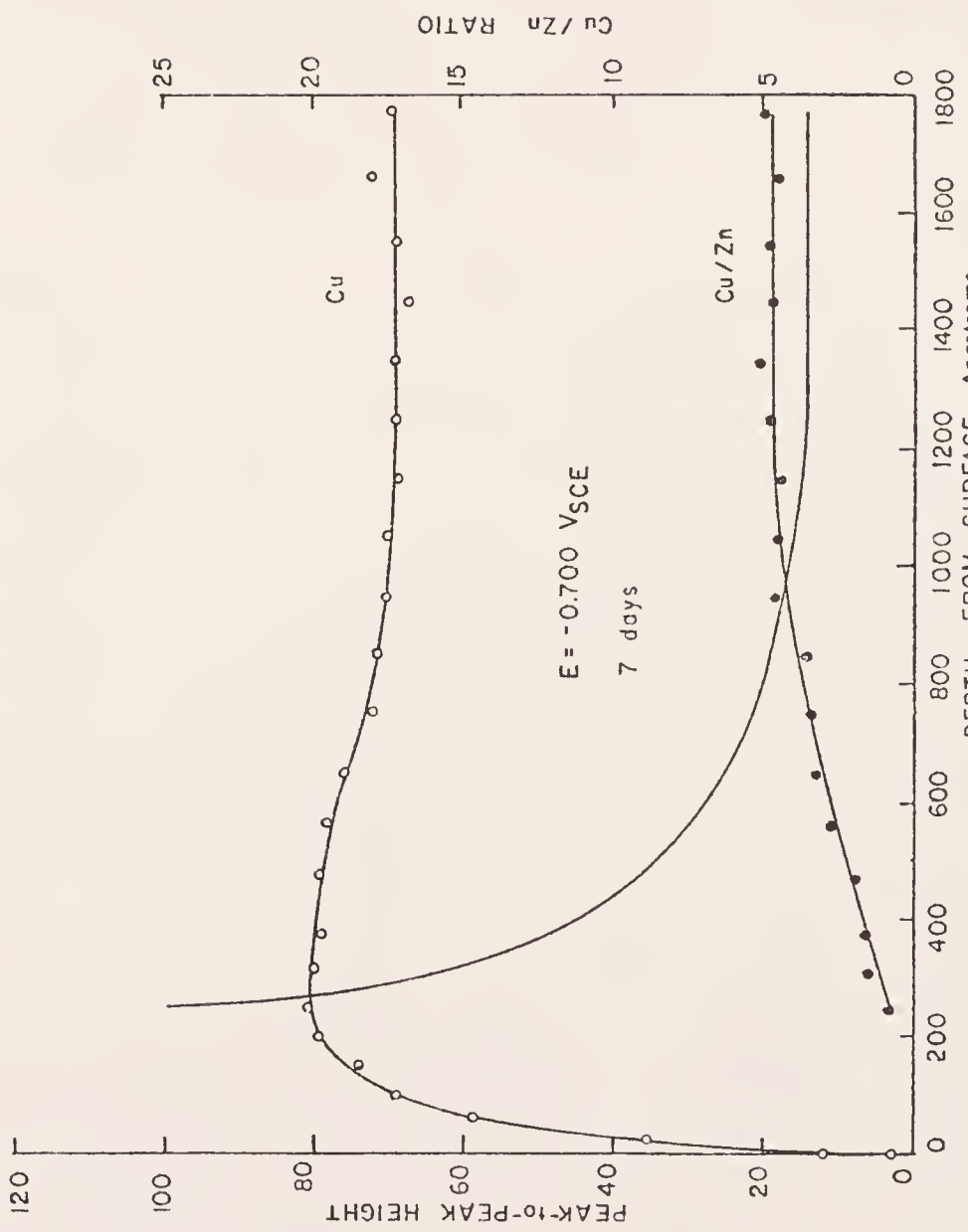

Figure 24c. Auger composition profile obtained from a Cu30Zn sample potentiostated at -0.700 V_{SCE} for 7 days.

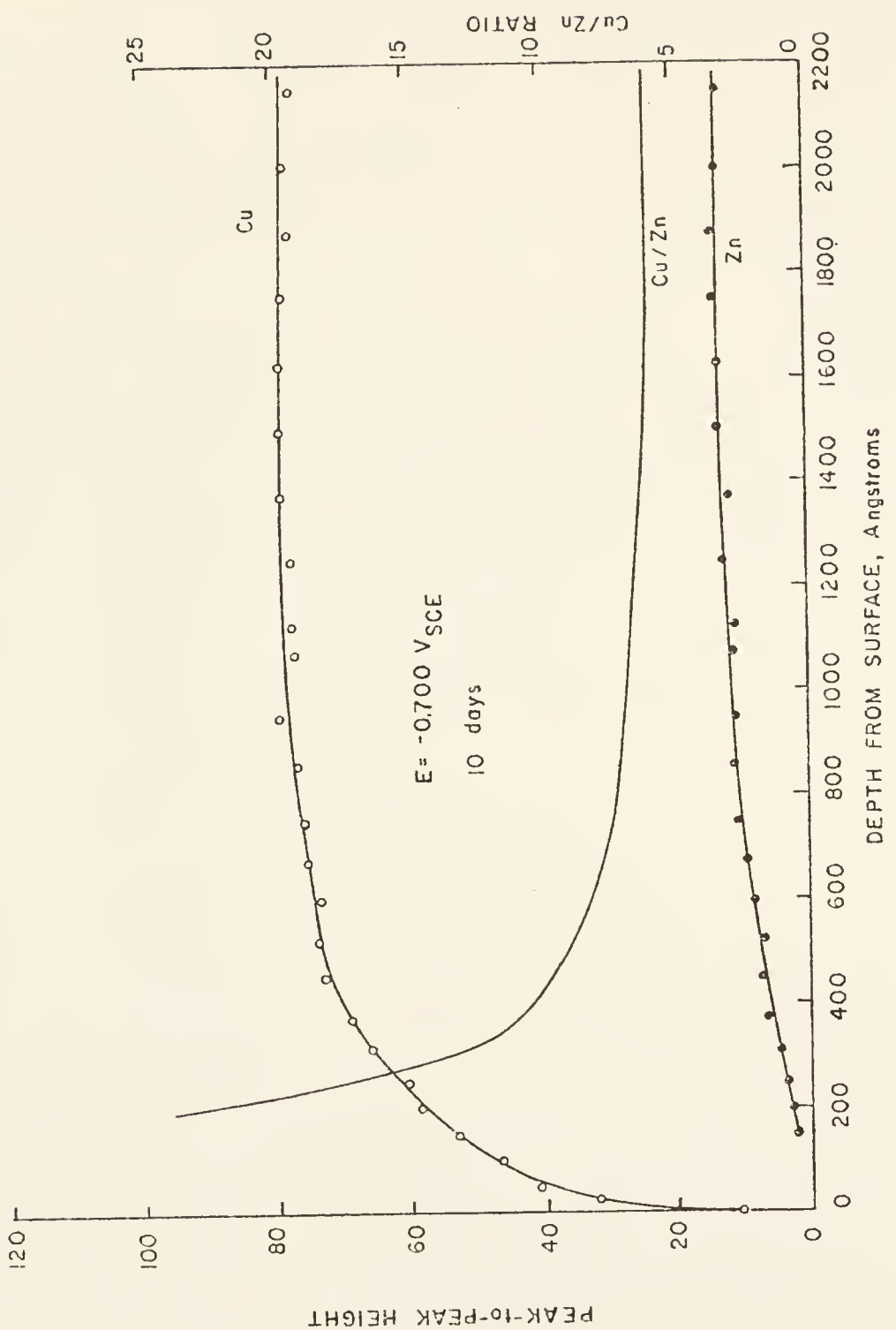

Figure 24d. Auger composition profile obtained from a Cu30Zn sample potentiostated at -0.700 V_{SCE} for 10 days.

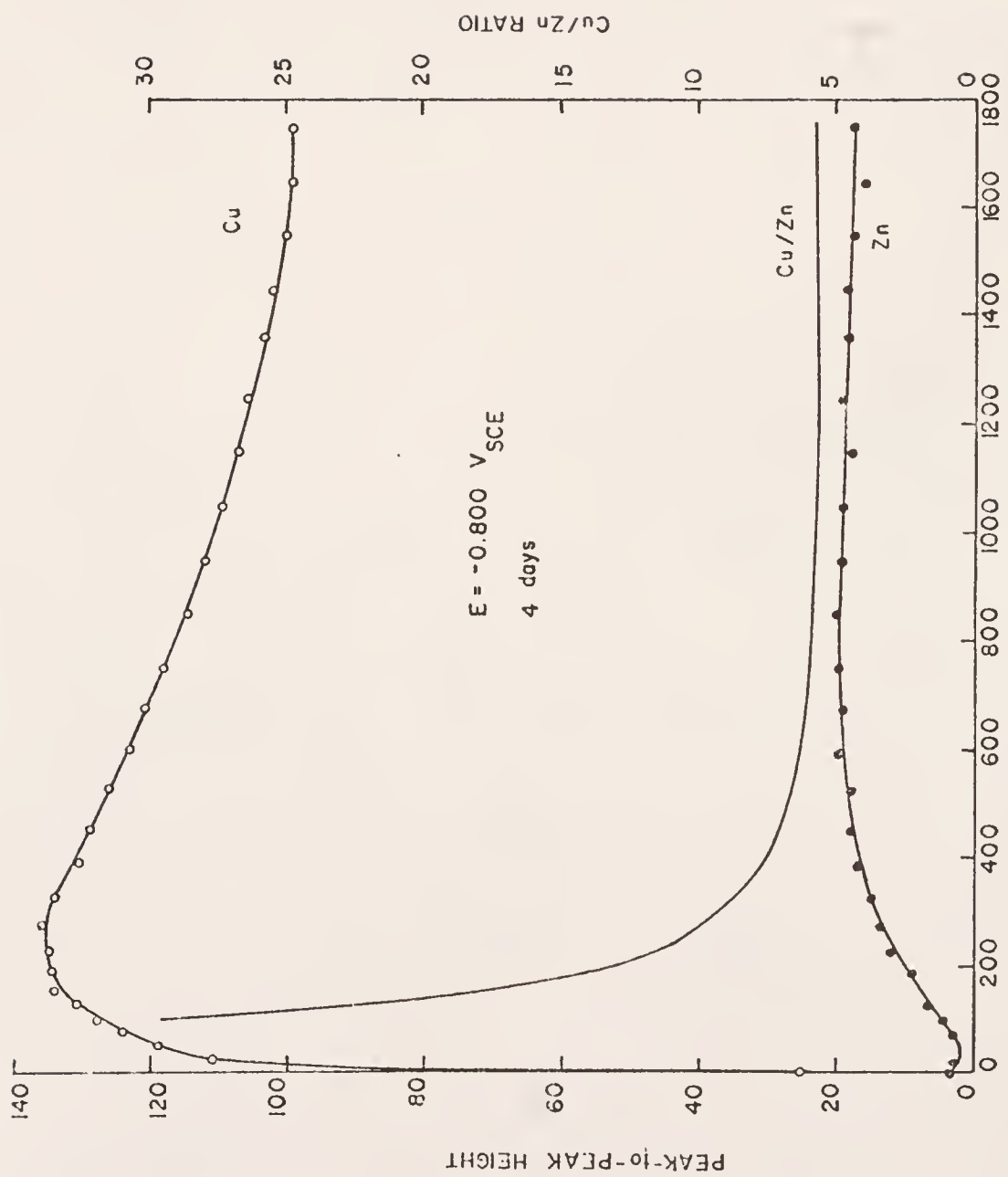

Figure 25. Auger composition profile obtained from a Cu30Zn sample potentiostated at -0.800 V_{SCE} for 4 days.

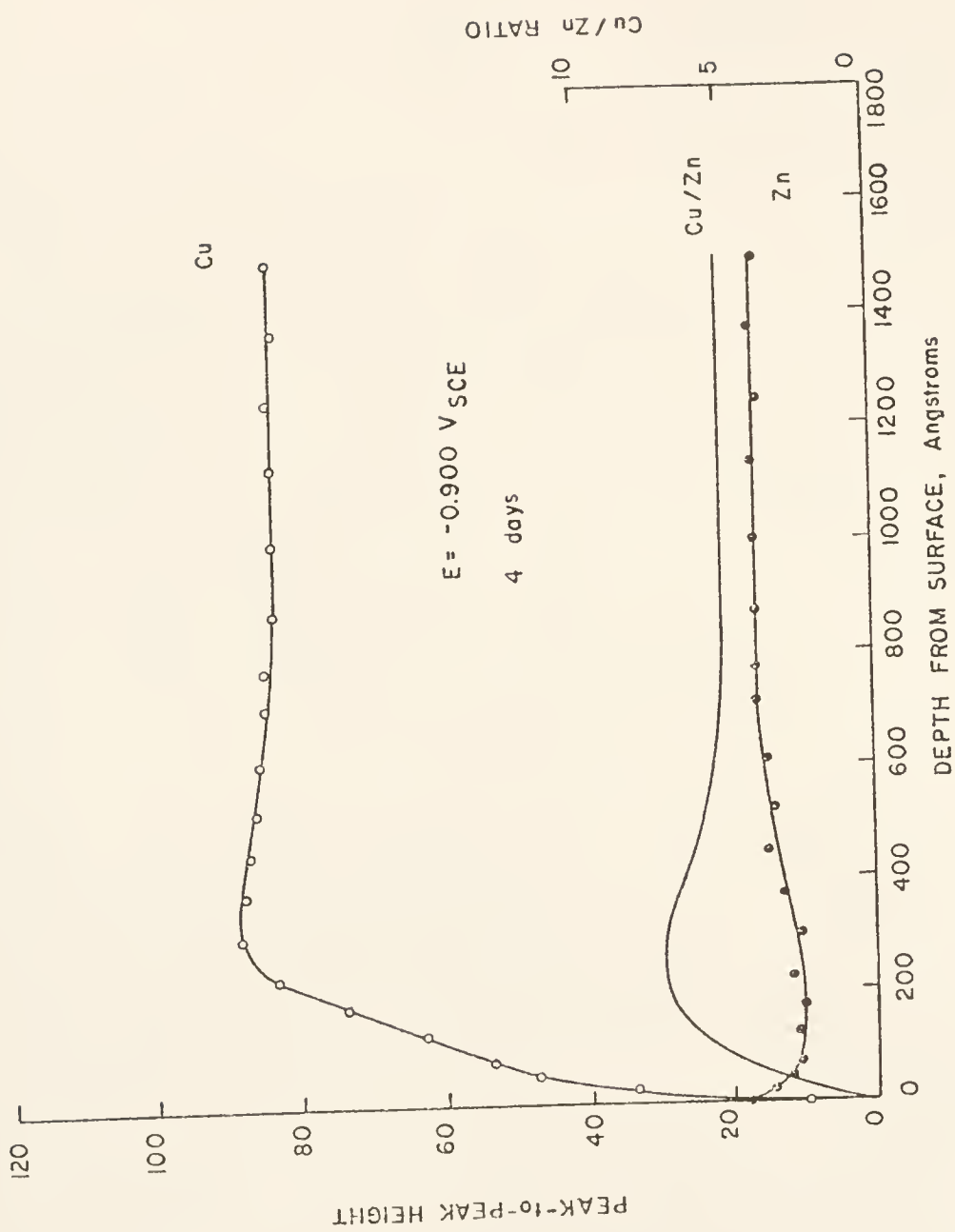

Figure 26. Auger composition profile obtained from a Cu30Zn sample potentiostated at -0.900 V_{SCE} for 4 days.

Consideration of its Cu/Zn ratio curve indicates the surface is enriched in zinc (Cu/Zn ratio < 5). At greater depths from the surface, however, slight depletion of the zinc content is noted.

The decrease in the level of enrichment of copper in the near-surface layers of the Cu30Zn sample potentiostated at -0.900 V_{SCE} is consistent with the solution analysis results reported in the previous section. Reference to table 2 shows that the current density due to zinc dissolutions drops off significantly at the lower electrode potentials. This behavior is in general agreement with the prediction that propensity for zinc to ionize decreases as its standard electrode potential is approached.

Estimates of the thickness of the zinc-depleted surface layers on the selectively leached Cu30Zn samples are listed in table 3. Reading of these thicknesses directly from the profiles is a somewhat subjective operation. The values listed in table 3 correspond to the depths (measured directly from the composition profile plots) at which the Cu/Zn ratio curves reach constant values. No attempt was made to account for the initial "depths" due to sputtering before the characteristic metal surfaces were reached. Thus, the recorded values probably overestimate true thicknesses of the zinc-leached layers, but the error is believed to be less than 125 Å Angstroms in all cases.

Table 3

Thicknesses of the Zinc-Depleted Surface Layers

Electrode Potential volts (S.C.E.)	Time days	Thickness Angstroms
-0.450	1	500
-0.450	4½	800
-0.450	7	2600
-0.500	4	700
-0.600	4	800
-0.700	2	600
-0.700	4	1600
-0.700	7	1300
-0.700	10	1700
-0.800	4	1100
-0.900	4	700

4.2.5. Diffusion Analysis

An effort was made to determine whether or not the selective leaching of zinc from the Cu30Zn samples proceeds via a volume diffusion process. The set of Auger compositional profiles taken from the Cu30Zn samples potentiostated at -0.700 V_{SCE} for 2, 4, 7, and 10 days was analyzed according to the method outlined below.

A simple infinite diffusion model for transport of zinc from the metal interior to the solution-solid interface is outlined schematically in figure 27. Zinc atoms diffuse in one dimension normal to the planar Cu30Zn surface. Initially, the composition of zinc is uniform throughout the Cu30Zn. The dissolution of zinc atoms arriving at the surface is considered to be very fast, so that their concentration at the surface is virtually zero. Thus the boundary conditions can be stated as

$$C_{Zn} = 0, \quad \text{for } x = 0, \text{ at } t > 0 \qquad (14a)$$

$$C_{Zn} = C^{\circ}_{Zn} \text{ for } x > 0, \text{ at } t = 0 \qquad (14b)$$

where C_{Zn} is the mole fraction of zinc atoms at any x and t, and C_{Zn} (= 0.295) is the mole fraction of zinc in the Cu30Zn alloy. The solution to the diffusion equation for these conditions is given by (75)

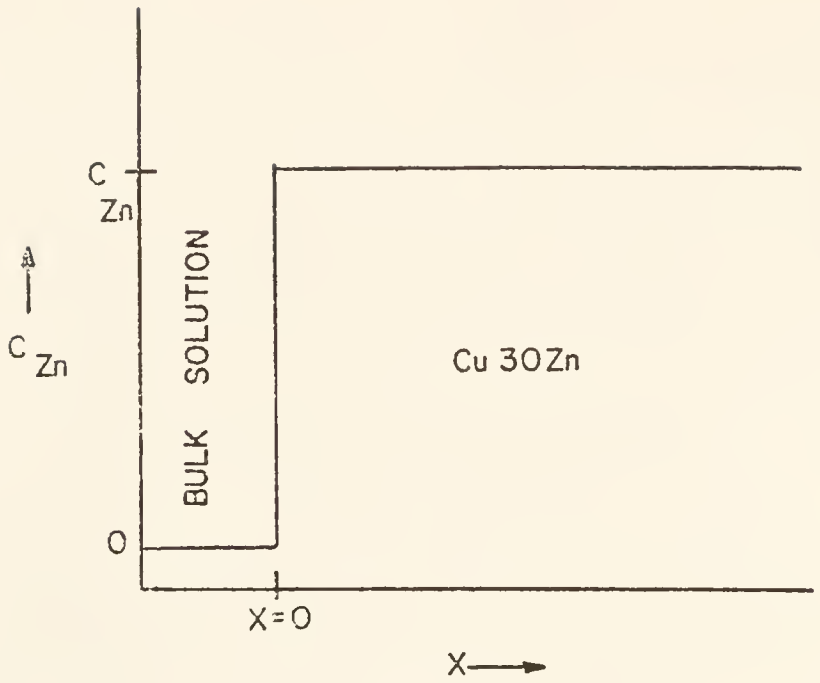

Figure 27. Infinite diffusion model used in zinc diffusion analysis.

$$C_{Zn} = C^{\circ}_{Zn} \text{ erf} \left(\frac{x}{2\sqrt{Dt}} \right) \tag{15}$$

where the interdiffusion coefficient D is assumed to be independent of composition and location.

For the binary Cu30Zn alloy, the mole fraction of copper is given by

$$C_{Cu} = 1 - C_{Zn} \, . \tag{16}$$

The ratio, N, of the mole fractions of copper to the mole fraction of zinc is given by

$$N = \frac{1 - C_{Zn}}{C_{Zn}} \, . \tag{17}$$

Each value of N corresponds to a unique Cu-Zn alloy composition. The relationship between brass compositions lying between 10 and 30 w/o zinc and the Cu/Zn ratios measured by AES for these compositions was defined in figure 8. Thus, each point on the Cu/Zn ratio curves, reported for the selectively leached Cu30Zn samples in the previous section, can be unambiguously associated with a single value of N.

Substitution of equation (15) into equation (17) gives after rearrangement

$$\text{erf} \left(\frac{x}{2\sqrt{Dt}} \right) = \frac{1}{C^{\circ}_{Zn}(1 + N)} \, . \tag{18}$$

Further arrangement gives

$$x = 2K\sqrt{Dt} \tag{19}$$

where K is given by

$$K = \text{erf}^{-1}\left[\frac{1}{C^{\circ}_{Zn}(1 + N)}\right] . \tag{20}$$

Taking logarithms,

$$\log x = \log (2K\sqrt{D}) + 1/2 \log t . \tag{21}$$

Equation (21) relates the depth x at which a certain zinc concentration (defined by K and, hence, N) would be detected in a Cu30Zn sample exposed under selective leaching conditions for time t. If the selective leaching process is diffusion-controlled, then for each value of N, a plot on logarithmic coordinates of the depth of zinc depletion (corresponding to that value of N) versus the time of exposure should yield a straight line of slope = 1/2. Further, the intercept on the log x - axis at t = 1 should be $2K\sqrt{D}$.

Data from the Cu/Zn ratio curves measured for each of the four -0.700 V_{SCE} samples were analyzed for three values of N, corresponding to 25, 20, and 15 w/o of zinc. Cu/Zn ratios measured for each composition value were taken from figure 8. The depth at each time of exposure corresponding

to the Cu/Zn ratios were read from the Auger composition profiles. The data are summarized in table 4.

Figure 28 shows the data plotted on log-log coordinates. The data points have been fitted to lines of slope = 1/2. Fair agreement between the data and the predicted slope of 1/2 is noted. Extrapolation of the lines to the ordinate at time = 1 day yields intercepts of 135, 180, and 215. These intercepts are related to the diffusion coefficient D by

$$\text{intercept} = 2\sqrt{D}\ \text{erf}^{-1}\left[\frac{1}{C^{\circ}_{Zn}(1 + N)}\right] . \qquad (22)$$

Substitution of the measured intercepts into equation (22) yields values of D of about 2×10^{-17} cm^2/sec.

The values of the diffusion coefficient measured above are considerably higher than diffusion coefficients extrapolated to the test temperature (89°C) from high temperature diffusion data. For example, Anusavice and DeHoff (76) have measured tracer diffusion coefficients for zinc in Cu30Zn at temperatures between 700 and 902°C. Extrapolation of these values to 89°C gives a diffusion coefficient of about 4.5×10^{-25} cm^2/sec. Substitution of this value into equation (19) predicts the depth of zinc depletion (to a level equivalent to 25 w/o Zn) of 4×10^{-2} Ångstroms after 4 days' exposure. It is apparent from this

Table 4

Summary of Diffusion Analysis Data

	Time of Exposure days	Depth of Zinc Depletion Angstroms
w/o Zn = 25	2	290
Cu/Zn ratio = 7.9	4	480
N = 3.08	7	540
	10	650
w/o Zn = 20	2	230
Cu/Zn ratio = 9.4	4	370
N = 4.10	7	470
	10	480
w/o Zn = 15	2	180
Cu/Zn ratio = 11.5	4	300
N = 5.85	7	390
	10	350

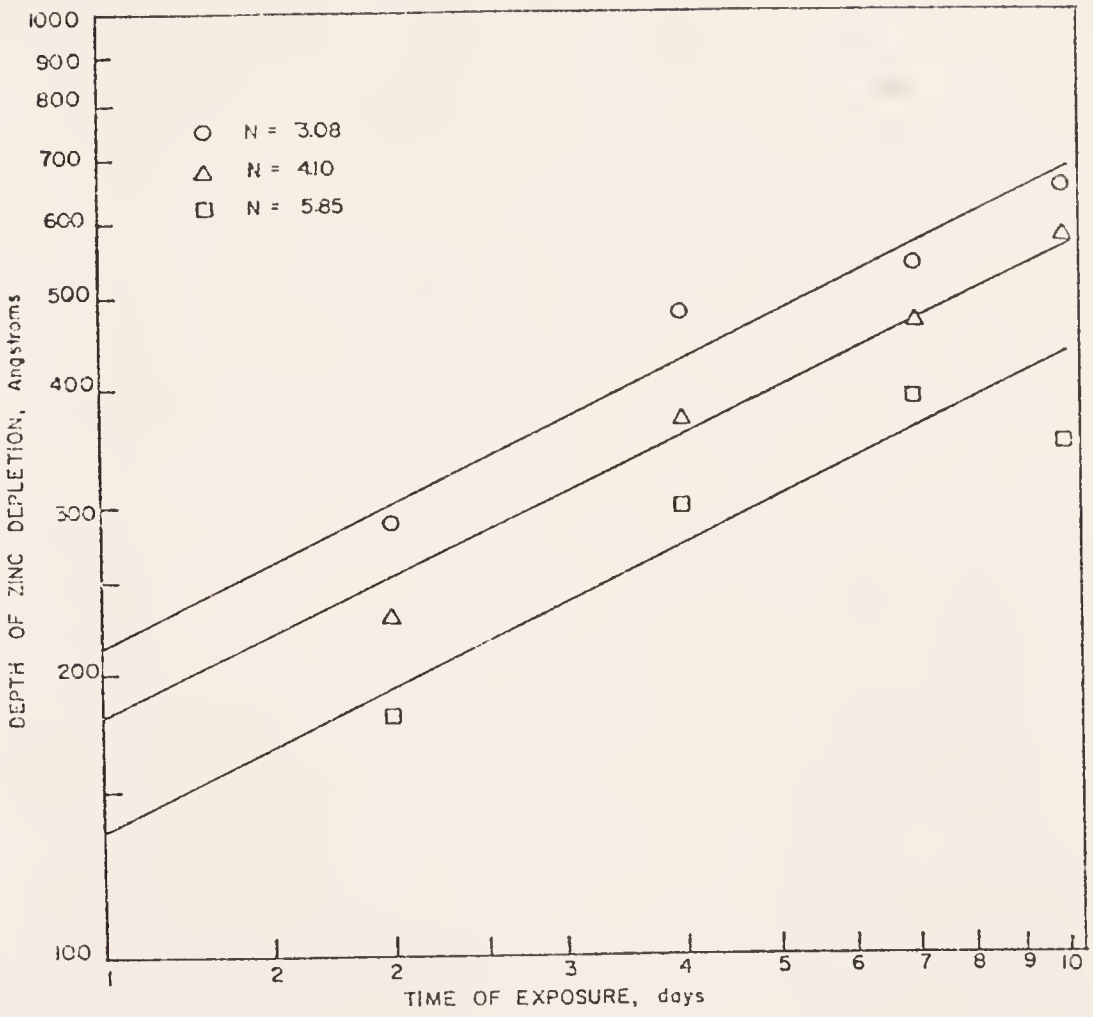

Figure 28. Log-log plot of the zinc diffusion data taken from composition profiles obtained by AES from Cu30Zn samples selectively leached at -0.700 V_{SCE}.

calculation that the amount of selective leaching measured on Cu30Zn alloy samples in this investigation cannot be accounted for by simple volume diffusion of zinc based on extrapolated diffusion coefficients.

The contributions to volume diffusion made by short circuit diffusion paths at ambient temperatures are not well characterized. Small angle grain boundaries, subgrain boundaries and dislocations are all considered to provide faster paths for low temperature transport than does volume diffusion (16). However, an important feature of these paths is normally overlooked. This is the fact that they act only as conduits for atoms which must be supplied by volume diffusion. As an example, a dislocation pipe can conduct to the solid-solution interface only those atoms which are capable of diffusing to it from its immediate surroundings. Thus, unless the metal structure is unusually concentrated in these features (not the case in this investigation), then their contributions to the total diffusion rate cannot be significantly larger than the volume diffusion contribution.

Enhancement of volume diffusion by the injection of excess vacancies and divacancies into the near-surface metal layers has been proposed by Pickering and Wagner (16). Details of the model were discussed in section 2.2. Based on the authors' published calculations, such a mechanism could well be involved in interpretation of the results reported

in this investigation. However, the validity of the mechanism remains in question (17) and awaits experimental justification that excess vacancies and divacancies can be easily introduced into the lattice at ambient temperatures.

Surface diffusion of mobile atoms on the solid surface has received relatively little attention. Feller (25) has proposed that diffusion and agglomeration of more noble atoms on the surface could act, in a manner similar to surface roughening, to expose fresh alloy surface to the solution. It is difficult to imagine that this mechanism could operate without producing surface roughening of a scale at least as large as the depth of diffusion-affected layer. No surface roughening of this magnitude was detected in connection with the selective leaching produced in this investigation.

4.2.6. Summary

Selective leaching of zinc from the Cu30Zn occurs under the conditions of electrode potential predicted by Verink and Heidersbach (18). The rate of zinc dissolution at each electrode potential level is approximately constant, at least for times up to 4 days. The magnitudesof the zinc dissolution currents are comparable to those found in an earlier investigation (20).

The thicknesses (measured by Auger electron spectroscopy) of the surface layers depleted in zinc average about 800 Ångstroms after 4 days' exposure. The mechanism by which zinc atoms are transported to the solid-solution interface is diffusional in nature. The mechanism apparently involves enhanced volume diffusion.

4.3. Dealloying of Cu30Zn by Dissolution and Replating

The results of experiments presented in section 4.2. indicated the validity of the selective leaching mechanism in producing dezincification of Cu30Zn. It is evident, however, that the slowness with which that mechanism operates eliminates it as the culprit in the majority of dezincification failures.

In this section, the results of investigations into the operation of the dissolution and replating mechanism of dezincification are described. Particular emphasis is placed on the equilibria governing the dezincification of Cu30Zn in chloride-containing environments.

4.3.1. Conditions of Exposure

Construction of an experimental potential versus pH diagram for Cu30Zn in 0.1M chloride solutions was described in section 4.1.3. A simplified version of this diagram is presented in figure 29. The predictions of Verink and

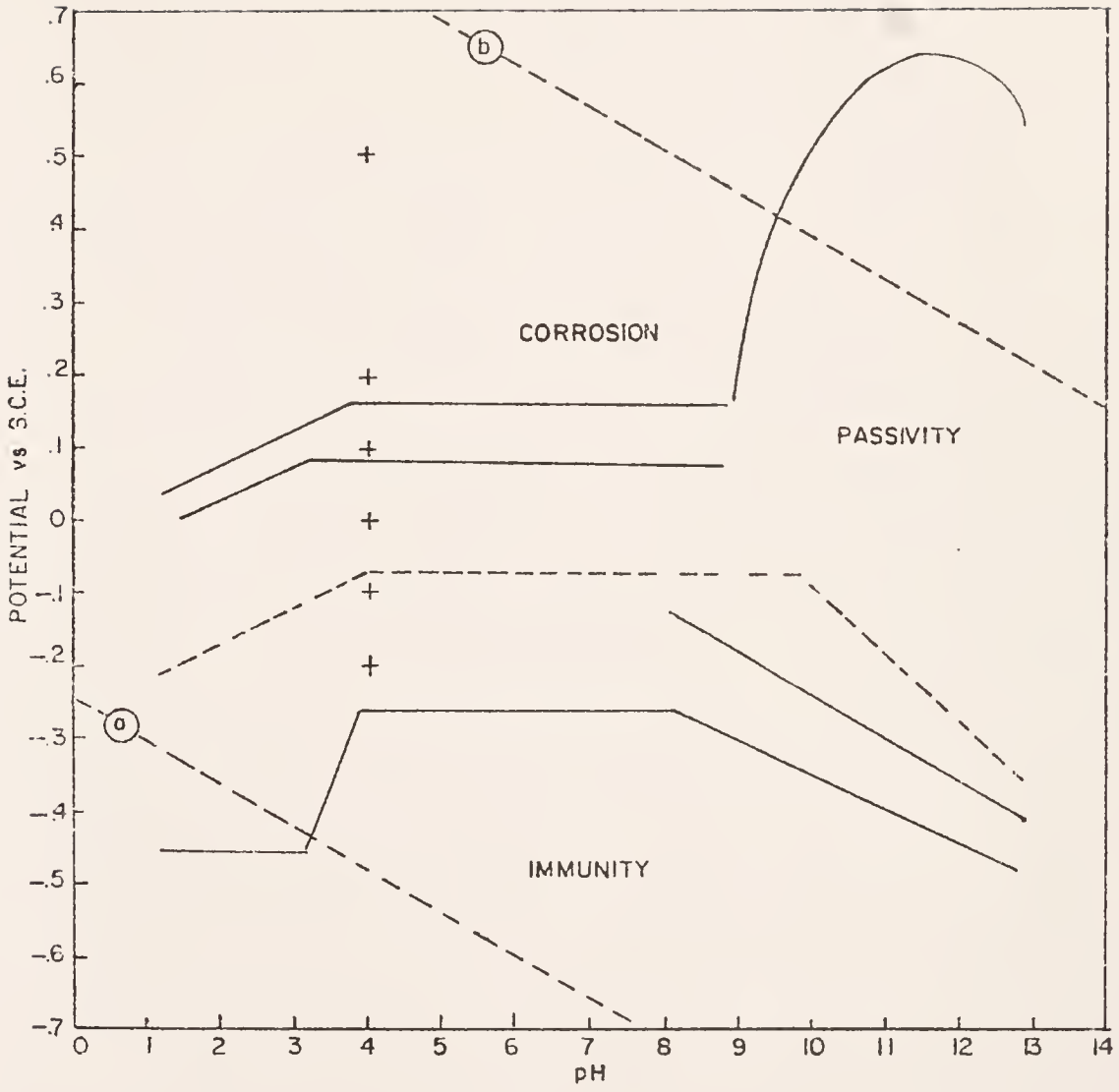

Figure 29. Simplified potential versus pH diagram for Cu30Zn in 0.1M chloride solutions outlining conditions of exposure for controlled anodic dissolution experiments.

Heidersbach (18) concerning the conditions of electrode potential which favor dezincification by dissolution and replating in this system were outlined in section 2.2. Referring to figure 29, the range of electrode potentials which favor dezincification in acid and neutral chloride solutions is bounded by the protection potential and the corrosion potential. At electrode potentials more noble than the protection potential, only complete dissolution of the alloy was predicted. These predictions were taken as the basis for a series of controlled anodic dissolution experiments conducted in stirred, nitrogen-saturated 0.1M chloride solutions of pH 4. The electrode potential conditions employed during these experiments are indicated by crosses on figure 29.

4.3.2. Results of Controlled Anodic Dissolution Experiments

The results of the controlled anodic-dissolution experiments on Cu30Zn in pH 4, 0.1M chloride solutions at 30°C are presented below in order of ascending electrode potential. Monitoring of the copper and zinc contents of the solutions during each experiment was undertaken to gain some insight into the equilibria operating under the conditions of exposure. The results of solution analysis are presented along with the other experimental results for experiments conducted at each electrode potential. Detailed interpretation of the solution analysis results will be presented subsequently. Details of the experimental procedure appear in section 3.3.

Three experiments were conducted at -0.200 V_{SCE}. Times of exposure were 3, 7, and 13 days. All three samples were observed to undergo crystallographic etching, an example of which is pictured in figure 30. No corrosion products could be detected on the sample surfaces by either visual or SEM examination. No reddening of the exposed surfaces was noted during the course of the experiments. However, a small region of dezincification was found on the 13-day sample, located beneath a section of the stop-off lacquer adjacent to the etched surface.

It must be noted that the dezincification described on the Cu30Zn samples exposed under anodic conditions is quite different in appearance than that resulting from selective leaching under cathodic conditions. In the latter cases, the exposed sample surfaces underwent slow, uniform changes in color from the characteristic yellow of the Cu30Zn alloy towards pink or red. Dezincification produced under anodic conditions develops very quickly, with an abrupt change in color (which is readily seen with the unaided eye), and often occurs only locally.

The concentrations, in ppm, of copper and zinc found by atomic absorption analysis of the solutions from the 7-day and 13-day experiments are illustrated in figure 31. The results are in general agreement with the observations of etching behavior for the samples. After the first few days of exposure, the amounts of copper and zinc in solution were

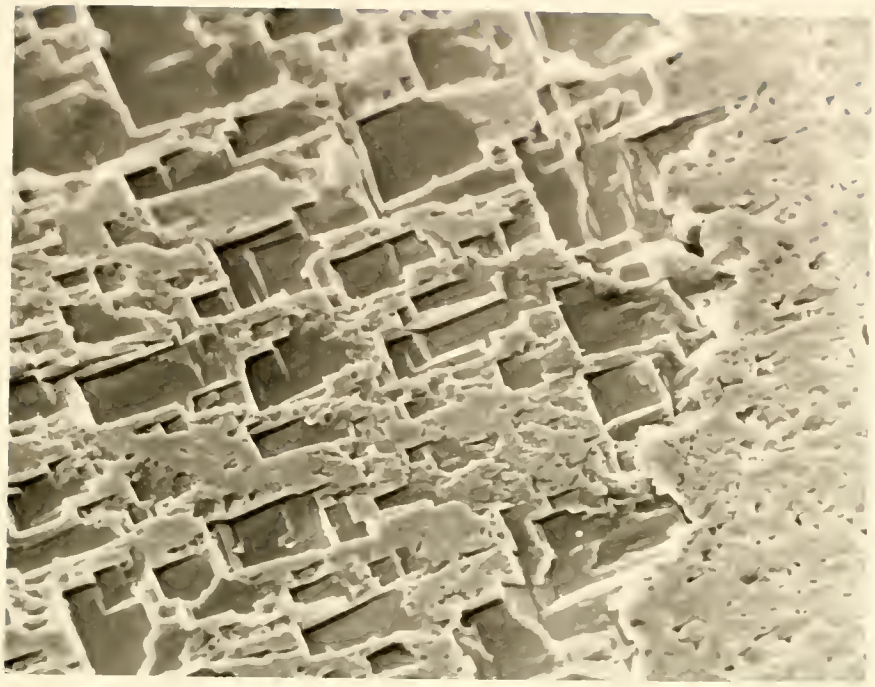

Figure 30. Etched surface of a Cu30Zn sample potentiostated 13 days at -0.200 V_{SCE} in pH 4, 0.1M chloride solution. 1500X

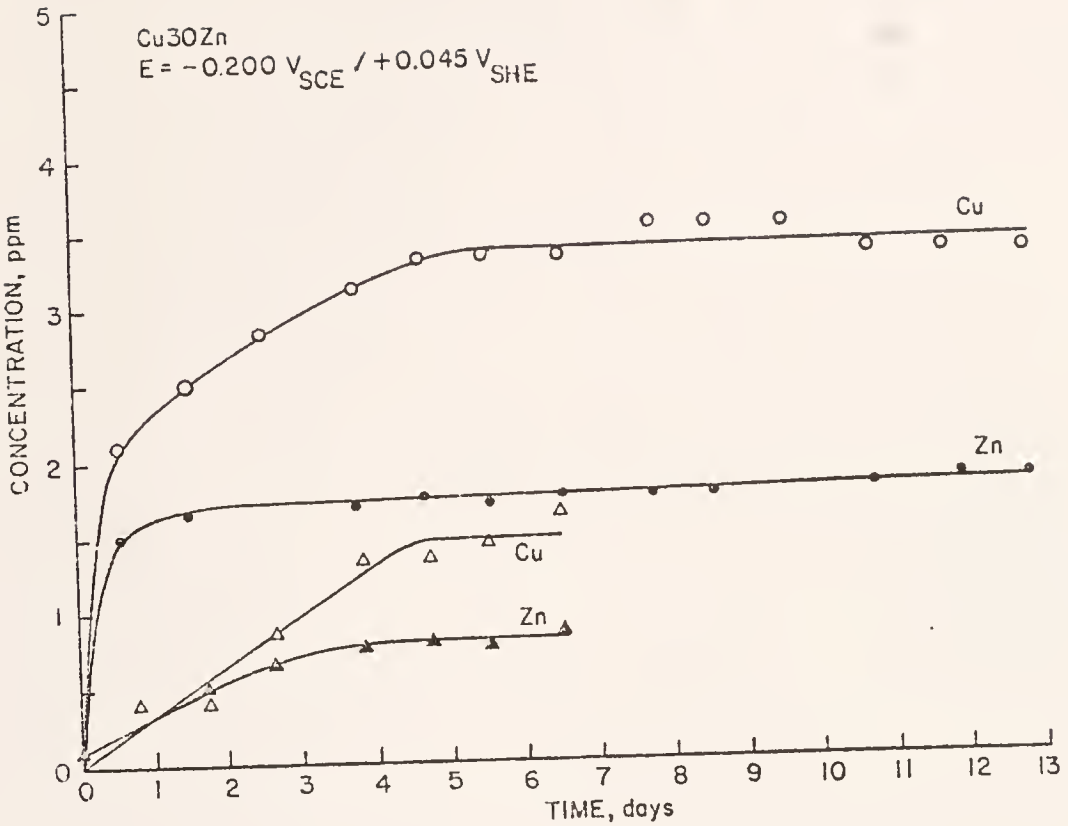

Figure 31. Curves showing the concentrations of copper and zinc present in solution during dissolution of Cu30Zn at -0.200 V_{SCE}.

roughly proportional to their respective concentrations in the Cu30Zn alloy. Assuming simultaneous dissolution of the alloy, the ratio of copper (in ppm) to zinc (ppm) dissolved in solution is expected to be 7/3 = 2.33. Referring to figure 31, it is evident that proportionately more zinc than copper entered solution during the first few days of dissolution. It is assumed that this initial disproportionate dissolution of zinc from the Cu30Zn samples influenced the zinc concentrations measured at later times during the experiments, thereby causing the apparent ratios of dissolved copper to zinc to be somewhat lower than 2.33. This observation is supportive of published results showing preferential dissolution of zinc from alpha brasses in acid sulfate solutions, followed by simultaneous dissolution (20, 38).

After about five days' exposure the measured concentrations of copper and zinc reached constant values less than 4 ppm. No subsequent increases in the concentrations of either metal in solution were noted.

Two experiments conducted at -0.100 V_{SCE} for 6 days and 10 days, respectively, gave results similar to those described above for the -0.200 V_{SCE} experiments. Both samples were observed to undergo crystallographic etching with no formation of visible solid corrosion products. On about the fourth day of exposure, however, a band of dezincification was observed forming around the edges of the exposed

surface of the 10 day-sample, adjacent to and beneath the stop-off lacquer. The exposed area of the sample showed no signs of dezincification (i.e., no reddening). On the ninth day of the experiment, small, discrete crystals of copper were observed forming on the etched surface.

SEM examination of the etched surface revealed a highly pitted surface structure, shown in figure 32a. Two of the copper crystals observed forming on the surface are visible in the photograph, and are marked by arrows. The smaller of the two crystals can be seen clearly to have formed at a triple point where three grain boundaries intersect the surface.

Another of the copper crystals is detailed in figure 32b. This crystal was formed in the shape of a tetrahedron, the vertical edges of which are apparent artifacts of the original brass grain boundaries. Similar ridges on several crystals were observed to be continuous with the brass grain boundaries upon which the crystals were situated. The copper character of the crystals was confirmed by nondispersive X-ray analysis.

A polished cross-section through one of the crystals is shown in figure 32c. It is apparent that dezincification attack has taken place beneath the initial copper deposit. Furthermore, the more dense parts of the dezincified structure are coincident with the brass grain boundaries which intersect the dezincified structure.

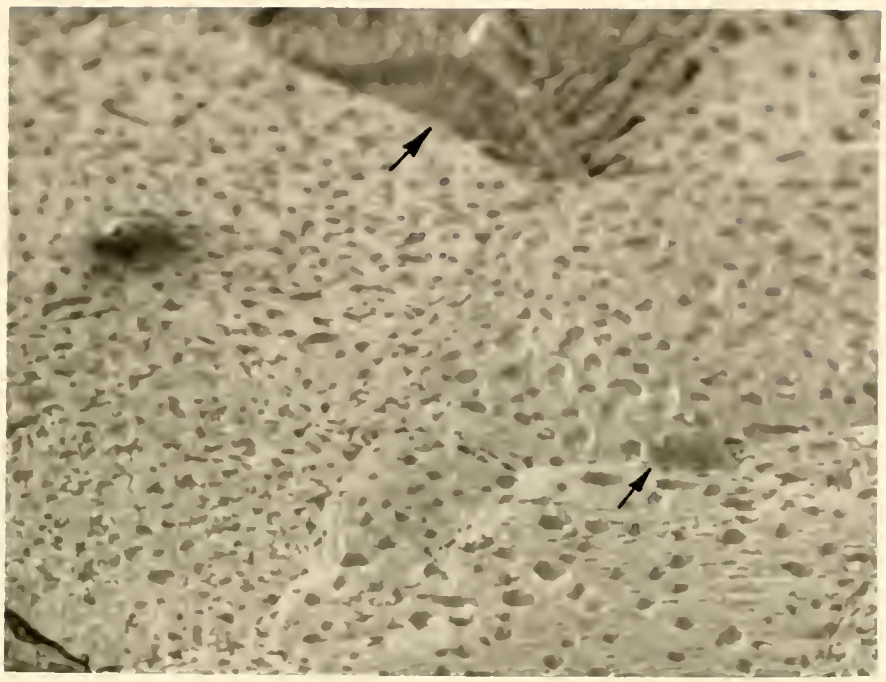

Figure 32a. Pitting observed on etched Cu30Zn sample exposed 10 days at -0.100 V_{SCE}. Two copper crystals formed on the surface are marked by arrows. 125X

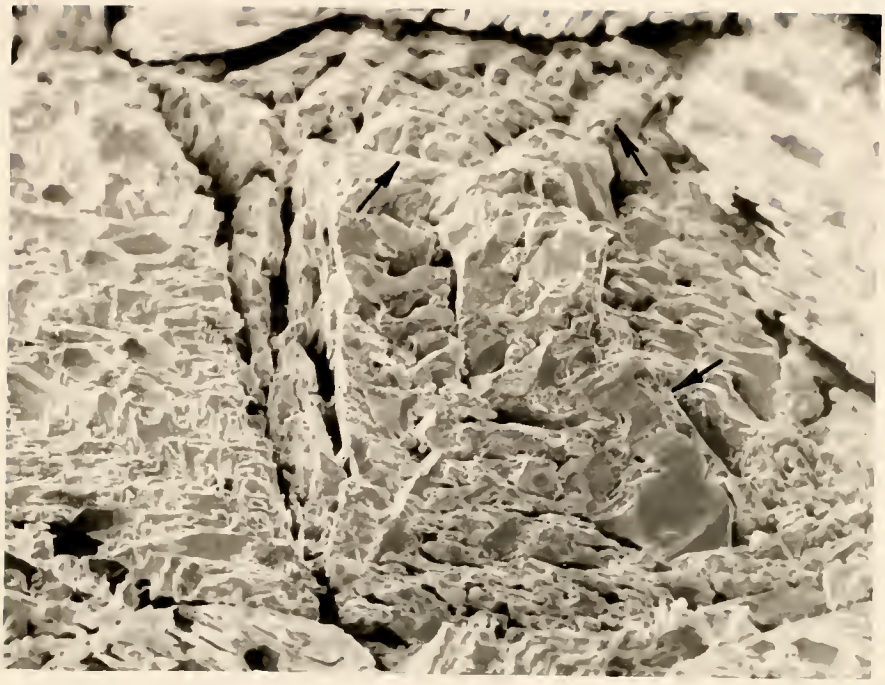

Figure 32b. Detail of one of the crystals found on the sample described in figure 32a. The tetrahedral shape is outlined in the accompanying sketch. 300X

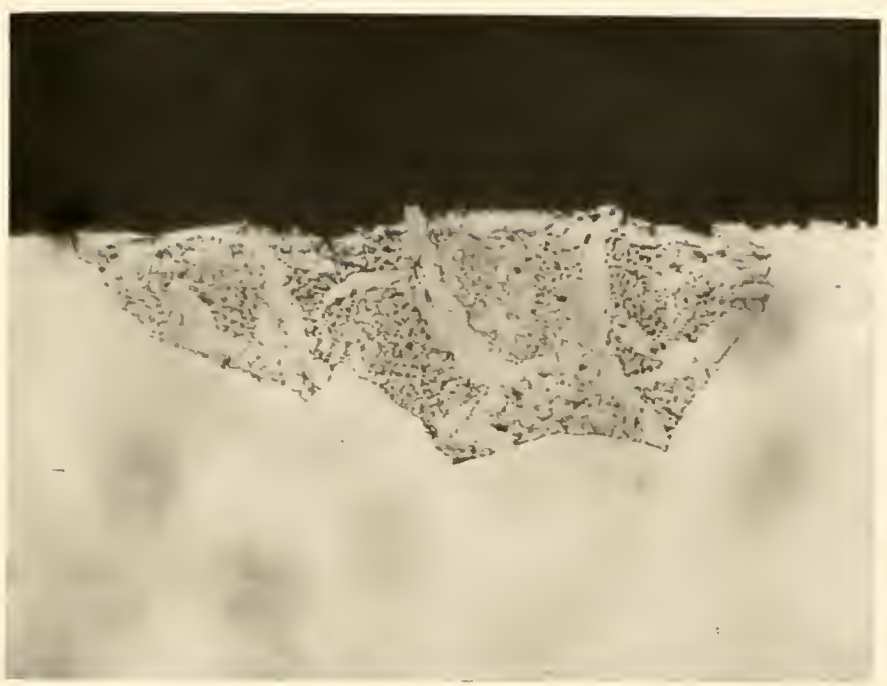

Figure 32c. Cross section of one of the copper crystals detailing the Cu30Zn grain boundary artifacts visible in the dezincified structure. 75X

The results of solution analysis for the 10-day sample, figure 33, reflect some of the observations described above. Initially, when only etching was observed, copper and zinc entered solution at rates proportional to their respective amounts in the Cu30Zn alloy. However, after three days' exposure (approximately the time at which dezincification around the edges of the sample bacame evident), the concentration of zinc in the solution began a drastic increase. The measured amount of copper reached a plateau value after about 7 days. It was on the ninth day of the experiment, after the concentration of copper in solution had reached a level of "saturation," that copper crystals were observed forming on the sample surface.

The large increase in the zinc concentrations measured after dezincification was observed on the sample is significant when viewed in terms of the dissolution and replating mechanism. For simultaneous dissolution of the Cu30Zn alloy, the rate of zinc dissolution can be taken as proportional to the total alloy dissolution rate. Referring to figure 33, the increase in the dissolution rate (ppm/day) of zinc from the Cu30Zn sample measured after dezincification had begun denotes an increase of the total alloy dissolution rate in the dezincifying areas. The expected corresponding increase in the copper content of the solution was not realized. Apparently, the major amount of copper dissolved was plated-out of solution to form residual dezincified structure.

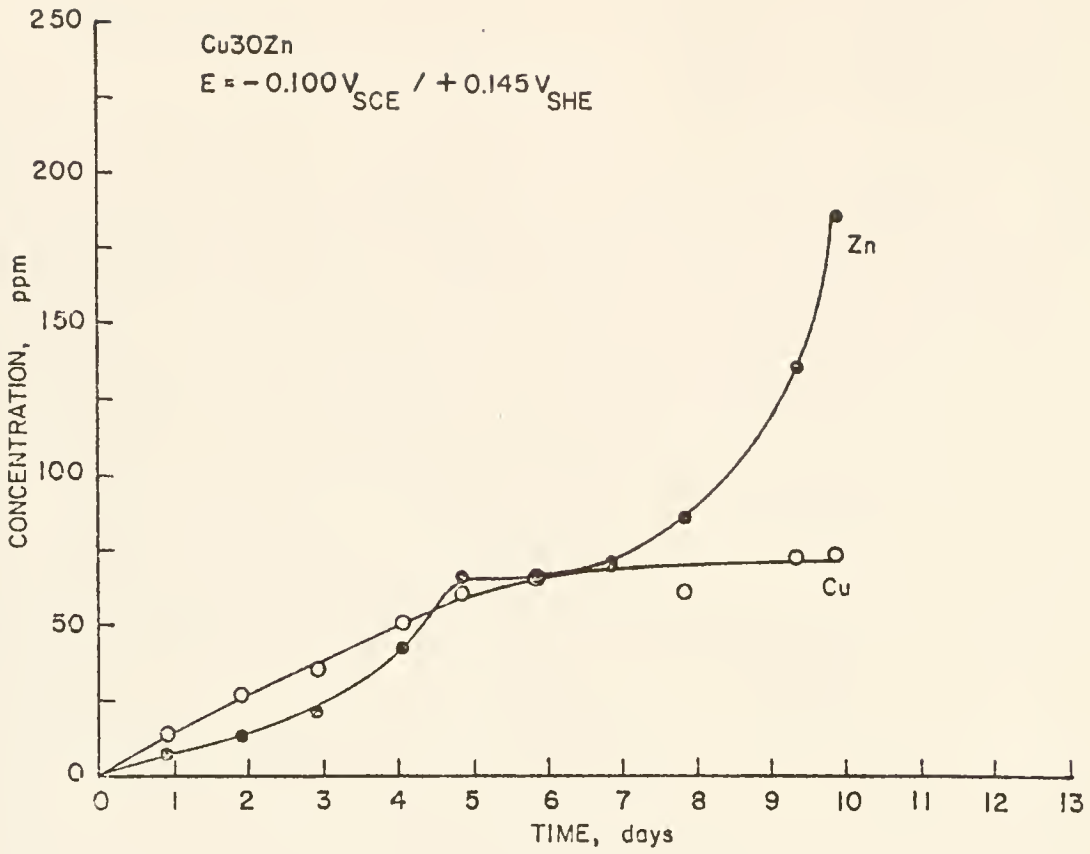

Figure 33. Concentrations of copper and zinc measured in the solution of a cell containing a Cu30Zn sample polarized 10 days at -0.100 V_{SCE}.

Thus, it is evident that the conditions which fostered dezincification in this instance also caused local increases in the dissolution rate of the brass.

Cu30Zn samples exposed at 0.000 V_{SCE} exhibited behavior very different from that exhibited by samples exposed at more active electrode potentials. Three experiments were conducted at this potential, for 3, 7, and 13 days, respectively. Immediately upon polarization, the exposed surfaces took on a uniform dull-red color indicative of dezincification occurring beneath a permeable, white cuprous chloride (CuCl) layer. Figures 34 and 35 depict the extent of dezincification attack found after 3 days and 13 days, respectively. Referring to figure 34, the attack initially occurred as local "plugs". After 13 days, however, the attack was more uniform in character, figure 35. The presence of a CuCl layer on the sample surface could not be positively demonstrated by X-ray diffraction methods because of its thinness. However, the formation of such a layer on the brass surface at this value of electrode potential is consistent with the polarization data presented in section 4.1.3.

The results of solution analysis for the 7- and 13-day experiments at 0.000 V_{SCE} are plotted in figure 36. For both experiments, the copper concentrations measured in solution reached plateau values between 200 and 300 ppm while the zinc concentrations continued to increase. It is

Figure 34. Dezincification noted on a Cu30Zn sample exposed 3 days at 0.000 V_{SCE}. 1000X

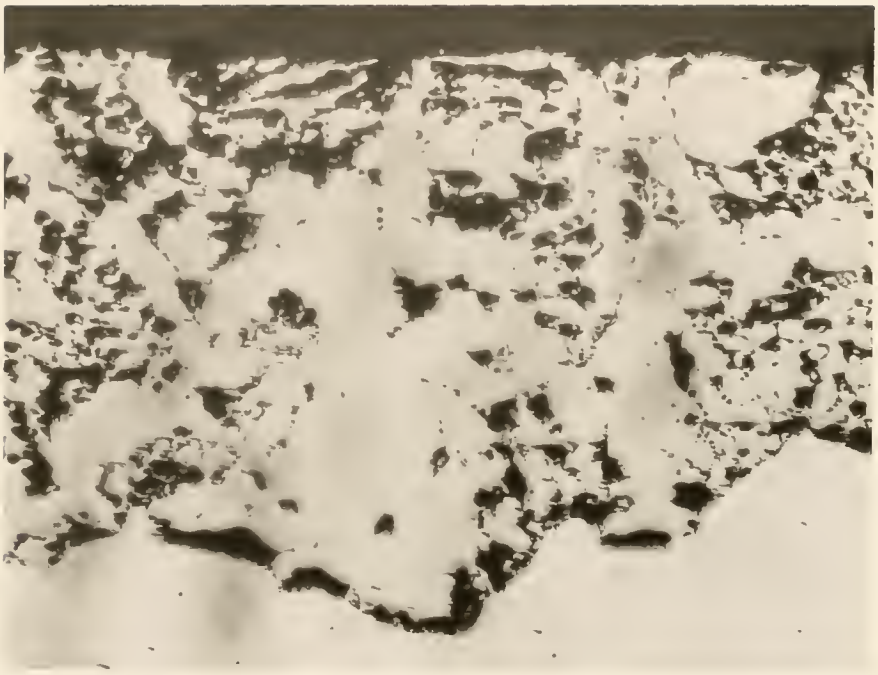

Figure 35. Dezincification noted on a Cu30Zn sample exposed 13 days at 0.000 V_{SCE}. 60 X

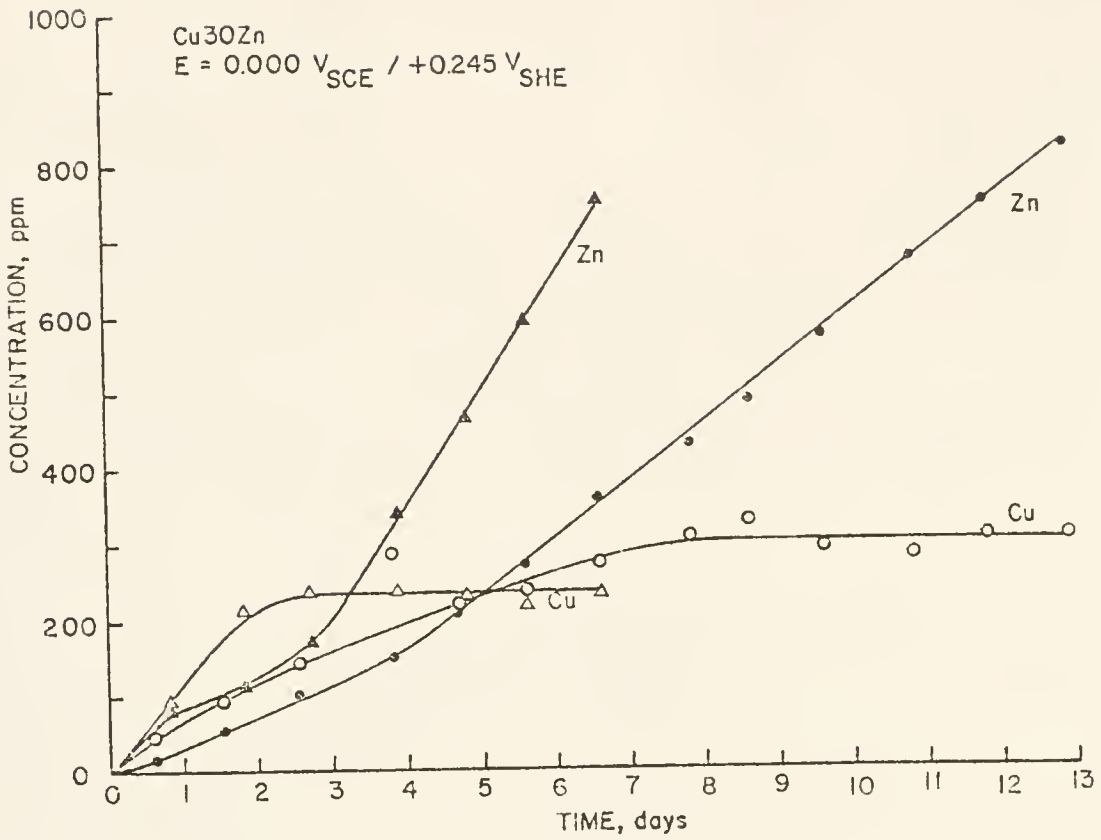

Figure 36. Results of solution analysis of Cu30Zn samples potentiostated at 0.000 V_{SCE} for 7 days and 13 days.

clear that rapid increases in the zinc content of the solutions without corresponding increases in their copper concentrations are indicative of accelerated dissolution of the underlying brass accompanied by dezincification. The significance of the increases in the plateau concentration of copper with increasing electrode potential will be discussed subsequently.

Results similar to those reported above for the 0.000 V_{SCE} experiments were found for two experiments conducted at +0.100 V_{SCE} for 3 days and 10 days, respectively. The Cu30Zn samples developed the uniform, dull-red appearance characteristic of dezincification occurring beneath a permeable, white CuCl layer. The dezincification, noted after 10 days' exposure, figure 37, can be characterized as generally "uniform".

The results of solution analysis for the 10-day experiment conducted at +0.100 V_{SCE} are plotted in figure 38. Again, the zinc concentration continued to increase while the copper concentration reached a plateau value of approximately 400 ppm. The cause of the increase after 8 days in the copper concentration above the plateau value is unknown.

Three experiments were conducted at +0.200 V_{SCE}, for 3, 7, and 13 days, respectively. All three samples exhibited the same dull-red appearance characteristic of samples exposed at 0.000 V_{SCE} and +0.100 V_{SCE}. Figure 39

Figure 37. Dezincification noted on a Cu30Zn sample exposed 10 days at +0.100 V_{SCE}. 1000X

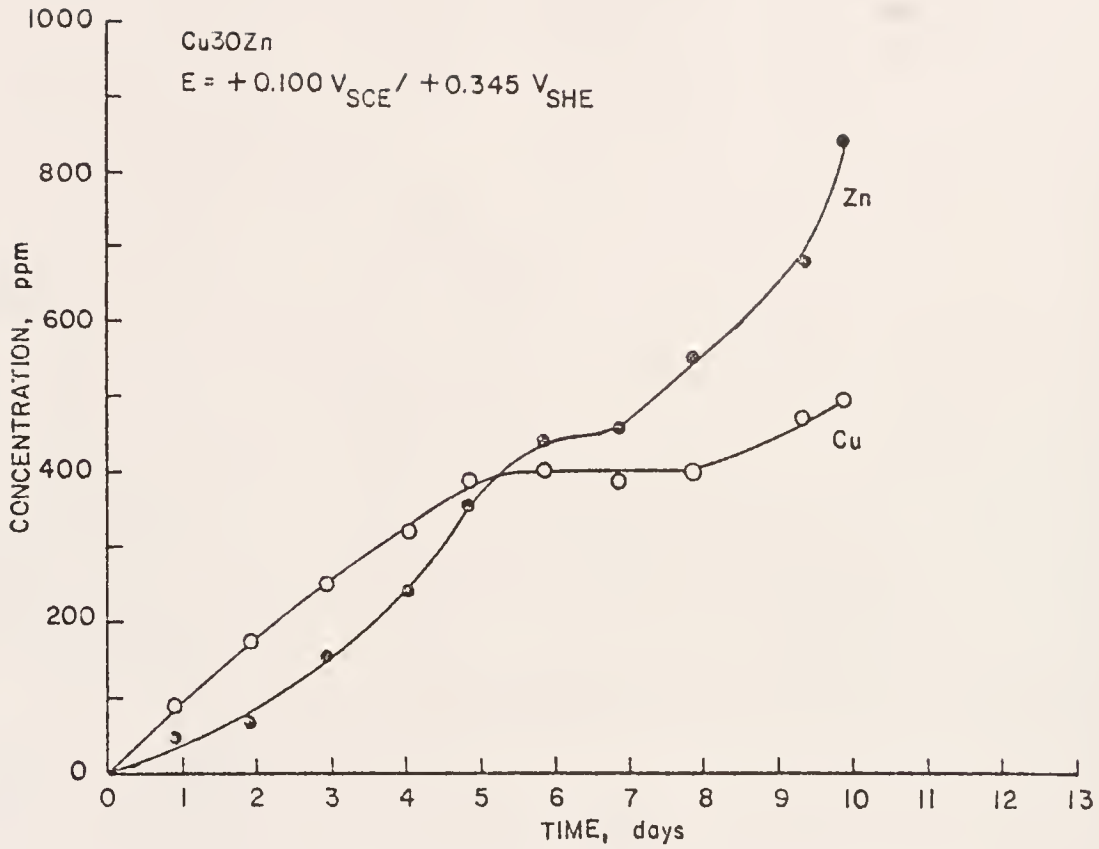

Figure 38. Results of solution analysis for a Cu30Zn sample potentiostated 10 days at +0.100 V_{SCE}.

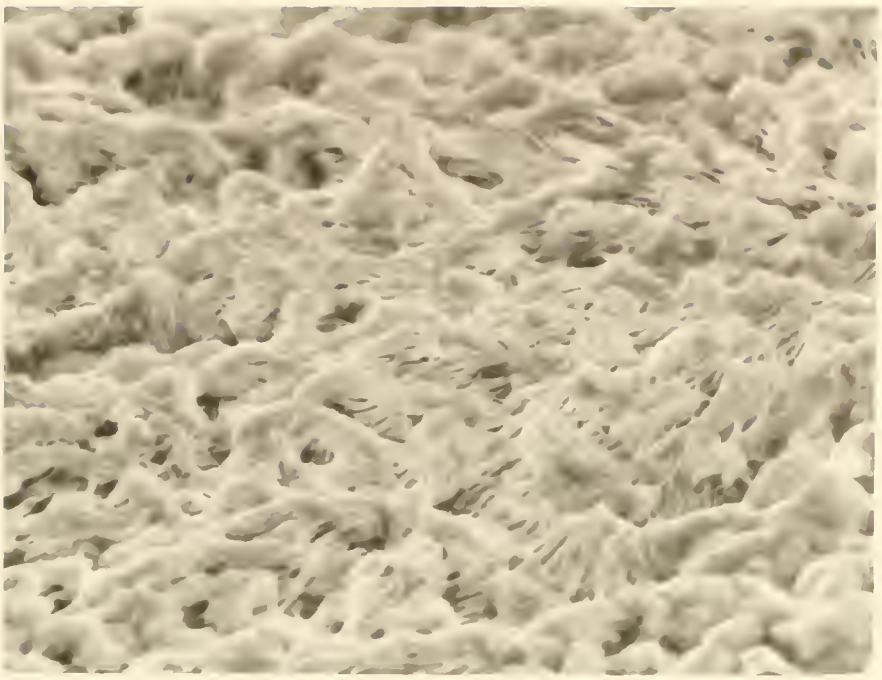

Figure 39. Detail of sample surface of Cu30Zn sample exposed 13 days at +0.200 V_{SCE}, covered by a layer of cuprous chloride. 1500X

details an area on the surface of the 13-day sample, and provides evidence of the physical character of the thin, permeable layer of corrosion product found on many of the samples. Nondispersive X-ray analysis of this area revealed that the principal detectable elements present in the layer were copper and chlorine. Thus the product was assumed to be CuCl.

The results of solution analysis for the 13-day experiment conducted at +0.200 V_{SCE} are plotted in figure 40. The pattern established at more active electrode potentials (i.e., that the copper concentration in solution reaches a plateau value which increases with the level of polarization) is also evident here. At this potential, the copper plateau concentration reached a value in excess of 800 ppm.

The same plateau copper concentration found at +0.200 V_{SCE} was also measured for a 10-day experiment conducted at +0.500 V_{SCE}, figure 41. Two Cu30Zn samples were exposed at this electrode potential, for 3 days and 10 days, respectively. During the course of the experiments, both samples became covered by voluminous green-colored corrosion products identified by X-ray diffraction as paratacamite, $3Cu(OH)_2 \cdot CuCl_{2\gamma}$. The extent of dezincification noted on the 10-day sample, revealed in figure 42, is comparable to that noted on samples exposed at lower electrode potentials.

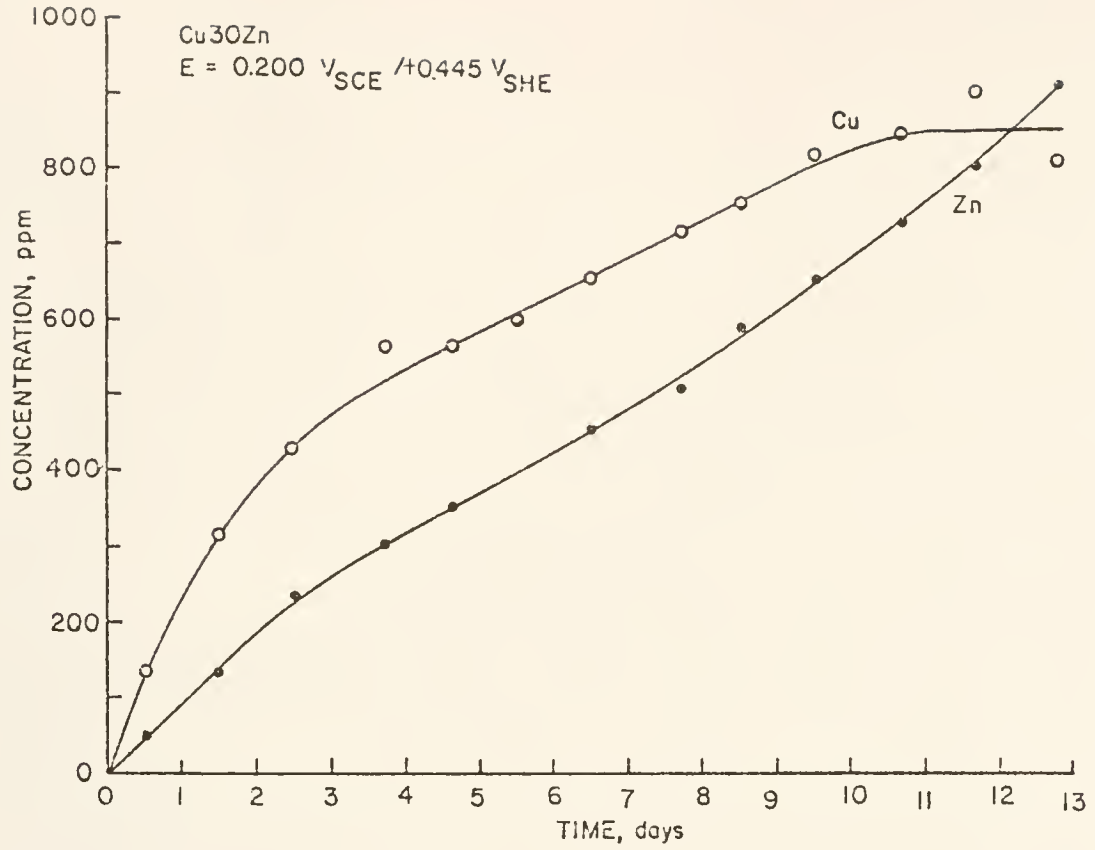

Figure 40. Results of solution analysis for a Cu30Zn sample potentiostated 13 days at +0.200 V_{SCE}.

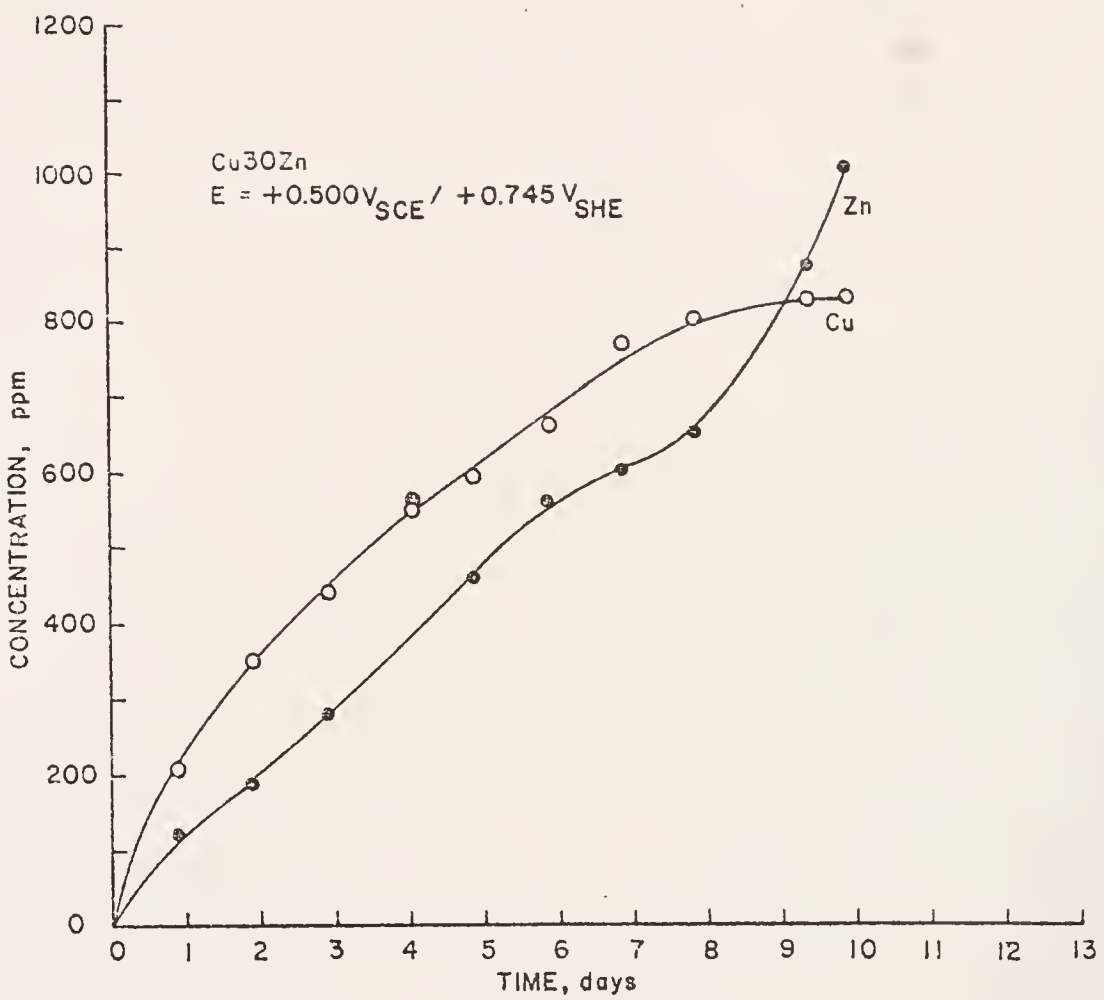

Figure 41. Results of solution analysis for a Cu30Zn sample potentiostated 10 days at +0.500 V_{SCE}.

Figure 42. Extent of dezincification noted on a Cu30Zn sample exposed 10 days at +0.500 V_{SCE}. 60X

The results of this series of controlled anodic dissolution experiments at pH 4 can be summarized as follows.

(1) Cu30Zn samples potentiostated at -0.100 V_{SCE} and -0.200 V_{SCE} underwent crystallographic etching with no visible solid corrosion product formation. This result is in agreement with the report of Taylor (77) that no selective leaching or replating of copper occurs on naval brass polarized to low anodic overpotentials in 0.5M NaCl solution. Nonetheless, dezincification was detected at both of these electrode potential levels. In both cases the dezincification was associated with stagnant conditions occurring beneath the edge of the stop-off lacquer. The appearance of copper deposits at triple points on the -0.100 V_{SCE} sample occurred after the concentration of dissolved copper in solution had reached saturation. This saturation condition is equivalent to the stagnant conditions present in the crevice formed between the non-adhering stop-off lacquer and the Cu30Zn surface. The resulting copper deposits occurred at triple points, which are among the more active areas on the surface (as are pits, etc.). It is reasonable to assume that the local dissolved copper concentration adjacent to triple points may be slightly greater than the average, and, hence, that copper may deposit preferentially at these locations. Similarly, stagnant conditions were present adjacent to the surface beneath the deposited copper crystals, and dezincification proceeded into those areas. These results are

consistent with the predictions of Verink and Heidersbach (18) that the occurrence of dealloying in this electrode potential region depends on the presence of stagnant conditions.

(2) Cu30Zn samples potentiostated at 0.000 V_{SCE}, +0.100 V_{SCE}, and +0.200 V_{SCE} all underwent dezincification in a more-or-less uniform fashion over their entire exposed surfaces. The attack was observed to initiate long before large concentrations of copper ions were built up in the solutions. In this region of electrode potential, CuCl is the stable solid copper species (see figure 11), and the dullness of the dezincifying surfaces certainly suggests their covarage by thin layers of CuCl. As discussed in section 2.2., the formation of CuCl layers on brass surface has been associated with dezincification (51). It seems plausible that such a layer could act as a crevice, fostering the build-up of locally high copper ion concentrations adjacent to the Cu30Zn surface. The results of dissolved metal analysis of the solutions used in these experiments indicated that the local dissolution rate of the brass was increased in areas where crevice conditions were evident. This action certainly could result in local high copper concentrations.

(3) Cu30Zn samples potentiostated at +0.500 V_{SCE} underwent dezincification attack, and were found to be covered by voluminous corrosion products composed, at least partially, of paratacamite. Again it is reasonable to assume that the role of the corrosion product in dezincification may be to

produce crevice or occluded cell conditions adjacent to the active brass surface.

The occurrence of dezincification at the four more noble electrode potentials is contrary to the prediction of Verink and Heidersbach that only simultaneous dissolution would occur. Other investigators have noted that no detectable dezincification could be produced on alpha brasses polarized to similar high anodic overpotentials in acid sulfate solutions (20, 24, 38). However, at least one other investigation in acid chloride solutions has demonstrated dezincification of Cu30Zn in this range of electrode potential (78). Thus it seems that the presence of chlorides in solution, and the accompanying solid copper complexes which form on the Cu30Zn sample surfaces, may play a pivotal role in producing dezincification at more noble electrode potentials.

4.3.4. Results of Solution Analysis

The results of the analyses for copper and zinc dissolved in the solutions employed in the pH 4 controlled anodic dissolution experiments were presented in figures 31, 33, 36, 38, 40, and 41. Reference to these figures shows that at each level of electrode potential, the dissolved copper concentration of the solution in contact with the anodically dissolving Cu30Zn sample attained a plateau value.

These measured plateau concentrations were higher for each higher level of polarization up to 0.200 V_{SCE}. Table 5 lists the plateau concentrations of copper measured at each electrode potential.

As described previously, the standard polarization cell was modified for these experiments so that copper in solution could not plate-out (in significant quantities) onto the platinum auxilliary electrode. In this way the measured copper concentrations in the solution were not influenced significantly by experimental constraints, but were allowed to build up according to the equilibria established between the copper dissolved in solution and the Cu30Zn electrode at each level of electrode potential. Further, the build-up of constant copper concentrations in the bulk solutions implies that no higher dissolved copper concentrations are present in the cell. Thus, the plateau copper concentrations are indicative of the maximum concentrations which can be established in crevices, such as those produced by non-adhering stop-off lacquer, copper deposits, CuCl surface layers, and paratacamite corrosion products in contact with the Cu30Zn surfaces.

The significance of the measured plateau copper concentrations is revealed in figure 43. In this figure the plateau concentrations listed in table 5 are plotted on log-copper-concentration versus electrode-potential coordinates.

TABLE 5

Plateau Values of Dissolved Copper Concentrations
Measured in Controlled Anodic Dissolution Experiments

Electrode Potential		Dissolved Copper Concentration	
		ppm	molar
V_{SCE}	V_{SHE}		
+0.500	+0.745	820	1.3×10^{-2}
+0.200	+0.445	850	1.3×10^{-2}
+0.100	+0.345	400	6.3×10^{-3}
0.000	+0.245	300	4.7×10^{-3}
0.000	+0.245	230	3.6×10^{-3}
-0.100	+0.145	70	1.1×10^{-3}
-0.200	+0.045	3.4	5.3×10^{-5}
-0.200	+0.045	1.5	2.4×10^{-5}

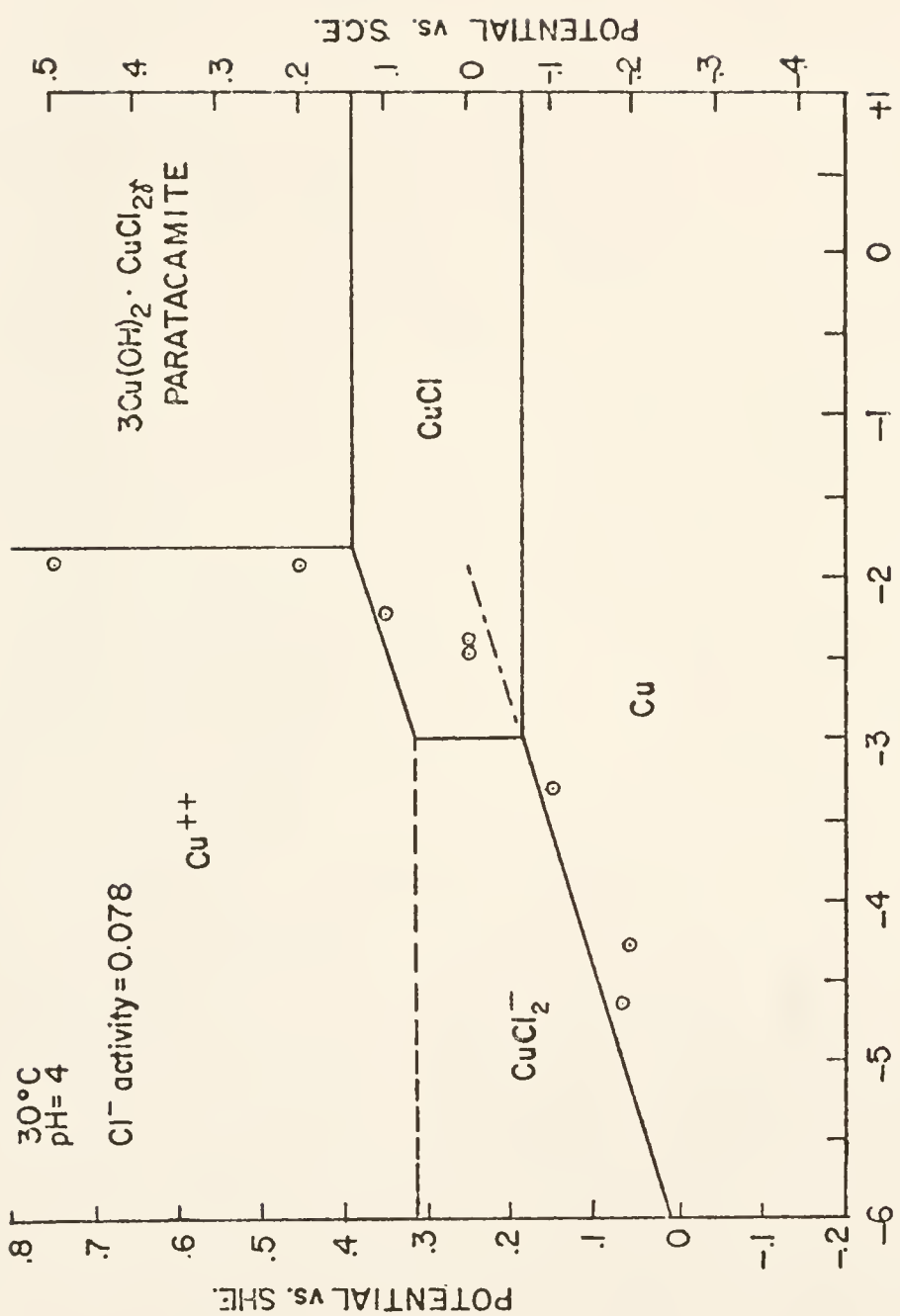

Figure 43. Equilibria calculated for the $Cu\text{-}Cl^{-}\text{-}H_2O$ system at pH = 4 showing agreement between equilibrium calculations and constant copper concentrations observed in the controlled anodic dissolution experiments.

Also plotted are lines representing the electrochemical equilibria calculated between the solid and dissolved copper species indicated by the previously reported, potentiokinetic polarization experiments and controlled anodic dissolution experiments as having domains of stability in pH 4, 0.1M chloride solutions. Equilibrium calculations were made using the free energy of formation data tabulated in Appendix 7. The calculations reflect the experimental conditions employed in the controlled anodic dissolution experiments (i.e., 30°C, pH 4, 0.1M chloride). The activity coefficient of the chloride ion for 0.1M concentration was taken as 0.78 (79).

Referring to figure 43, it can be seen that the measured copper plateau concentrations fall along the lines representing equilibria between the dissolved copper species ($CuCl_2^-$ and Cu^{++}) and the solid copper species (Cu, CuCl, and paratacamite). The interpretation of plateau concentration values then is straightforward. At each level of electrode potential, the maximum attainable concentration of copper in solution containing the polarized Cu30Zn electrode is limited by the equilibrium between the predominant copper ion and the corresponding stable solid metallic species. This result is supportive of the thoery advanced by Pourbaix (52) that the maximum dissolved metal concentration attainable in an active corrosion pit is determined by the solubility of the least soluble metal species present. Cu30Zn

samples polarized to -0.200 V_{SCE} and -0.100 V_{SCE} underwent dissolution until the concentrations of dissolved copper (as $CuCl_2^-$) in solution reached the maximum values dictated by the Cu-$CuCl_2^-$ equilibrium. On the crevice portions of the samples, however, dissolution continued at an increased rate. The copper entering solution as a result of this dissolution redeposited nearby, apparently because its equilibrium concentration in solution was exceeded. This action resulted in the dezincification noted beneath the stop-off lacquer and in the precipitation of copper crystals on the brass surface potentiostated at -0.100 V_{SCE}. The dissolved zinc was not affected by the copper-chloride equilibrium, and so it continued to concentrate in the solution.

At more noble electrode potentials, the situation is more complicated. For example, Cu30Zn samples potentiostated at 0.000 V_{SCE} were quickly covered by a CuCl corrosion product layer. The effects of such a layer on the brass surface are in some ways analogous to the effects of a crevice. Restriction of solution flow decreases the effective mobilities of ions in solution adjacent to the brass surface, causing local increases in the dissolved metal content of the solution adjacent to the dissolving Cu30Zn surface. In this case, however, the maximum dissolved copper concentration was limited by the CuCl-$CuCl_2^-$ equilibrium

$$CuCl_2^- \rightleftarrows CuCl + Cl^- , \qquad (23)$$

which is a chemical rather than an electrochemical equilibrium. Thus, when the dissolved copper concentration of the solution exceed the equilibrium value given by the equilibrium constant for equation (23), the reaction proceeded to the right and more CuCl was formed.

An important consequence of the controlling nature of the CuCl-$CuCl_2^-$ equilibrium can be described by reference to figure 43. A metastable extension of the Cu-$CuCl_2^-$ equilibrium is drawn as a phantom line into the CuCl domain on the diagram. This line represents the locus of maximum dissolved copper concentrations which would be allowed by the Cu-$CuCl_2^-$ equilibrium in the absence of CuCl. It is evident from this construction that at a given electrode potential more noble than about -0.07 V_{SCE} (+0.18 V_{SHE}), the maximum concentration of dissolved copper (as $CuCl_2^-$) allowed by the CuCl-$CuCl_2^-$ equilibrium is less than would be allowed by the Cu-$CuCl_2^-$ equilibrium. Thus, when CuCl is present on the Cu30Zn surface, it acts to limit the concentration of dissolved copper adjacent to the exposed portions of the brass surface to such an extent that the Cu-$CuCl_2^-$ equilibrium cannot be established. Consequently, the dissolved copper concentration of the solution adjacent to a Cu30Zn surface covered by CuCl layers can never exceed saturation with respect to the Cu-$CuCl_2^-$ equilibrium and cause plating-out of copper on the brass surface.

Similar reasoning can be applied at each more noble level of electrode potential. The significance of the argument remains the same. The effect of solid copper-chloride complex layers on brass surfaces in promoting dezincification is not merely to form crevices which allow local increases of dissolved copper concentration above saturation values. Clearly the role of such corrosion product layers is more complex, and greater understanding of the equilibrium conditions present at the attack interface is required.

4.3.5. Results of Artificial Occluded Cell Experiments

The artificial occluded cell experiment was designed as a method to gain insight into the electrochemical and equilibrium conditions present at the interface between the corroding brass surface and the residual copper sponge layer on a dezincifying brass sample. Lucey (27) was first to recognize that the copper sponges resulting from dezincification were not always continuous with the uncorroded brass, and that solution-filled gaps existed between the two structures. An example of this separation can be seen in figure 44. The copper sponge structure can be seen to contact the brass surface only at discrete points in the plane of observation.

The design of the occluded cell sample holder, described in detail in section 3.4., represents a model of such

Figure 44. Cu30Zn sample potentiostated 4 days at +0.500 V_{SCE}, showing separation between the brass and the copper sponge structure. 250X

a dezincified structure. The Cu30Zn sample was positioned parallel to a porous copper screen, and connected to it electrically through a zero-resistance ammeter. In this way the current, i_c, passing between the brass sample and the copper screen could be monitored. Additionally, provision was made to monitor the electrode potential, E_c, inside the occluded cell compartment (formed between the Cu30Zn sample and the copper screen) with the saturated calomel electrode, SCE 1.

The occluded cell assembly was made the working electrode in a polarization cell. Referring to figure 5 in section 3.4., this working electrode assembly was polarized against the platinum counter electrode to applied potentials, E_b, monitored by the saturated calomel electrode, SCE 2. The copper screen acts as a source of resistance in the solution portion of the electrical circuit between the Cu30Zn sample and the platinum auxilliary electrode. When current is flowing in the circuit (i.e., when the potentiostat is switched on), a potential drop across the copper screen results. Consequently, the measured occluded cell potential, E_c should be less noble than the applied potential, E_b. The value of E_c measured at each applied potential, E_b,is expected to provide information about the equilibria which are established inside the occluded cell compartment adjacent to the Cu30Zn sample surface.

Occluded cell experiments were conducted at room temperature ($25 \pm 3°C$) in nitrogen-saturated 0.1M chloride solutions of pH 4. Monitoring of E_c and i_c was begun after the solution was introduced into the cell and the solution connections to the reference electrodes, SCE 1 and SCE 2, were completed. In each case the measured corrosion potential of the electrode assembly was about -0.200 V_{SCE}, and the difference in corrosion potentials measured against SCE 1 and SCE 2 was less than 3 mV. This potential difference was less than the rated accuracy of the saturated calomel electrodes and, therefore, was considered not to be significant. No detectable occluded cell currents were measured (≥ 0.1 μa). When the potentiostat was switched on, E_c and i_c were recorded as a function of time.

Experiments were conducted at applied electrode potentials, E_b, of 0.000, +0.200, +0.350, and +0.500 V_{SCE}. Referring to figure 43 in section 4.3.4., controlled anodic dissolution experiments in this region of electrode potential produced dezincification beneath layers of CuCl or layers of CuCl and paratacamite.

Figure 45 summarizes the results obtained from the occluded cell experiments. On the upper section of the plot, the occluded cell potential, E_c, measured as a function of time, is plotted for each level of applied potential, E_b. On the lower section of the plot, the corresponding

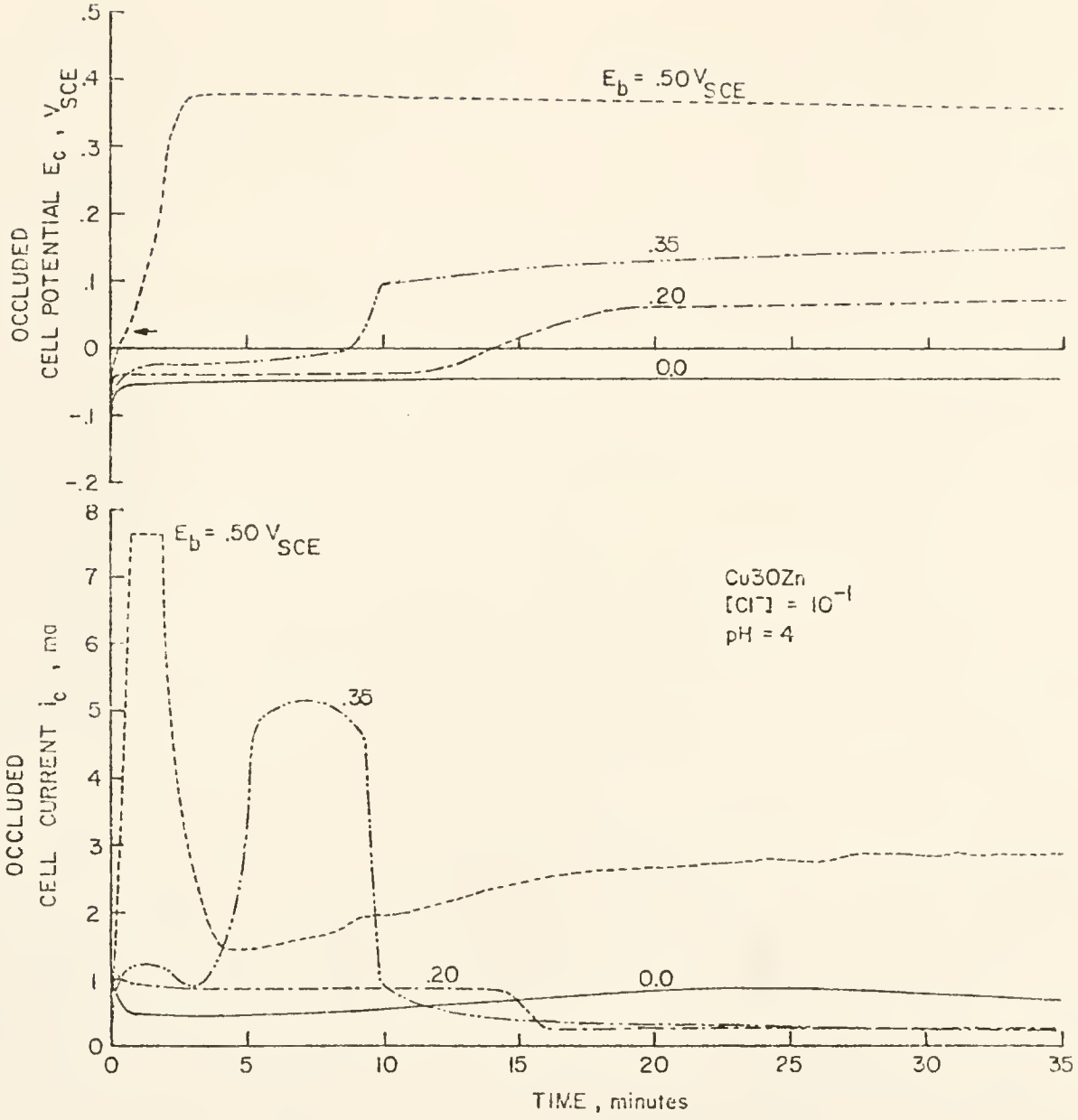

Figure 45. Results of artificial occluded cell experiments showing occluded cell potential and occluded cell current measured as a function of time.

occluded cell current, i_c, is similarly plotted as a function of time for each applied potential. In all cases, the Cu30Zn sample was anodic with respect to the copper screen, and the measured occluded cell currents represent positive direct current flowing from the copper screen through the ammeter to the Cu30Zn sample.

When the potentiostat was switched on, the working electrode assembly immediately assumed the value of the polarizing potential, E_b. However, by reference to the E_c versus time plot (figure 45), it can be seen that the electrode potential, E_c, measured inside the occluded cell increased initially to a plateau value between about -0.07 and -0.03 V_{SCE}. The measured E_c versus time curve recorded for the experiment conducted at E_b = 0.50 V_{SCE} did not maintain a plateau potential value. However, the inflection in this curve (see arrow) at about 1 min is taken to be indicative of a tendency to do so. After certain amounts of time, which can be seen to be highly dependent on E_b, the occluded cell potential increased (except in the experiment where E_b = 0.0 V_{SCE}) to values more noble than the initial plateau value. After several hours (data not shown in figure 45), E_c continued slowly to increase towards E_b.

The measured value of the plateau in the occluded cell potential is significant in that it matches closely the calculated potential, -0.07 V_{SCE}, of the Cu-CuCl equilibrium. This suggests that the initial species formed

adjacent to the Cu30Zn electrode in the occluded cell compartment is CuCl. This is predictable when the applied potential, E_b = 0.0 V_{SCE}, since CuCl is stable at this electrode potential (refer to figure 43). However, when Cu30Zn samples were polarized to electrode potentials more noble than about +1.40 V_{SCE} in the controlled anodic dissolution experiments, the Cu^{++} - $3Cu(OH)_2 \cdot CuCl_2$ equilibrium was apparently established. Thus, the establishment of the Cu-CuCl equilibrium in the occluded cell of samples polarized at the more noble potentials is surprising.

Upon disassembly of the occluded cell sample holder assemblies after each experiment, it was observed that the Cu30Zn surfaces exposed in the occluded cell in all cases exhibited the dull-red appearance characteristic of dezincification occurring beneath a porous layer of white CuCl (see section 4.3.2.). This observation is supportive of the establishment of the Cu-CuCl equilibrium at the Cu30Zn surfaces.

Referring again to figure 45, the occluded cell current, i_c, was essentially zero before polarization was begun. When the potentiostat was switched on, i_c increased to a more-or-less constant value depending on E_b. However, after times corresponding to increases in the E_c versus time curves, the occluded cell currents, i_c, decreased to relatively low values. In the case of the experiment conducted

at 0.0 V_{SCE} (the results of which indicated no increase in E_c), only a small decrease in i_c can be discerned after about 25 min of polarization.

Interpretation of those phenomena requires that both the increases in E_c and the decreases in i_c be accounted for. The initial reactions at the Cu30Zn sample surface were the dissolution of copper and zinc to CuCl and Zn^{++} respectively. Formation of CuCl on the brass surface is confirmed by the measurement of constant values of E_c nearly equal to the Cu-CuCl equilibrium potential at short times of polarization. According to the results of Bonfiglio *et al*. (73), transfer of dissolved copper away from the Cu30Zn surface occurs by further complexation of CuCl by the reaction

$$CuCl + Cl^- \rightarrow CuCl_2^- \quad . \qquad (24)$$

The $CuCl_2^-$ ions can migrate in the occluded cell cavity towards the copper screen. The occluded cell current, i_c, arises from the subsequent discharge of $CuCl_2^-$ ions at the copper screen

$$CuCl_2^- + e^- \rightarrow Cu + 2Cl^- \quad . \qquad (25)$$

Intuitively, the measured dependence of the maximum occluded cell current reached on the level of polarization, E_b, can be explained in terms of increasing ion mobility in the occluded cell cavity as the driving force (E_b) is increased.

The transfer of copper from an anodically dissolving beta brass sample to a copper screen placed in contact with it has been demonstrated previously (27). In that experiment, as well as in the present one, copper deposition took place on the surfaces of the copper screen directly opposite the brass surface while anodic dissolution of the screen took place on surfaces directly opposite the cathode of the polarization cell (i.e., on the backside of the screen).

As the reaction sequence proceeds, the CuCl layer on the Cu3OZn surface eventually thickens to such dimensions that it acts, in a manner analogous to that of the copper screen, as a barrier to diffusion of ions in solution. In this way the CuCl layer forms a new occluded cell adjacent to the Cu3OZn surface having much smaller dimensions than the artificial occluded cell formed between the brass surface and the copper screen. Several consequences of such a formation can be envisioned.

The limitation of ion mobility by the CuCl layer may lead to local build-up of copper ion concentration adjacent to the Cu3OZn surface. It has been shown (section 4.3.4.) that the maximum concentration of dissolved copper is limited in the presence of CuCl to values less than those required to satisfy the Cu-$CuCl_2^-$ equilibrium. Thus, if the chloride concentration of the solution remains constant, then copper may not deposit via the Cu-$CuCl_2^-$ equilibrium.

However, potential drops across the CuCl can result in a lowering of the electrode potential adjacent to the Cu30Zn surface. This is analogous to the potential drops measured across the artificial copper screen. If the Cu-CuCl equilibrium is active at the brass surface, then a decrease in the local electrode potential to a level more active than Cu-CuCl equilibrium potential (-0.70 V_{SCE}) near the brass surface could result in deposition of copper at sites on or adjacent to the brass surface, according to the reaction

$$CuCl + e^- \rightarrow Cu + Cl^- . \qquad (26)$$

Similarly, it may be argued that local reductions of the chloride content of the solution may occur due to restriction of flow by the CuCl layer. In this case the CuCl would tend to decompose to produce more chloride, possibly by reaction (26).

At any rate, the resulting deposition of copper adjacent to the Cu30Zn surface provides sites for further copper deposition. Further, deposition of copper at these local sites short-circuits the cathodic copper reduction reaction at the artificial copper screen, thereby causing the measured reductions in occluded cell current, i_c. Similarly, this cathodic reaction occurring at sites on or near the brass surface would tend to increase the local dissolution rate of the brass. Such an effect can account for the

large increases in dissolution when dezincification was initiated in crevices.

The measured increases in the occluded cell potential, E_c, at times corresponding to the fall-offs in i_c can be accounted for by consideration of the limitations of migration of dissolved copper away from the brass surface. This effect leads to increased polarization of the brass surface in the occluded cell cavity. Under these conditions of increased overpotential, oxidation of CuCl to cupric ions may occur

$$CuCl \rightarrow Cu^{++} + Cl^{-} + e^{-} . \qquad (27)$$

This would result in the increases noted in the occluded cell potentials in experiments where E_b was greater than 0.0 V_{SCE}. For the experiment conducted at E_b = 0.0 V_{SCE}, the applied potential is not noble enough to cause oxidation of CuCl. Hence, no increase in E_c was noted for this experiment.

The explanations detailed above for the results of the artificial occluded cell experiments are significant in that they provide a basis for a broader understanding of the equilibria which control dezincification. It has been shown that at least some CuCl is present at the corroding brass surface polarized at electrode potentials more noble than about -0.07 V_{SCE}, even in the domain in which paratacamite is stable. The dezincification reaction can be assigned to

reduction of CuCl to copper, at local sites adjacent to the dissolving brass surface.

In the controlled anodic dissolution experiments, dezincification was produced at electrode potentials considerably more active than the lower limit of the domain of stability for CuCl, as shown in figure 43. In all cases, the dezincification initiated at crevices or areas of restricted solution flow. Under these conditions, it is possible to envision a mechanism whereby CuCl plays an active role in the attack.

The results of Bonfiglio et al., discussed previously, showed that copper undergoes dissolution in acidic chloride solutions via a series of complexing reactions. At low anodic overpotentials, copper dissolves as cuprous ions and combines with chloride ions to produce CuCl at the surface. CuCl likewise dissolves by further complexing to form the $CuCl_2^-$ ion. At higher overpotentials, the second complexing reaction is stifled since $CuCl_2^-$ ions cannot migrate away from the copper surface fast enough. This leads to accumulation of CuCl on the copper surface (in the range of electrode potential where CuCl is thermodynamically stable).

Similar reasoning can be applied to a Cu30Zn surface undergoing anodic dissolution in a crevice situation where solution flow is restricted. If the migration of $CuCl_2^-$ ions away from the brass surface is severely restricted, then accumulation of CuCl on the brass surface may occur at

electrode potentials less noble than the Cu-CuCl equilibrium potential (-0.07 V_{SCE} in 0.1M chloride solution). Assuming such a process to be operative, reduction of CuCl at local sites on the corroding Cu30Zn surface can proceed over the entire range of anodic overpotentials investigated.

4.3.6. Summary

The results of the experiments on dezincification of Cu30Zn in 0.1M chloride solutions by dissolution and replating provide a basis for understanding the phenomena involved. The formation of CuCl layers on dissolving brass surfaces has been shown experimentally to occur at electrode potentials more noble than the equilibrium electrode potential for the Cu-CuCl reaction. Similar formation of CuCl has been hypothesized to occur at less noble electrode potentials when crevice conditions are present.

Initiation of dezincification attack occurs by the deposition of copper by reduction of CuCl at sites adjacent to the brass surface. Potential drops across the CuCl layer itself are believed to cause the reduction reaction to proceed.

The initial copper deposition locally increases the kinetics of brass dissolution by providing a local cathodic reaction site. Under equilibrium conditions it was shown that the predominant solid copper-containing species present limits the maximum attainable concentration of the dissolved

copper species. Under conditions of high-rate dissolution of the brass, however, the concentrations of dissolved copper in local areas near the brass surface may exceed these limitations, and supersaturation may occur. Thus, propagation of dezincification attack may proceed by a combination of CuCl reduction and reduction of other ionic species present in higher than equilibrium quantities near the brass surface.

4.4. Effect of Arsenic Additions on the Dealloying of Cu30Zn

The effect on dealloying of arsenic additions to the Cu30Zn alloy was investigated in terms of the dissolution and replating mechanism. No attempt was made to determine whether or not arsenic may also influence the selective leaching of zinc from Cu30Zn. The experimental approach used in this part of the investigation is similar to that used in section 4.3. on dealloying of Cu30Zn by dissolution and replating. Controlled anodic dissolution experiments and atomic absorption spectrophotometric analysis of the resulting solutions were employed to gain information concerning the effects of arsenic on the copper-chloride equilibria found to play roles in dealloying of Cu30Zn.

4.4.1. Results of Controlled Anodic Dissolution Experiments

Controlled anodic dissolution experiments were conducted on arsenical (0.048 w/o arsenic) Cu30Zn samples

according to the procedure outlined in section 3.3. Stirred, nitrogen-saturated 0.1M chloride solutions maintained at 30±1°C were used in all cases. The applied electrode potentials were the same as those employed in previous controlled anodic dissolution experiments on Cu30Zn samples, i.e., -0.200, -0.100, 0.000, +0.100, +0.200, and +0.500 V_{SCE}. All experiments were run for 16 days. The results of the experiments are presented below in order of ascending electrode potential.

The arsenical Cu30Zn samples potentiostated at -0.200 and -0.100 V_{SCE} were observed to develop light tarnishes within a few hours of exposure. Because of their thinness, these tarnish layers could not be identified by x-ray diffraction. Similarly formed tarnish films on arsenical alpha brasses have been identified by electron diffraction as containing As_2O_3 (60). The dissolution behavior of both samples was observed to be similar to that exhibited by non-arsenical Cu30Zn exposed at the same electrode potentials. In both cases the samples underwent crystallographic etching. However, the arsenical Cu30Zn samples did not undergo dezincification in areas where the stop-off lacquer lost adherency. Instead, only tarnishing of the brass surfaces in these areas was observed.

Arsenical Cu30Zn samples potentiostated at 0.000, +0.100 and +0.200 V_{SCE} also exhibited similar behavior.

Immediately upon polarization, these samples developed dark tarnishes which were observed to thicken and grow darker as the experiments progressed. X-ray diffraction analysis of a sample of this dark product taken from the +0.100 V_{SCE} sample revealed the presence of only CuCl. Since no species was detected which could account for the dark color of the layer, it is assumed that such a species was present in quantities too small to detect. It is also possible that the apparent dark color of the layer may be an optical effect related to the particle size of the deposit. A slight roughening of the surface could disperse the incident light, thereby causing the surface to appear dark.

As was observed for the samples exposed at more active electrode potentials, only tarnishing took place on the brass surfaces under non-adhering stop-off lacquer. Metallographic examination of sample cross-sections revealed no detectable dezincification at magnifications up to about 500X.

The arsenical Cu30Zn sample potentiostated at +0.500 V_{SCE} also developed a dark corrosion product layer upon polarization. However, within a few hours of exposure, paratacamite was observed forming at the edges of the exposed surface. The volume of the paratacamite increased with time until the entire surface was covered. After five days' exposure a finely divided red corrosion product was formed in

the polarization cell. It was observed that the product apparently did not form on the Cu30Zn sample. By the end of the experiment, copious quantities of this product, identified by X-ray diffraction as Cu_2O, were present in the cell.

Subsequent visual and metallographic examination of the arsenical Cu30Zn sample exposed at +0.500 V_{SCE} revealed no detectable dezincification. Again, only tarnishing was observed on surfaces not protected by the stop-off lacquer.

4.4.2. Results of Solution Analysis

Analysis by atomic absorption spectrophotometry of the solutions used in the controlled anodic dissolution experiments on arsenical Cu30Zn was undertaken to provide a point for comparison of the results of the present experiments with those found for non-arsenical Cu30Zn. The concentrations of copper, zinc, and arsenic in solution were determined periodically throughout each experiment.

The results of solution analysis for the experiments conducted at -0.200 and -0.100 V_{SCE} are presented in figures 46 and 47, respectively. For both experiments, the relative amounts of copper and zinc dissolved in the solutions were nearly proportional to their respective concentrations in the alloy (i.e., about 7 to 3). This result, and the values of maximum attained copper concentration, are comparable to the results obtained for non-arsenical

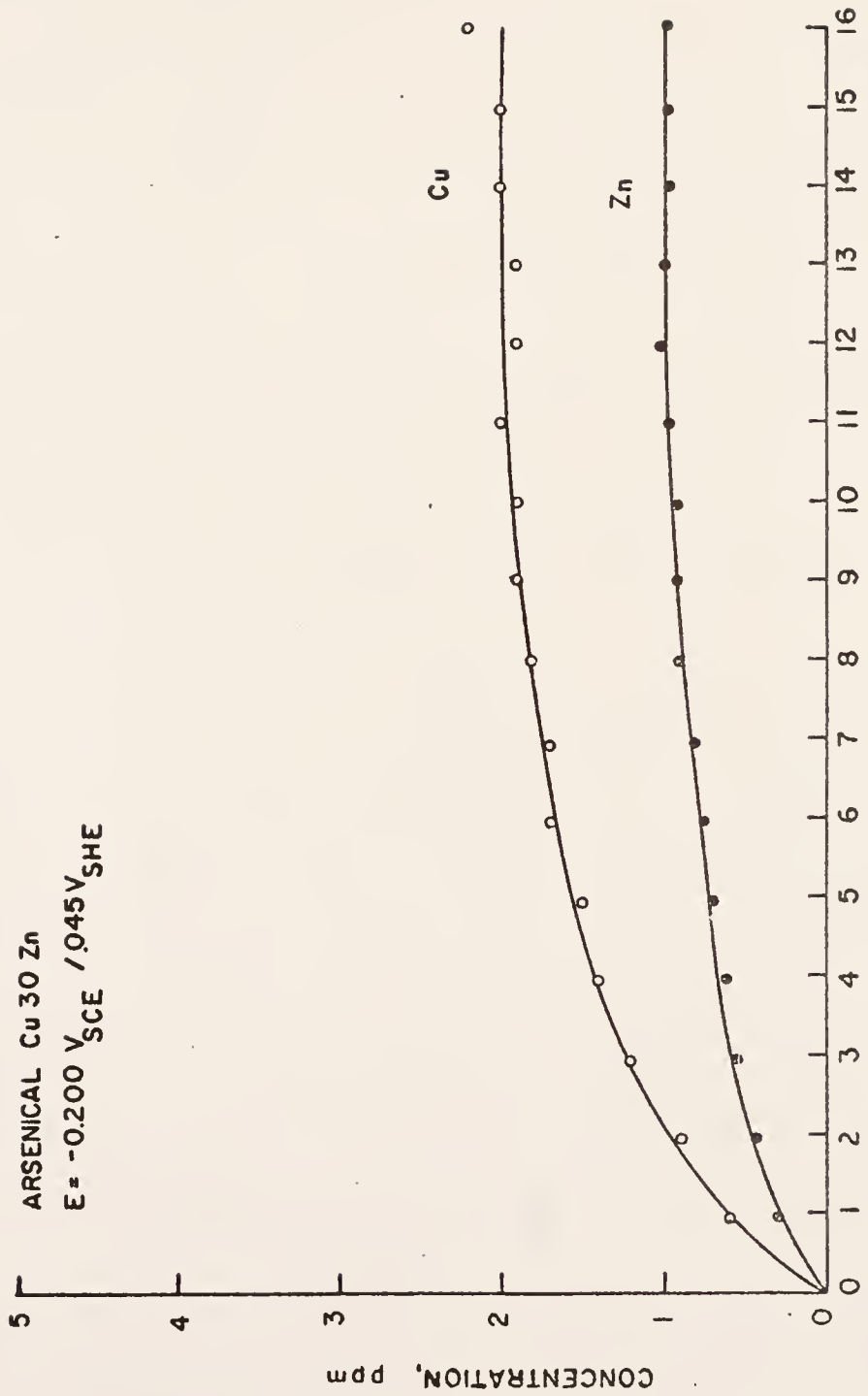

Figure 46. Results of solution analysis for arsenical Cu30Zn potentiostated at -0.200 V_{SCE} in pH 4, 0.1M chloride solution.

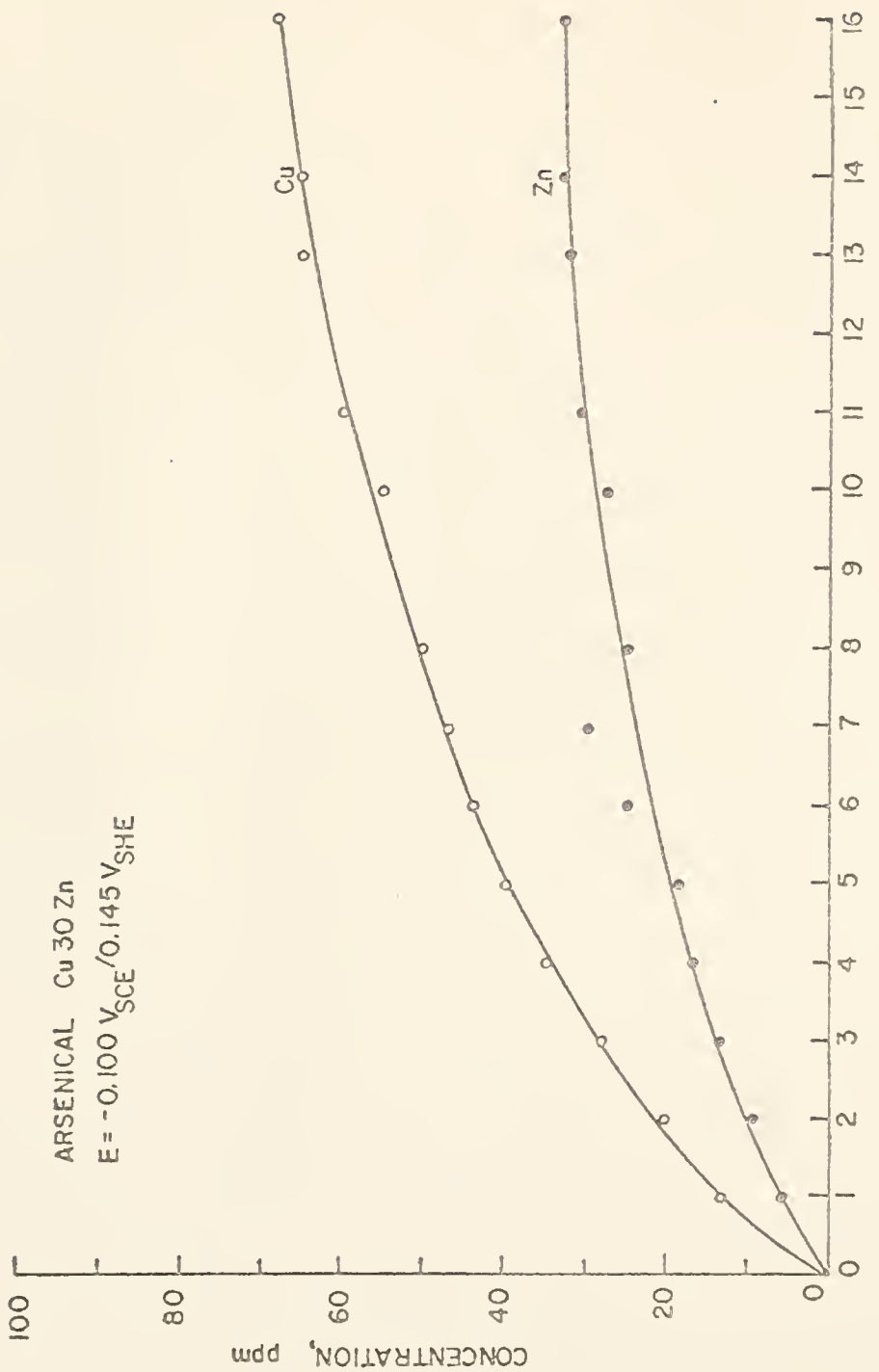

Figure 47. Results of solution analysis for arsenical Cu30Zn potentiostated at -0.100 V_{SCE} in pH 4, 0.1M chloride solution.

Cu30Zn exposed under the same conditions. In both the present experiments, however, the measured zinc concentrations also approach limiting values, but showed no tendency to increase with respect to the copper concentrations. This result is consistent with the observed absence of dezincification on the arsenical Cu30Zn samples.

No arsenic was detected in the solutions from either of these experiments. The experimental limit of detection for arsenic was 0.01 ppm.

The results of solution analysis for the experiments conducted at 0.000, +0.100, and +0.200 V_{SCE} are presented in figures 48, 49, and 50, respectively. These results denote simultaneous dissolution of the arsenical Cu30Zn samples. Again, no disproportionate increases in zinc content of the solutions were noted. The copper concentrations in the 0.000 and +0.200 V_{SCE} experiments reached plateau values after about 13 days' exposure. For the +0.100 V_{SCE} experiment, however, the copper concentration continued to increase until the end of the experiment. The maximum concentrations of copper measured for these experiments are in reasonable agreement with those measured for the experiments on non-arsenical Cu30Zn.

Significant concentrations of arsenic were measured in the solutions from all experiments conducted at electrode potentials more noble than -0.100 V_{SCE}. Reference to figures 48, 49, and 50 reveals that the arsenic contents of the

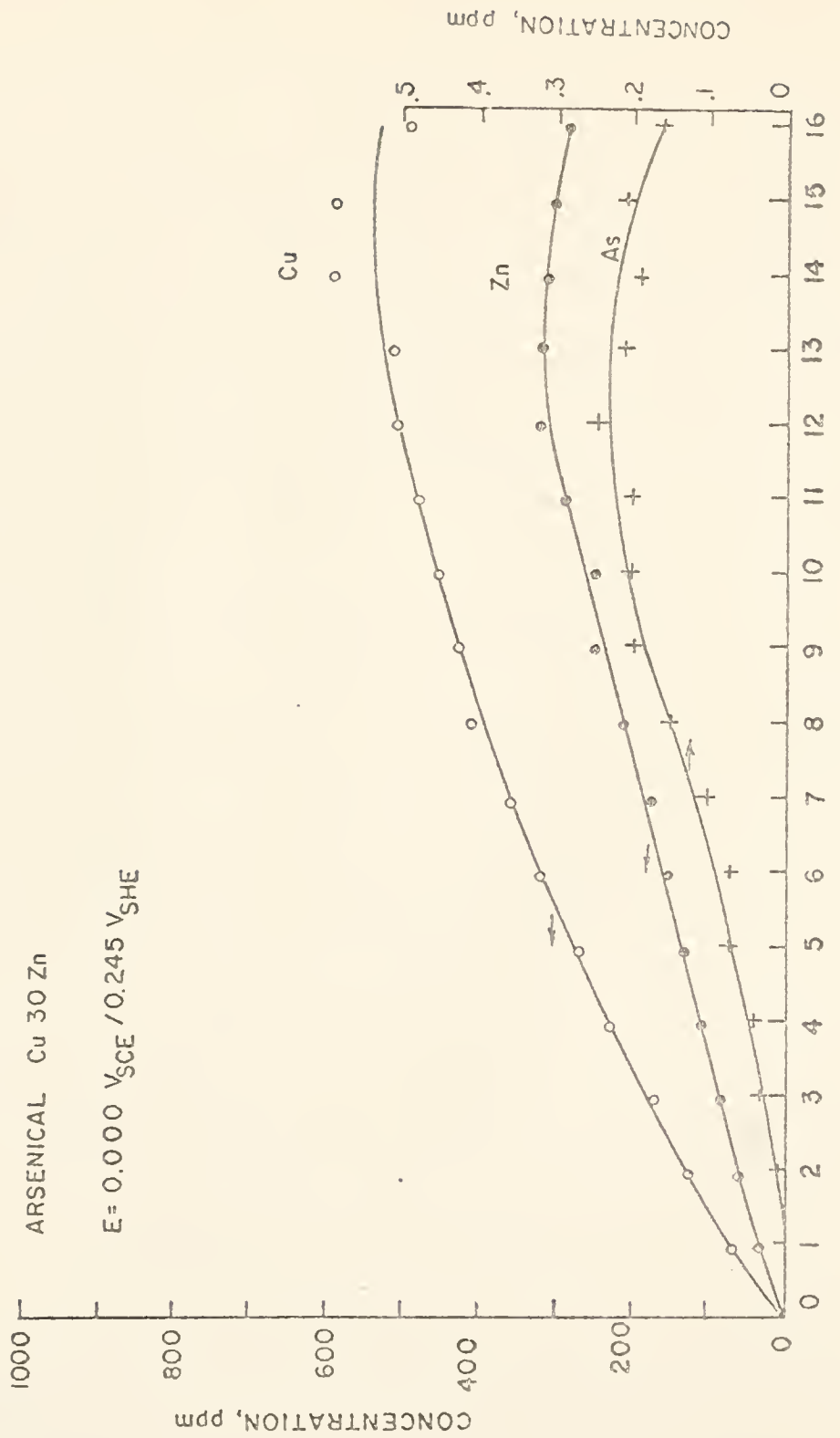

Figure 48. Results of solution analysis for arsenical Cu30Zn potentiostated at -0.000 V_{SCE} in pH 4, 0.1M chloride solution.

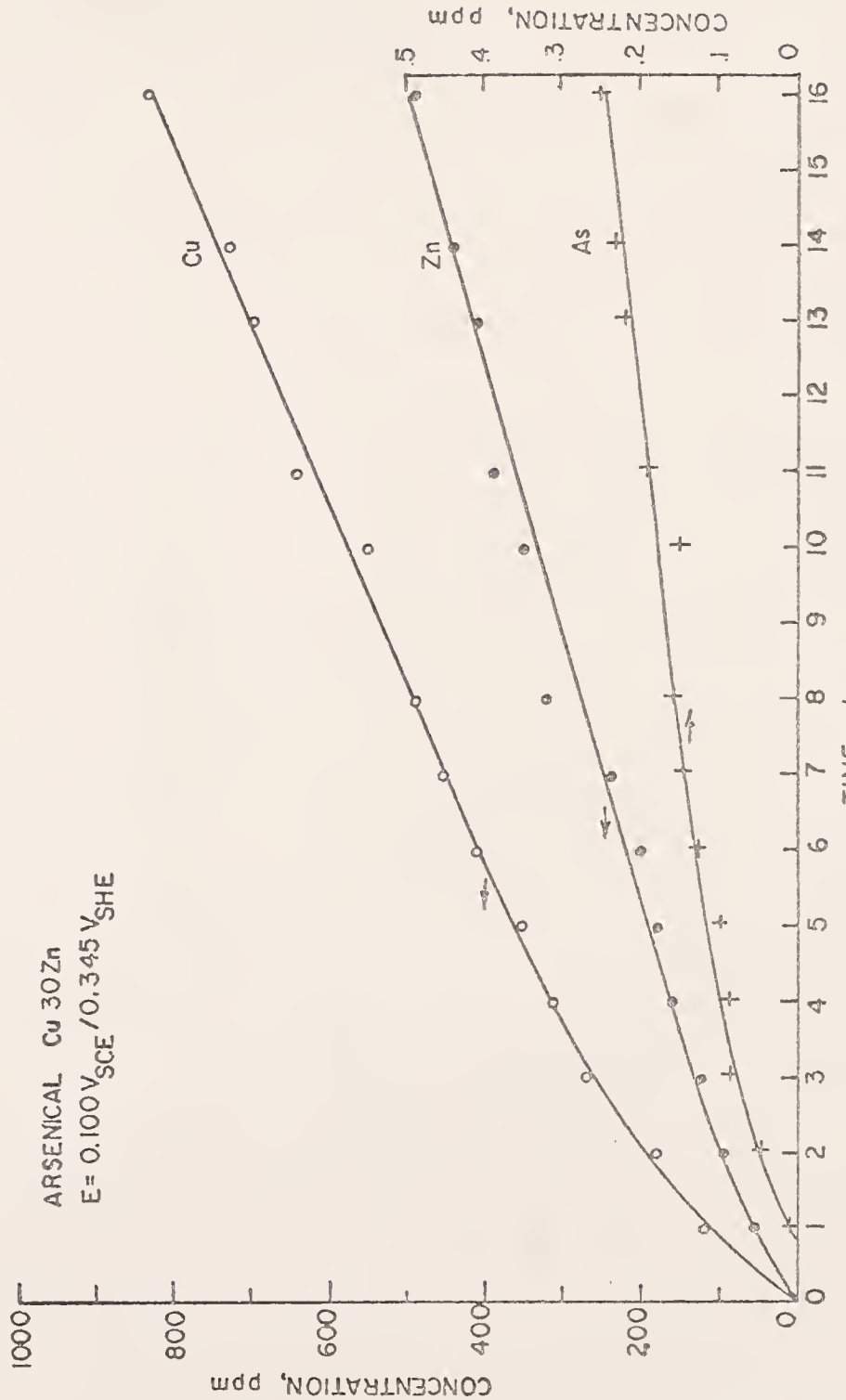

Figure 49. Results of solution analysis for arsenical Cu30Zn potentiostated at +0.100 V_{SCE} in pH 4, 0.1M chloride solution.

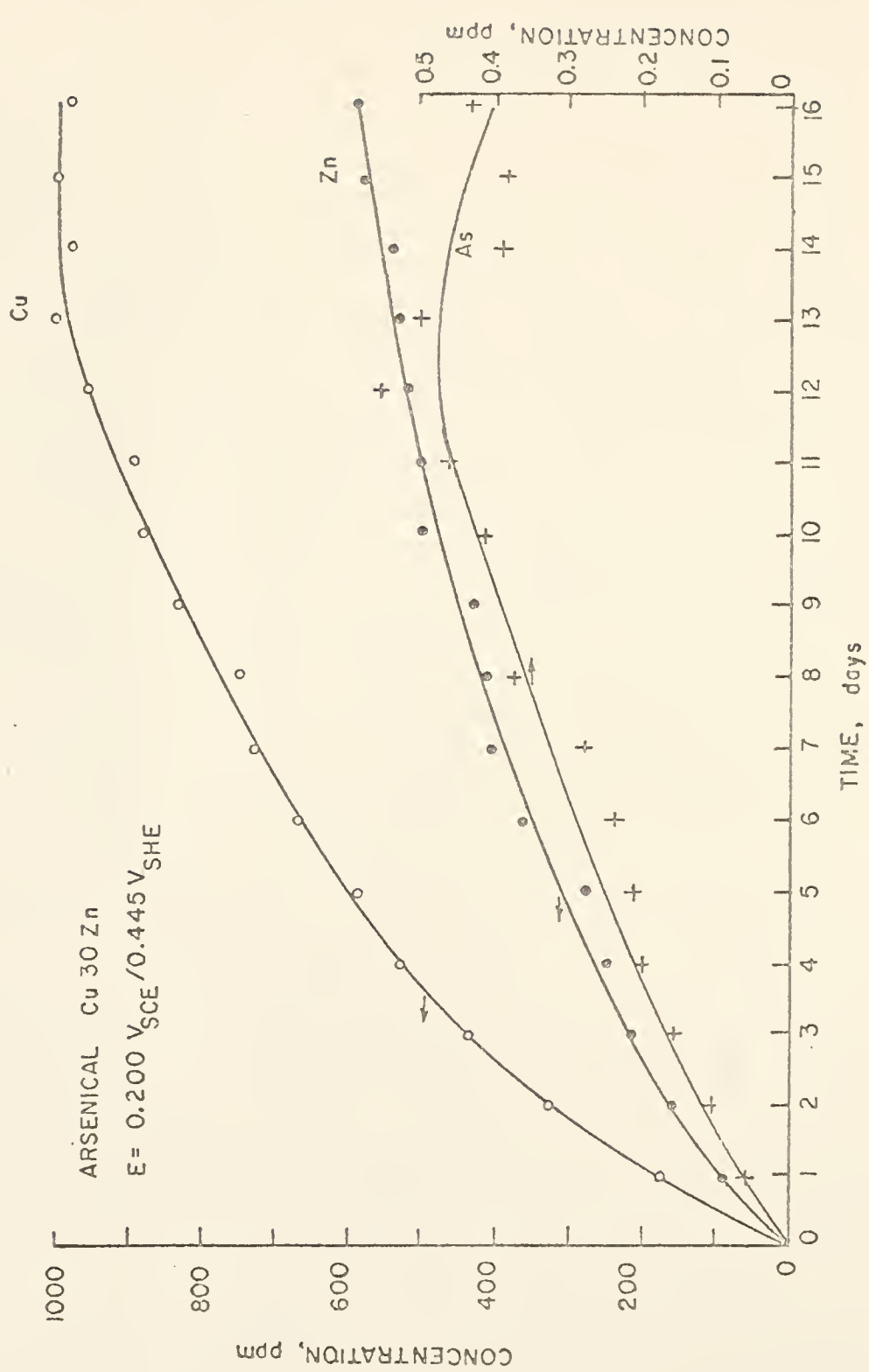

Figure 50. Results of solution analysis for arsenical Cu30Zn potentiostated at +0.200 V_{SCE} in pH 4, 0.1M chloride solution.

solutions from the 0.000, +0.100, and +0.200 V_{SCE} experiments were roughly proportional to the copper and zinc contents measured at each time during the experiments. Consideration of the relative concentrations of arsenic, copper, and zinc in solution reveals that proportionately less arsenic was present in solution than would be predicted from total dissolution of the brass. This observation could be explained by the presence of arsenic compounds in the dark films found on the brass surfaces.

Results of solution analysis for the experiment conducted at +0.500 V_{SCE}, figure 51, reveal behavior very different from that observed at lower electrode potentials. The concentration of copper dissolved in the solution attained a plateau value after about 6 days' exposure. This stabilization of the copper concentration in solution corresponds to the observed formation of Cu_2O in the cells.

The measured zinc concentration of the solution was at all times higher with respect to the copper concentration than would be predicted from simultaneous dissolution of the alloy. In this case, the formation of voluminous solid copper corrosion products resulted in limitations of the measured dissolved copper concentrations. It is, however, significant that the amount of zinc entering solution from this sample potentiostated at +0.500 V_{SCE} continued to increase after the copper concentration reached a limiting value. For the investigations conducted on non-arsenical

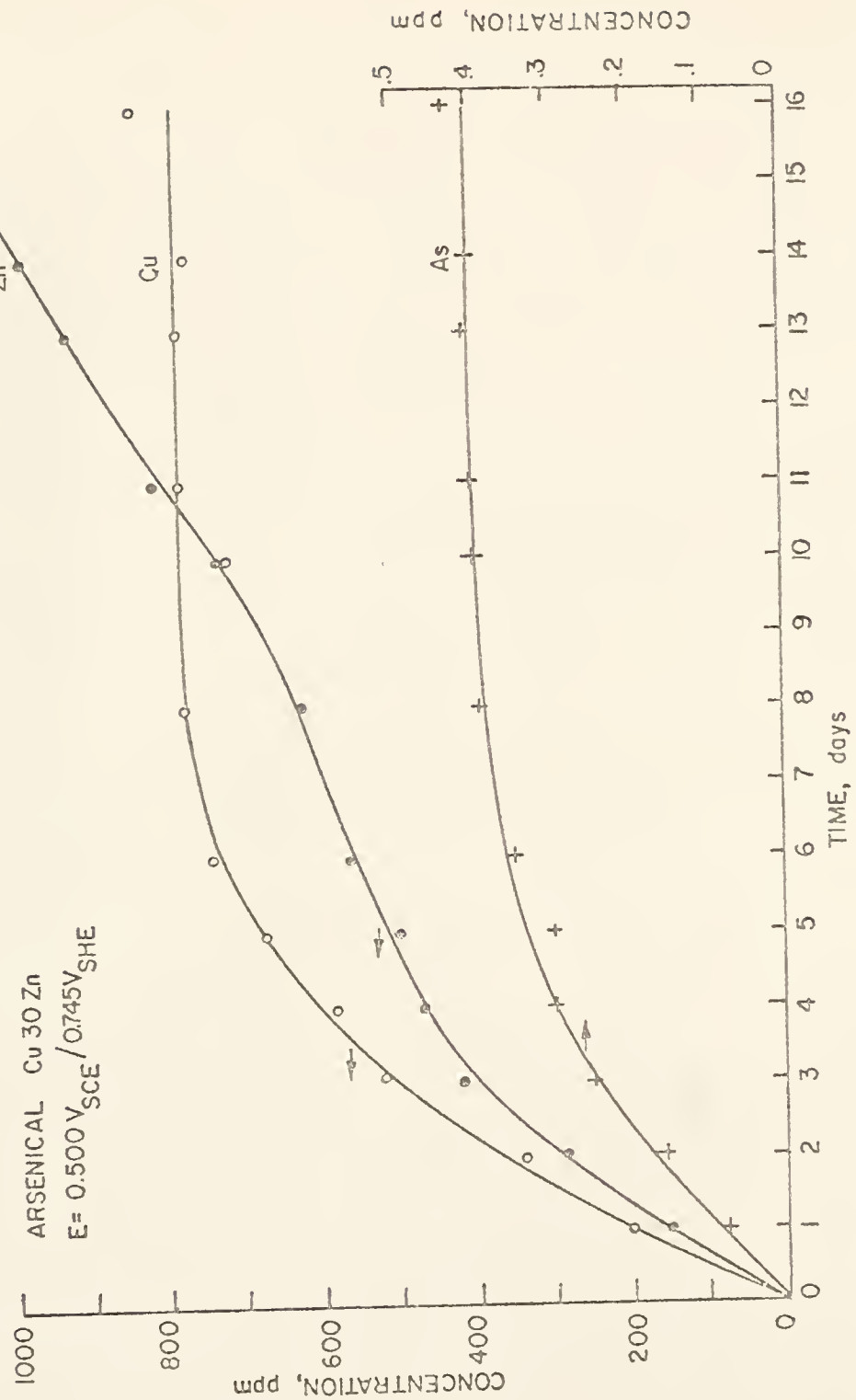

Figure 51. Results of solution analysis of arsenical Cu30Zn potentiostated at +0.500 V_{SCE} in pH 4, 0.1M chloride solution.

Cu30Zn, such increases in zinc concentration were always accompanied by dezincification. The arsenical Cu30Zn sample, however, did not dezincify.

In section 4.3.6. the dezincification of Cu30Zn in 0.1M chloride solutions was discussed in terms of initiation and propagation. The results of the controlled anodic dissolution experiments on non-arsenical Cu30Zn indicated that initiation of dezincification in crevices was always associated with local increases in the brass dissolution rate. The present results of similar experiments on arsenical Cu30Zn indicate that such increases in the brass dissolution rate did not occur when crevice conditions were present.

The solution analysis results presented in this section indicate that the presence of arsenic in the brass has no significant effect upon the establishment of the copper-chloride equilibria. X-ray diffraction analysis of corrosion products indicated that CuCl was present on the surfaces of Cu30Zn sample potentiostated within the range of electrode potentials in which CuCl is the stable species. Thus, it seems likely that the role of arsenic in inhibiting dezincification may be to prevent the reduction of CuCl to copper at the brass surface.

The identity of the black films observed on corroding arsenical brasses has not been well established. The only report available indicates that As_2O_3 was present on arsenical

brass samples after exposure in HNO_3 and in HCl (60). This is in agreement with calculated equilibria (72) which indicate that As_2O_3 is the stable solid arsenic species over a wide range of electrode potential and pH conditions. In the present investigation, no arsenic species were identified.

It is significant that measurable quantities of dissolved arsenic were detected in the solutions from the experiments conducted at the higher electrode potentials. This finding implies that solid copper-arsenic or zinc-arsenic complex species are not formed to any large extent. If such complexing were the case, then it would be expected that the amounts of arsenic detected in solution would be only a small fraction of the total dissolved from the alloy. It is, however, possible that solid complex species could be present as a colloidal suspension of fine particles. The atomic absorption spectrophotometric technique is insensitive to the chemical and physical character of species in the measured solution volume. Therefore, the presence of such a solid species could account for the measured arsenic concentrations of the solutions. Additionally, the existence of ionic complex species can not be ruled out.

The characteristic dark color observed on the corroding arsenical brass surfaces in this investigation strongly suggests the presence of a thin layer of some arsenical product. The effect, in inhibiting dezincification, of a thin

compact layer of arsenic-containing corrosion product on the brass surface could be to limit reduction of CuCl adjacent to the surface. The mechanism involved could be physical separation and perhaps electrical isolation of the CuCl layer from the brass. Since the CuCl reduction reaction, equation (26), requires an accompanying oxidation reaction, isolation of the CuCl from the metal surface might stifle the charge transfer necessary for the reduction reaction to proceed.

4.4.3. Summary

The addition of a small amount of arsenic ($\sim$ 0.048 w/o) to Cu30Zn has been shown to inhibit the initiation of dezincification of the brass in pH 4, 0.1M chloride solutions over a wide range of electrode potential conditions. The presence of arsenic in the system appears not to affect the establishment of copper-chloride equilibria. Significant quantities of dissolved arsenic (up to 0.5 ppm) were detected in the test solutions.

The effect of arsenic in inhibition of dezincification under the conditions of exposure was attributed to interference in the reduction of CuCl to copper adjacent to the brass surface. The mechanism by which it interferes may be the isolation of the CuCl layer from the Cu30Zn surface.

CHAPTER 5

CONCLUSIONS

1. Experimental potential versus pH diagrams for a binary alloy and its less noble component may be compared to predict the conditions of electrode potential and pH under which dealloying may occur.
2. Dealloying by the selective leaching of zinc from Cu30Zn alloy surfaces occurs at electrode potentials which are both less noble than the corrosion potential of Cu30Zn and more noble than the corrosion mixed potential of pure zinc.
3. Significant selective leaching of zinc from Cu30Zn can occur after as little as 2 days' exposure at 89°C in nitrogen-saturated, 0.1M chloride solution of pH 4.
4. The rate of selective leaching of zinc from Cu30Zn, measured as the amount of zinc entering solution with time, is constant for each value of electrode potential, at least for times up to four days.
5. Auger electron spectroscopy is a highly surface-sensitive analytical technique which can be employed to measure the component concentrations of dealloyed metal surfaces.

6. When used in conjunction with argon sputtering, Auger electron spectroscopy can be employed to generate qualitative composition versus depth profiles of dealloyed layers on alloy surfaces.
7. The thicknesses of selectively leached layers, measured on Cu30Zn by Auger electron spectroscopy, average about 800 Å Angstroms after 4 days' exposure.
8. Analysis of composition versus depth profiles indicates that the selective leaching of zinc from Cu30Zn at 89°C occurs via enhanced volume diffusion of zinc to the solution-solid interface.
9. The effective diffusion coefficient for transport of zinc to the solution-solid interface is estimated to be about 2×10^{-17} cm^2/sec at 89°C.
10. The selective leaching of zinc from Cu30Zn is apparently not accompanied by surface roughening.
11. Selective leaching and anodic dissolution may operate simultaneously on Cu30Zn exposed at low anodic overpotentials.
12. Dealloying of Cu30Zn by the dissolution and replating mechanism occurs at electrode potentials more noble than the corrosion potential (up to at least +0.500 V_{SCE}) in 30°C nitrogen-saturated, 0.1M chloride solutions of pH 4.

13. The occurrence of dealloying by this mechanism is always associated with occluded cell or crevice conditions or with saturation of the solution in copper.
14. The role of the chloride ion and resulting copper-chloride equilibria are pivotal in producing dezincification of brass by the dissolution and replating mechanism.
15. Solid CuCl forms on Cu30Zn surfaces exposed at potentials more noble than the Cu-CuCl equilibrium potential (-0.07 V_{SCE}). The effect of a CuCl surface layer is to produce occluded cell conditions.
16. Solid CuCl is believed to be present on Cu30Zn surfaces exposed in occluded cells or crevices at electrode potentials less noble than the Cu-CuCl equilibrium potentials.
17. Under equilibrium conditions, the maximum cooper content of the solution is limited by the thermodynamically stable solid copper species (either Cu, CuCl, or $3Cu(OH)_2 \cdot CuCl_{2Y}$) present on the Cu30Zn sample.
18. The "dezincification reaction" by which dealloying (by the dissolution and replating mechanism) initiates is the reduction of CuCl to copper at local sites on or adjacent to the brass surface

$$CuCl + e^- \rightarrow Cu + Cl^- .$$

19. The deposition of copper adjacent to the Cu30Zn surface increases the local rate of brass dissolution.
20. Supersaturation of the local copper content of the solution near the Cu30Zn surface may be important in the propagation of dealloying.
21 The addition of arsenic to Cu30Zn does not significantly alter the establishment of copper-chloride equilibria.
22. The role of arsenic in inhibiting dezincification may be to prevent the reduction of CuCl to copper. The mechanism is believed to be the isolation of CuCl from the Cu30Zn surface by an arsenical corrosion product film.

CHAPTER 6

RECOMMENDATIONS FOR FURTHER RESEARCH

The results of this investigation point up the fact that all aspects of the dealloying phenomenon are still not completely understood. Several areas of research which may significantly increase our knowledge of the subject are suggested below:

1. Application of the method of predicting the occurrence of dealloying based on the comparison of potential versus pH diagrams should be applied to other systems of interest. Improvements in our ability to correctly calculate such diagrams for complex equilibria should eventually allow even greater predictive capacity.
2. The unique surface analysis capacity of Auger electron spectroscopy makes it an ideal tool for the study of dealloying. The analysis carried out in this investigation should be improved by more careful surface preparation, refinement of the sputtering rate calibration, and correction for selective sputtering effects.
3. The selective leaching analysis on Cu30Zn should be extended to include the wide range of temperatures under which dealloying normally occurs. In this way, more

extensive and meaningful data concerning zinc transport can be generated. Application of the available enhanced volume diffusion theories to these data should result in the establishment of a more detailed selective leaching model.

4. Similarly, the selective leaching analysis should be applied to high brass alloys. The goal of such a project would be to determine the basis of the immunity of these brasses to dezincification.
5. Occluded cell experiments should be extended to investigate the effects on dezincification initiation and propagation of dissolved oxygen in the solution.
6. The effects of increased pH on the morphology and mechanism of dealloying should be investigated. The interplay of passivity, rupture, and dezincification should be of particular interest.
7. Detailed investigations of the nature of arsenical films formed on brasses should be undertaken. Auger analysis could prove to be of use in this area.

APPENDIX 1

SAMPLE CHARACTERIZATION AND PREPARATION

The 99.999% pure copper was supplied as annealed 19 mm diameter wire. Cu30Zn was supplied, courtesy of Chase Brass and Copper Co., as 18 mm diameter extruded and annealed wire. Its composition is listed below:

Cu	69.82 % by weight
Pb	<0.006% by weight
Fe	<0.004% by weight
Sb	<0.01 % by weight
Mn, Si	<0.002% by weight
Ni, Sn, Al	<0.001% by weight
Bi	<0.0005% by weight
Zn	remainder

The 99.99+% pure zinc was supplied as 13 mm diameter cast rod.

The arsenical Cu30Zn alloy was fabricated from 99.999+% pure copper, 99.99+% pure zinc and CDA 142 alloy (0.16 w/o As, 0.008 w/o P, balance copper).* A 200 g charge

---

*Courtesy of C. L. Bulow, Bridgeport Brass Co.

was encapsulated in an evacuated 18 mm diameter quartz tube. The composition of the charge was such that the resulting alloy composition would be 69.91 w/o copper, 30.04 w/o zinc, and 0.048 w/o arsenic. The charge was melted by induction and homogenized for 24 hours at 600°C.

Disk-shaped samples of copper, Cu30Zn, and arsenical Cu30Zn approximately 5 mm thick were cut transversely from the stock materials. The zinc rods were heated to 250°C, and forged to a cross section of approximately 5 mm by 22 mm. Samples approximately 15 mm were cut transversely from the forged bars.

An insulated copper connecting wire was soldered to the back of each sample. The face of each sample was wet-ground successively on 180, 240, 400, and 600 silicon carbide papers. Each sample was then rinsed in distilled and de-ionized water, followed by an acetone rinse.

Cu30Zn samples to be used in selective leaching experiments were further polished with 6 μm diamond paste on nylon cloths and 1 μm diamond paste on Microcloths,* with lapping oil as a lubricant. These samples were rinsed in water, degreased in trichloroethylene and rinsed in acetone.

Each copper and Cu30Zn sample was painted completely, except for an area of about 1 cm^2 on the polished face, with

---

*Trade name of Buehler Ltd.

two coats of Miccroflex* lacquer. Excellent protection of masked copper alloy surfaces was afforded by this treatment, particularly at elevated temperatures. Zinc samples were masked by similar coatings of Microshield* lacquer.

All samples were stored in dessicators over indicator grade activated alumina.

---

*Trade name of Michigan Chrome and Chemical Co.

APPENDIX 2

SOLUTION CHARACTERIZATION AND PREPARATION

The electrolyte solutions used in this investigation were prepared from reagent grade chemicals and distilled and deionized water. All solutions were 0.1M in chloride and buffered as follows:

pH 1-2 . . unbuffered
pH 2-7 . . 0.05M $KHC_8H_4O_4$
pH 7-11 . . 0.05M H_3BO_3
pH 11-13. . unbuffered.

The choice of buffers was based on the results of multiple polarization experiments run on copper samples in pH 4 and pH 8 solutions buffered with 0.005M to 0.1M of $KHC_8H_4O_4$ and H_3BO_3, respectively. No changes in the measured polarization curves with changes in buffer concentrations were noted.

Before use, solutions were vacuum deaerated and saturated with nitrogen. Details of the vacuum deaeration process are discussed elsewhere (53).

APPENDIX 3

STANDARD POLARIZATION CELL

A schematic representation of the polarazation cell is given in figure 52. The cell consists of a Pyrex* reaction kettle with glass and PTFE fittings. The sample is held in place by a glass tube through which the connecting wire passes out of the cell. The auxilliary electrode consists of a bright platinum screen, about 25 mm x 25 mm, spot welded to a thin platinum wire partially sealed in a glass tube. The asbestos-fiber-tipped Haber-Luggin probe is connected to an external beaker, containing a saturated calomel reference electrode, by an external salt bridge filled with the test solution. The gas inlet tube is fitted with a porous glass frit, which helps disperse the gas (nitrogen) throughout the solution. The gas outlet is connected to a bubble bottle, which prevents back leakage of air into the cell. Vigorous stirring is accomplished by a PTFE-coated magnetic stirring bar.

The cell was purged continuously before and throughout each test with nitrogen gas. Bottle gas was used for

---

*Trade Name of Corning Glass Works.

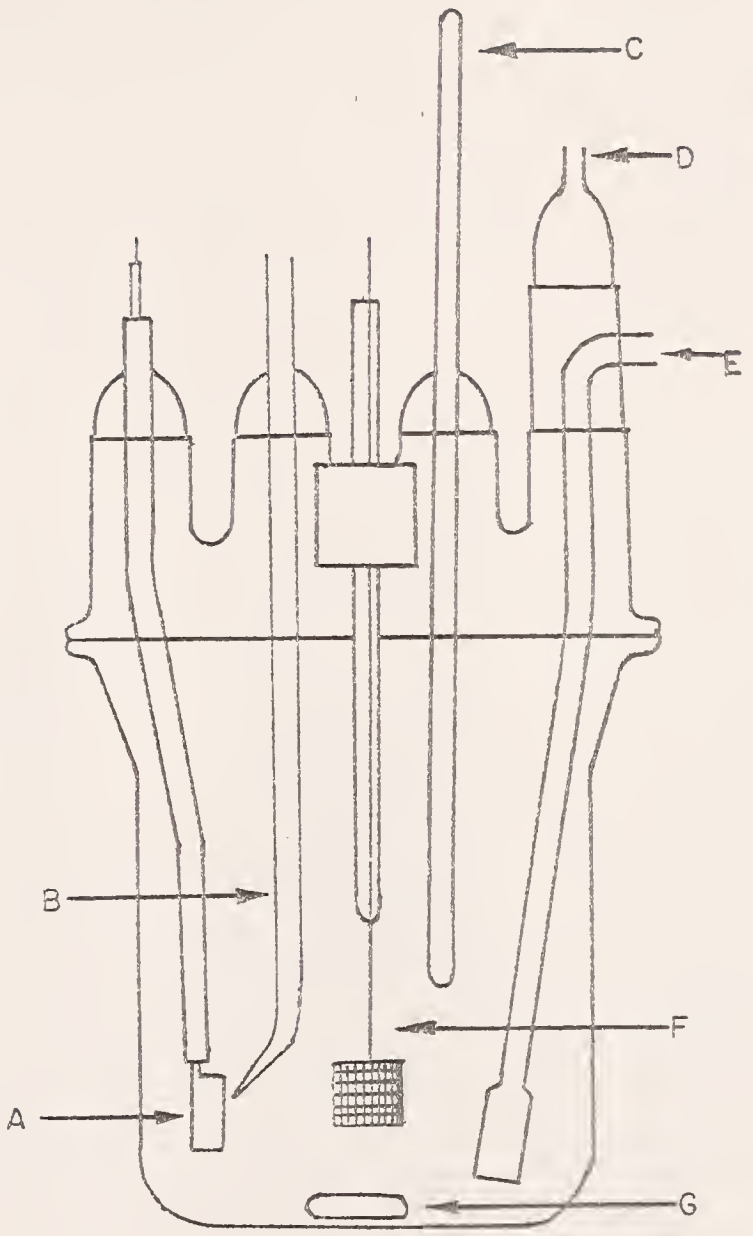

Figure 52. Standard polarization cell.
A - sample
B - Haber-Luggin probe
C - thermometer
D - gas outlet
E - gas inlet diffuser
F - Pt auxilliary electrode
G - magnetic stiring bar

the potentiokinetic tests. In all subsequent tests the nitrogen was purified by passage through a plug of clean copper turnings maintained at 600°C.

For the high temperature selective leaching experiments the cell was operated in a heated water bath. To minimize evaporation losses from the cell, suitable cell joints were sealed with Miccroflex stop-off lacquer, and a vertical, water-cooled condenser was attached to the gas outlet. In these tests, the magnetic stirrer was not used. Instead, the gas diffuser was positioned close to the sample so as to make maximum use of turbulence caused by the gas bubbling action.

For the controlled anodic dissolution tests, the platinum auxilliary electrode was inserted into a glass tube closed at the bottom end with a 1 μm fritted glass disk of about 1 cm^2 projected area. The effect of this modification was to isolate the platinum electrode from copper ions entering solution at the anode, thus preventing their discharge.

APPENDIX 4

LIST OF EQUIPMENT

1. Wenking Potentiostat Model 68TA1 with attached Motor Potentiometer Model MP165.
2. Hewlett-Packard Sanborn Differential Amplifier Model 8875A.
3. Hewlett-Packard Logarithmic Coverter Model 7561A.
4. Hewlett-Packard X-Y Recorder Model 7005B.
5. Keithley Electrometer Model 602.
6. Hewlett-Packard Moseley Strip Chart Recorder Model 680.
7. Beckman pH Meter Expandomatic Model SS-2.
8. Keithley Digital Multimeter Model 160.
9. Hewlett-Packard D.C. Power Supply Model 6261A.
10. Techne Thermoregulator Model TE-4.
11. Cambridge Stereoscan II Scanning Electron Microscope.
12. Sloan Instruments M100 Ångstrometer.
13. Physical Electronics Industries Auger System Control PHI Model 11-500M.
14. Physical Electronics Industries Cylindrical-Auger Electron Optics System PHI Model 10-150.
15. Physical Electronics Industries Sputter Ion Gun PHI Model 04-161.

APPENDIX 5

AUGER ELECTRON SPECTROSCOPY

Auger Electron Spectroscopy (AES) is a highly surface-sensitive technique which is now enjoying application in several areas of materials research, including catalysis, impurity segregation, corrosion and oxidation, and thin film characterization. Several recent review are available [80-83].

The basis of AES can be rather simply explained with the aid of figure 53. An atom in the path of an electron beam loses an electron from its inner K shell as the result of an electron-electron collision. The atom, now in an excited state, seeks to fill the resulting K shell vacancy. To do so, an electron from a higher energy electron shell, and L shell electron in this case, falls into the K shell vacancy. In doing so, it releases a quantity of energy which may be emitted as a photon, or be given to an electron in a higher energy state. If, for example, the energy is given to an M shell electron, then the electron will have sufficient energy to be ejected from the atom. This sequence of events describes a KLM Auger transition. Several

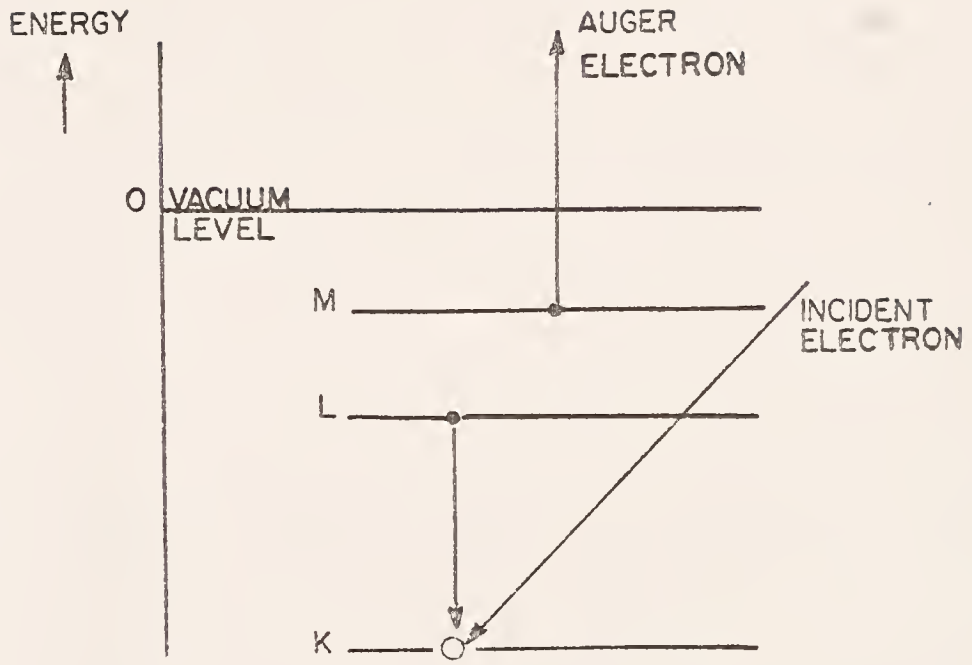

Figure 53. Energy level diagram depicting a KLM Auger transition

combinations of events are possible, e.g., KLL, LMM etc.

The energy of the ejected Auger electron is determined by its transition sequence. Each Auger transition for each element has a unique energy. Thus the element of the atom from which the Auger electron emanates can be positively identified through measurement of the energy of the Auger electron. Typically, the electron energy region measured is between 10 and 1500 eV. Electrons in this energy range have a short mean free path in solids. Consequently, only Auger electrons resulting from transitions in atoms close (3 to 50 Ångstroms, approximately) to the solid surface can emerge from the solid and be measured. This characteristic of AES that only low energy electrons are measured gives the technique its particular surface sensitivity.

Experimentally, when an electron beam irradiates a surface, secondary electrons of four principal types are emitted. These can be identified by reference to the energy spectrum, N(E), for pure silver shown in figure 54. Elastically scattered primary electrons account for the large energy peak at 1000 eV, the energy of the incident beam. Inelastically scattered primary electrons are responsible for the large background signal in the high energy half of the spectrum. True secondary electrons generated by collisions with valence band electrons cause the broad energy peak at very low energies. Superimposed on the curve are

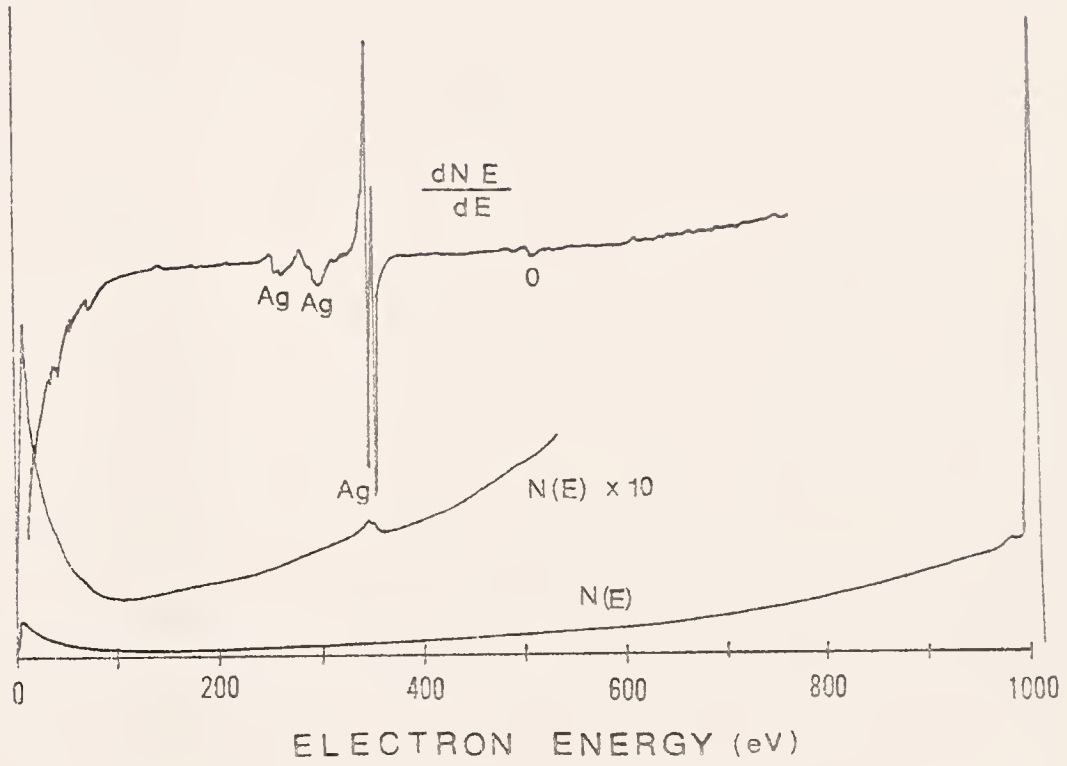

Figure 54. Schematic energy spectrum and experimental AES curve for silver excited in a 1000 eV electron beam.

relatively small peaks due to the Auger transitions in silver, detailed in the N(E) x 10 curve. In practice, the N(E) curve is electronically differentiated, as in the dN(E)/dE curve shown for silver.

Quantitative analysis with AES is currently in the developmental stage. The primary problem seems to be uncertainty in the depth, or volume, from which the Auger electrons are generated. Further complications arise from backscattering of the incident beam and the multiplicity of transition sequences which create Auger electrons for a given element. Semiquantitative analysis is possible, however. The variation in the peak-to-peak height of a differentiated Auger peak (more specifically, the integrated peak area) measured for an element is roughly proportional to the change in concentration of that element in the measured volume. In practice, however, absolute calibration of peak-to-peak heights with concentrations is very difficult, particularly when the measured surface is altered by ion sputtering.

It is often convenient to use the ratio of the measured peak-to-peak heights for two elements as an indication of their relative concentrations in a sample. It should be noted that such ratios measured for a sample are not necessarily equal to the actual compositional ratios of the elements in the sample. The efficiencies of Auger electron

production vary from element to element, thereby making calibration of the peak-to-peak height ratios necessary if semiquantitative information is desired. In such cases, however, calibration is much simpler, since the volume of material contributing to the measurement is the same for each element.

Depth profiles of near-surface concentrations can be obtained through combination of the AES technique with ion sputtering. By this method, energetic ions of a noble gas, such as Ar^+, are used to bombard the sample surface. The action of the ion bombardment is to sputter atoms off the surface. Alternate sputtering and measurement of the Auger surface spectra produces a depth profile of sample composition.

Several experimental complications can be introduced by the ion-sputtering process. These have been most recently detailed by Chang (84), and are briefly summarized below.

(1) The ion-sputtering process can introduce surface roughening, which exposes layers beneath those of interest.

(2) The bombardment process tends to homogenize the surface.

(3) Different materials exhibit different sputtering rates. This can result in preferential sputtering of one or more components of the sample, thereby changing the measured surface concentrations.

APPENDIX 6

CALIBRATION OF THE ARGON SPUTTERING RATE

A thin layer of copper was evaporated in vacuum simultaneously onto the surfaces of a clean glass microscope slide and a 20 mm x 20 mm piece of pure zinc finely polished according to the method used for polishing the selective leaching samples (see Appendix 1). The thickness of the copper film, measured on the glass slide with an Ångstrometer, was found to be 1026±25 Ångstroms. This was facilitated by evaporating thin aluminum film over the step produced by an edge of the copper film on the glass surface.

The copper-coated zinc sample was submitted to successive argon sputtering and Auger analysis until a composition versus sputtering time profile, figure 55, was obtained. The time at which the peak-to-peak heights for copper and zinc reached about one-half of their average maximum values, 41 minutes, was taken as the time required to mill through the copper film. Comparison of this value with the measured copper film thickness gives a sputtering rate of 25 Ångstroms/min. This value, determined for pure copper, was applied to the composition profiles obtained from the Cu30Zn selective leaching samples.

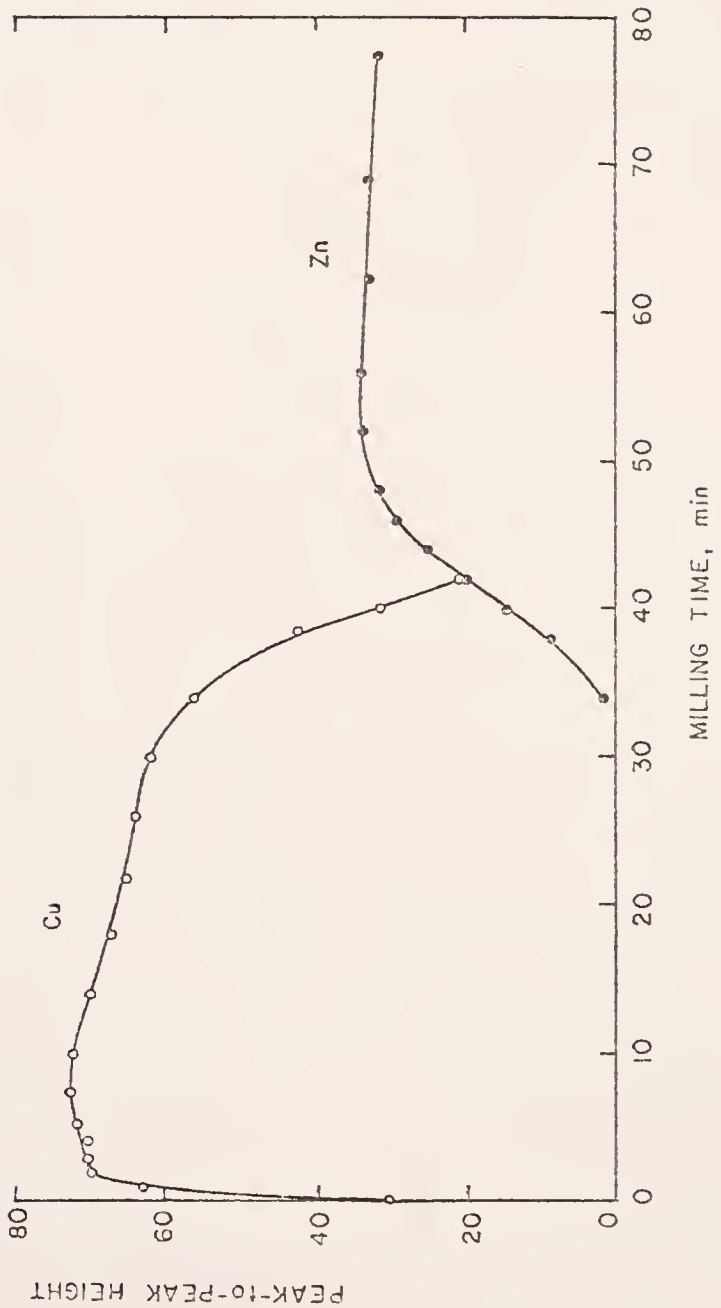

Figure 55. Composition profile of a 1026±25Å copper film deposited on a zinc substrate, used to calibrate the argon sputtering rate.

APPENDIX 7

FREE ENERGY DATA USED IN CALCULATED EQUILIBRIA

Species	Free Energy kcal/mol	Reference
H_2O	-56.69	72
H^+	0.0	72
OH^-	-37.59	72
Cl^-	-31.37	72
Cu	0.0	85
Cu_2O	-34.9	85
CuCl	-28.65	85
CuO	-31.0	85
$3Cu(OH)_2 \cdot CuCl_{2\gamma}$	-320.2	85
Cu_2O_3 hydr.	-41.5	71
Cu^+	11.95	85
$CuCl_2^-$	-57.4	85
$CuCl_3^{--}$	-90.0	85
Cu^{++}	11.95	85
$HCuO_2^-$	-61.8	85
CuO_2^{--}	-43.9	85
Zn	0.0	72
$Zn(OH)_2$	-76.94	72
Zn^{++}	-35.14	72
$HZnO_2^-$	-109.26	72
ZnO_2^{--}	-91.85	72

BIBLIOGRAPHY

1. Calvert and Johnson, J. Chem. Soc., 19, 436 (1866); referenced by M. N. Desai, J. D. Talati, and A. M. Trivedi, J. Indian Chem. Soc., 38, 565 (1961).

2. G. D. Bengough, R. M. Jones, and R. Pirret, J. Inst. Metals, 23, 65 (1920).

3. R. H. Heidersbach, Corrosion, 24, 38 (1968).

4. H. W. Pickering and P. R. Swann, Corrosion, 19, 373t (1963).

5. H. W. Pickering and P. J. Byrne, Corrosion, 29, 325 (1973).

6. H. W. Pickering, Corrosion, 25, 289 (1969).

7. R. Bakish and W. D. Robertson, J. Electrochem. Soc., 103, 320 (1956); ibid., Trans. AIME, 206, 1277 (1956).

8. A. J. Forty. Conference on the Fundamental Aspects of Stress Corrosion Cracking, Columbus, Ohio (1967), NACE, p. 64. Ed. R. W. Staehle (1969).

9. B. Upton, Corrosion, 19, 204t (1963).

10. R. E. Maersch and J. M. Cieslewicz, Matl. Prot., 3, 54 (1964).

11. S. Goldspiel, J. Kirshner and G. Wacker, Modern Castings, 47, 818 (1965).

12. L. Piatti and R. Grauer, Werkstoffe u Korr., 14, 551 (1963).

13. M. C. Steele, Australasian Corr. Eng., 1, 13 (1963).

14. G. T. Colegate, Metal Ind., 73, 483, 507, 531 (1948).

15. L. Kenworthy and W. G. O'Driscoll, Corrosion Tech., 2, 247 (1955).

16. H. W. Pickering and C. Wagner, J. Electrochem. Soc., 114, 698 (1967).

17. B. T. Rubin, PhD Dissertation, University of Pennsylvania, 1969.

18. E. D. Verink, Jr. and R. H. Heidersbach, Jr., Special Technical Publication 516, ASTM, Philadelphia, 1972.

19. R. H. Heidersbach, Jr. and E. D. Verink, Jr., Corrosion, 28, 397 (1972).

20. H. W. Pickering and P. J. Byrne, J. Electrochem. Soc., 116, 1492 (1969).

21. H. W. Pickering and P. J. Byrne, J. Electrochem. Soc., 118, 209 (1972).

22. H. Gerischer and H. Rickert, Z. Metallkunde, 46, 681 (1955).

23. H. W. Pickering, J. Electrochem. Soc., 115, 690 (1968).

24. J. E. Holliday and H. W. Pickering, J. Electrochem. Soc., 120, 470 (1973).

25. H. G. Feller, Corr. Sci., 8, 259 (1968).

26. R. P. Tischer and H. Gerischer, Z. Elektrochem., 62, 50 (1968).

27. V. F. Lucey, Br. Corr. Jnl., 1, 7 (1965); ibid., 2, 53 (1965).

28. L. Graf, Metallwirtschaft, 11, 77, 91 (1932).

29. L. Graf, Korrosion u Metallschutz, 11, 34 (1935).

30. H. W. Pickering, J. Electrochem. Soc., 115, 143 (1968).

31. H. W. Pickering. Conference on the Fundamental Aspects of Stress Corrosion Cracking, Columbus, Ohio (1967), NACE, p. 159, Ed. R. W. Staehle (1969).

32. R. H. Heidersbach, Jr., PhD Dissertation, University of Florida, 1971.

33. C. W. Stillwell and E. S. Turnipseed, Ind. and Eng. Chem., 26, 740 (1934).

34. H. W. Pickering, J. Electrochem. Soc., 117, 8 (1970).

35. F. deWurstemberger, Rev. Met., 18, 687 (1921).

36. F. W. Fink, T. Electrochem. Soc., 75, 441 (1939).

37. U. R. Evans, The Corrosion and Oxidation of Metals, Edward Arnold, Ltd., London, 1960.

38. J. Bumbulis and W. F. Graydon, J. Electrochem. Soc., 109, 12 (1962).

39. R. B. Abrams, T. Electrochem. Soc., 42, 39 (1922).

40. C. F. Nixon, T. Am. Electrochem. Soc., 45, 297 (1924).

41. J. C. Rowlands, Proc. Second International Congress on Metallic Corrosion, Houston, Texas, NACE, p. 795 (1966).

42. W. D. Clark, J. Inst. Metals, 73, 263 (1947).

43. T. J. Lennox, Jr., M. H. Peterson, and R. E. Groover, Matls. Prot. and Perform., 10, 31 (1971).

44. J. T. Crennell and J. E. Sawyer, J. Appl. Chem., 12, 4 (1962).

45. E. E. Langenegger and F. P. A. Robinson, Corrosion, 24, 12 (1968); ibid., 25, 2 (1969).

46. I. G. S. Falleiros and A. Pieske, Metallurgica, 26, 146 (1970).

47. J. Van Muylder, M. Pourbaix, and P. Van Laer, Report No. 127, CEBELCOR, May, 1965, Brussels, Belgium.

48. K. D. Efird, MS Thesis, University of Florida, 1970.

49. I. K. Marshakov and V. P. Bogdanov, Russ. J. Phys. Chem., 38, 1041 (1964).

50. F. P. A. Robinson and M. Shalit, Corr. Tech., 6, 11 (1964).

51. H. Sugawara and H. Ebiko, Corr. Sci., 7, 513 (1967).

52. M. Pourbaix, Personal communication, 1972.

53. K. K. Starr, PhD Dissertation, University of Florida, 1973.

54. G. D. Bengough and R. May, J. Inst. Metals, 32, 81 (1924).

55. U. R. Evans, T. Am. Electrochem. Soc., 75, 446 (1939).

56. J. M. West, Electrodeposition and Corrosion Processes, D. Van Nostrand Company, Ltd., London, 1965.

57. G. Masing, Wiss. Veröff. Siemens-Konzern, 10, 35 (1931).

58. H. Sugawara and S. Shimodaira, Nippon Kinzoku Gakkaishi, 30, 775 (1966).

59. E. D. Verink, Jr., and T. S. Lee, III, Proceedings: Third International Congress on Marine Corrosion and Fouling, Gaithersburg, Maryland, p. 241 (1972).

60. J. H. Hollomon and J. Wulff, TAIME, 143, 93 (1941); ibid., 147, 183 (1942).

61. T. M. Chen and S. R. Chu, Scienta Sinica, 6, 1764 (1963).

62. R. L. Cusumano, M S Thesis, University of Florida, 1971.

63. E. D. Verink, Jr. and M. Pourbaix, Corrosion, 27, 495 (1971).

64. Recommended Practice for Standard Reference Method for Making Potentiostatic and Potentiodynamic Anodic Polarization Measurements, ASTM Designation: G5-72, Annual Book of ASTM Standards, Part 10 (1974).

65. B. D. Cullity, Elements of X-ray Diffraction, Addison-Wesley Publishing Company, Inc., Reading, Massachusetts, 1967.

66. W. Feitknecht and K. Maget, Helvetica Chimica Acta, 32, 1639 (1949).

67. M. Pourbaix, Corrosion, 26, 431 (1970).

68. R. S. Cooper, J. Electrochem. Soc., 103, 307 (1965).

69. H. Sugawara and S. Shimodaira, J. Japan, Inst. Metals, 30, 626 (1966).

70. H. P. Leckie, J. Electrochem. Soc., 117, 1478 (1970).

71. J. Van Muylder, N. deZoubov, and M. Pourbaix, Report No. 101, CEBELCOR, July, 1962, Brussels, Belgium.

72. M. Pourbaix, Atlas of Electrochemical Equilibria in Aqueous Solutions, First English Edition, Pergamon Press, Oxford, 1966.

73. C. H. Bonfiglio, H. C. Albaya, and O. A. Cobo, Corr. Sci., 13, 717 (1973).

74. B. E. Wilde and E. Williams, J. Electrochem. Soc. 116, 1539 (1969).

75. P. G. Shewmon, Diffusion in Solids, McGraw-Hill Book Company, Inc., New York, 1963.

76. K. J. Anusavice and R. T. DeHoff, Met. Trans., 3, 1279 (1972).

77. A. H. Taylor, J. Electrochem. Soc., 118, 854 (1971).

78. R. K. Flatt and P. A. Brook, Corr. Sci., 11, 185 (1971).

79. W. Latimer, Oxidation Potentials, Prentice-Hall, New York, 1952.

80. D. F. Stein, J. Vac. Sci. Technol., 12, 268 (1975).

81. N. A. Gjostein and N. G. Chavka, JTEVA, 1, 183 (1973).

82. G. J. Dooley, III and T. W. Haas, JOM, 22, 17 (1970).

83. T. W. Haas and D. J. Pocker, J. Vac. Sci. Technol., 11, 1087 (1974).

84. C. C. Chang, Analytical Auger Electron Spectroscopy, in P. E. Kane and G. B. Larrabee, Characterization of Solid Surfaces, Plenum Press, New York, 1974, p. 509.

85. NBS Technical Note 270-4, National Bureau of Standards, U.S. Government Printing Office, Washington, D.C. (1969).

BIOGRAPHICAL SKETCH

William Clarence Fort, III was born September 12, 1948, at Lake Wales, Florida. He attended public schools in Jacksonville, Florida. He attended the Georgia Institute of Technology for two years, and was graduated from the University of Florida in 1971, with the degree of Bachelor of Science in Metallurgical and Materials Engineering. Since that date he has pursued the degree of Doctor of Philosophy in the Department of Materials Science and Engineering.

William Clarence Fort, III is married to the former Deborah Cameron-Bruce Hore. He is the father of one daughter, Vanessa Margaret. He is a member of the American Institute of Mining, Metallurgical, and Petroleum Engineers, the American Society for Metals, the National Association of Corrosion Engineers, Tau Beta Pi, and Alpha Sigma Mu.

I certify that I have read this study and that in my opinion it conforms to acceptable standards of scholarly presentation and is fully adequate, in scope and quality, as a dissertation for the degree of Doctor of Philosophy.

Ellis D. Verink, Jr., Chairman
Professor of Materials Science
and Engineering

I certify that I have read this study and that in my opinion it conforms to acceptable standards of scholarly presentation and is fully adequate, in scope and quality, as a dissertation for the degree of Doctor of Philosophy.

Robert T. DeHoff
Professor of Materials Science
and Engineering

I certify that I have read this study and that in my opinion it conforms to acceptable standards of scholarly presentation and is fully adequate, in scope and quality, as a dissertation for the degree of Doctor of Philosophy.

Robert W. Gould
Professor of Materials Science
and Engineering

I certify that I have read this study and that in my opinion it conforms to acceptable standards of scholarly presentation and is fully adequate, in scope and quality, as a dissertation for the degree of Doctor of Philosophy.

Gerhard M. Schmid
Associate Professor of Chemistry

This dissertation was submitted to the Dean of the College of Engineering and to the Graduate Council, and was accepted as partial fulfillment of the requirements for the degree of Doctor of Philosophy.

August, 1975

Dean, College of Engineering

Dean, Graudate School

UNIVERSITY OF FLORIDA
3 1262 08554 0713